FUNCTIONAL POLYMERS FOR DRUG DELIVERY AND

OPTO-ELECTRONIC APPLICATIONS

by

Vasanthy Karmegam

APPROVED BY SUPERVISORY COMMITTEE:

Mihaela C. Stefan, Chair

Michael C. Biewer

Ronald A. Smaldone

Gabriele Meloni

To my family.

FUNCTIONAL POLYMERS FOR DRUG DELIVERY AND

OPTO-ELECTRONIC APPLICATIONS

by

VASANTHY KARMEGAM, BS, MS

DISSERTATION

Presented to the Faculty of

The University of Texas at Dallas

in Partial Fulfillment

of the Requirements

for the Degree of

DOCTOR OF PHILOSOPHY IN

CHEMISTRY

THE UNIVERSITY OF TEXAS AT DALLAS

December 2018

ACKNOWLEDGMENTS

Finally, I would like to thank my whole family, my parents (appa and amma) and my three sisters for being supportive and giving me blessings all the time, without whom I never would have been able to reach greater heights. My sincere gratitude goes to my husband Sandun, who has been supportive, helpful and giving me strength to achieve my goals in life.

November 2018

FUNCTIONAL POLYMERS FOR DRUG DELIVERY AND

OPTO-ELECTRONIC APPLICATIONS

Vasanthy Karmegam, PhD
The University of Texas at Dallas, 2018

Supervising Professor: Mihaela C. Stefan

Polymers are promising macromolecules that have been extensively used in a range of applications such as biomedical, optoelectronic, and catalysts. These polymer materials can be designed with a wide range of architecture and functionalities. The functionalization of the polymer backbone offers new properties to improve the existing polymer material. This study focuses on the synthesis of functionalized polycaprolactone and pyrimidine polymers and improvement in properties to apply in drug delivery and opto-electronic applications.

Chapter 1 discusses the recent advances in biodegradable polyesters for drug delivery systems. Polyesters are an attractive material which has been extensively used in biomedical application. There has been a significant amount of attention on modification of polyesters and its application in drug delivery systems. This chapter discusses the synthesis and design of aliphatic polyester materials and its various applications.

Chapter 2 describes the synthesis of thermo-responsive linear and star-like block copolymers from functionalized polycaprolactones, a class of biodegradable polyesters. The functionalized polycaprolactone was used to develop polymer micellar carrier to encapsulate anti-cancer drug,

Doxorubicin. The effect of polymer functionalization and architecture in polymer property and drug loading are discussed.

Chapter 3 discusses co-delivery of Doxorubicin and Resveratrol in linear and star-like polymer micellar drug carriers. The favorable interaction between drugs and functional groups of the polymer backbone significantly enhances the drug loading. The simultaneous delivery of DOX and Resveratrol is a promising approach for improving drug loading and antitumor activity.

Chapter 4 discusses the synthesis and characterization of a series of pyrimidine-containing donor acceptor conjugated polymers. The pyrimidine polymer was functionalized with electron-withdrawing and -donating pendent groups. The electron-withdrawing strength of the pendent groups was systematically varied to study its effect on opto-electronic properties of the conjugated polymer.

TABLE OF CONTENTS

LIST OF FIGURES

LIST OF TABLES

LIST OF SCHEMES

CHAPTER 1

BIODEGRADABLE ALIPHATIC POLYESTERS FOR DRUG DELIVERY

Authors: Vasanthy Karmegam, Pooneh Soltantabar, Erika Joy L. Calubaquib,
Ruvanthi, N. Kularatne, Mihaela C. Stefan

The Department of Chemistry and Biochemistry, BE26

The University of Texas at Dallas

800 West Campbell Road

Richardson, Texas 75080-3021

1.1 Abstract

The interest in the synthesis and tuning the properties of aliphatic polyesters has been growing in recent years, because of their unique properties and promising applications in drug delivery systems. Polyester based drug delivery systems have received considerable attention, because of their biocompatibility and biodegradability. Many polyesters have been synthesized by homopolymerization of substituted and/or unsubstituted monomers or co-polymerization with other monomers, mostly via ring-opening polymerization (ROP) of cyclic esters. The functionalization of aliphatic polyesters is a widely used strategy to tune the polymer properties such as hydrophilicity, hydrophobicity and degradation rate, making the materials suitable for drug delivery application. Here, we discuss the recent trends in the synthesis of these aliphatic polyesters and their potential application for drug delivery.

1.2 Introduction

Innovations in polymer technology have had a significant impact on the advancement of novel drug delivery systems. Most polymer-based drug delivery systems are designed to deliver a large dose of a therapeutic agent at a targeted site in a controlled manner, to reduce dosage frequency. However, the accumulation of polymer-based drug carriers in the body can pose a significant health risk and represents a major disadvantage of many polymer-based drug delivery systems. For example, the poor biodegradability of polystyrene (PS), poly(methyl methacrylate) (PMMA), and poly(N-isopropylacrylamide) (PNIPAM) have limited their potential applicability in drug delivery applications.[1]

In contrast, aliphatic polyesters have received significant traction as drug delivery systems due to their biodegradability and biocompatibility. The degradation of the polyester backbone *in vivo* avoids accumulation of the drug carrier products and its degraded products inside the body, which decreasing the long-term toxicity.[2] Common polyesters used in drug delivery applications include poly(lactide)s (PLA), poly(caprolactone)s (PCL), poly(glycolide)s (PGA), poly(dioxanone)s (PDO), poly(butyrolactone)s (PBL), poly(valerolactone)s (PVL), and poly(lactide-co-glycolide) (PLGA) (Figure 1.1).[3]
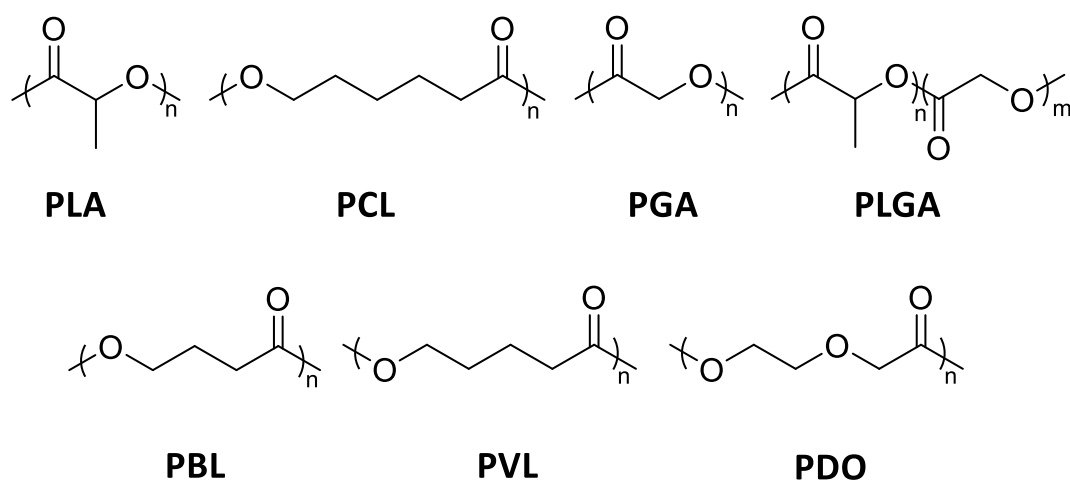
Figure 1.1. Polyesters commonly used in drug delivery applications.

A significant focus of current cancer therapy research is the delivery of anti-cancer drugs to tumor sites in a targeted manner, combined with activated release of the therapeutic payload. Stimuli-responsive polymeric drug carriers typically utilize nanocarriers (e.g., micellar systems, nanoparticles, polymersomes, or dendrimers) to release the drug at the tumor site by taking advantage of differences in the physiological environment between cancerous and healthy tissue. To further enhance the site-specificity of drug carriers, they can be conjugated with targeting moieties to allow for delivery at a specific tumor site. This article focuses on recent advances in

the development of aliphatic polyesters for cancer therapy, specifically polyester synthesis, stimuli-responsive drug carriers and active targeting.

1.3 Polyester Synthesis

There are several strategies for the synthesis of aliphatic polyesters, including the polycondensation of diacids and diols as well as the ring-opening polymerization (ROP) of cyclic esters. Disadvantages of polycondensation include the requirement of accurate stoichiometry between reactants, continuous removal of by-products (e.g., water), high temperatures, long reaction times, and difficulty obtaining high molecular weight polymers.[4] In contrast, ring-opening polymerization typically results in high molecular weight polyesters and features limited side reactions. Based on its ease of use and the wide variety of initiators and catalysts available, ROP is widely used to polymerize cyclic ester monomers. The three most common mechanisms used in cyclic ester ring-opening polymerization are coordination-insertion, enzymatic, and anionic.[4]

Coordination-insertion ROP is initiated by an alcohol or amine and catalyzed by metal complexes based on Lewis acidic metals such as tin, aluminum, and zinc.[1] While this method yields high molecular weight polymers, residual traces of the metal catalyst in the final polymer have been considered a major drawback limiting biological applications. For example, tin(II) bis(2-ethylhexanoate) (Aldrich Prod. No S3252), is an FDA-approved food additive commonly used for polyester synthesis, but due to the toxicity of tin, the residual concentration must remain below a certain threshold for use in food or biomedical applications.[4]

Enzymatic ROP commonly uses lipases as the catalyst in mild conditions, avoiding the use of toxic metals. While this method allows for the production of polyesters with stereo-, chemo- and regio-selectivity,[5] the resulting polyesters are commonly produced in relatively low yield with high

4

polydispersity.[3] Anionic ROP yields high molecular weight polyesters but these reactions frequently undergo side reactions due to backbiting.[4]

1.4 Polyester Drug Carriers and Drug Release

Choosing an appropriate polymer vehicle and aptly tuning its properties ensures increased drug loading efficiency, reduction of drug dose and dosing frequency, alleviation of side effects, improvement of patient compliance, and short *in vivo* half-lives for drug delivery. Micelles, nanoparticles, and polymersomes are the most commonly explored drug carriers from synthetic polymers, formed by the self-assembly of amphiphilic block copolymers. Nanoparticle formation can be controlled kinetically through the variation of temperature, pH, electrolytes, and solvents and typically range in size from 10 to 1000 nm.[3,7] Micelle formation is thermodynamically controlled,[6] proceeding only when unimers aggregate above the critical micelle concentration (CMC), to form particles with sizes ranging from 5 to 100 nm.[3,7] Upon interaction with hydrophobic segments, a hydrophobic drug will migrate into the core of the micelle to form a core-shell matrix. In contrast, polymersomes are composed of a core filled with aqueous solution surrounded by a bilayer membrane composed of hydrophilic coronas located both on the inside and outside of the sphere. This unique structure enables polymersomes to encapsulate both hydrophobic and hydrophilic drugs.

Polymeric drug carriers facilitate the delivery of high drug payload to the site of action and allow controlled and sustained drug release under physiological conditions through erosion or stimuli-triggered release.[2,3,8] Upon water permeation, polyesters can undergo degradation via hydrolysis resulting in loss of polymer mass. Depending on the identity of the polymer backbone, erosion can either occur at the bulk or the surface of the nanocarrier (Figure 1.2). Surface erosion

occurs when the rate of degradation is faster than the rate of water permeation into the bulk polymer. In contrast, bulk erosion occurs when water penetrates the bulk of the polymer at a faster rate than the erosion rate. The majority of biodegradable polyesters degrade via bulk erosion due to the increased ratio of aliphatic content. Recently, polymeric drug carriers with enhanced surface area have been utilized to control drug release, taking advantage of both surface and bulk erosion mechanisms.[2,5,8]
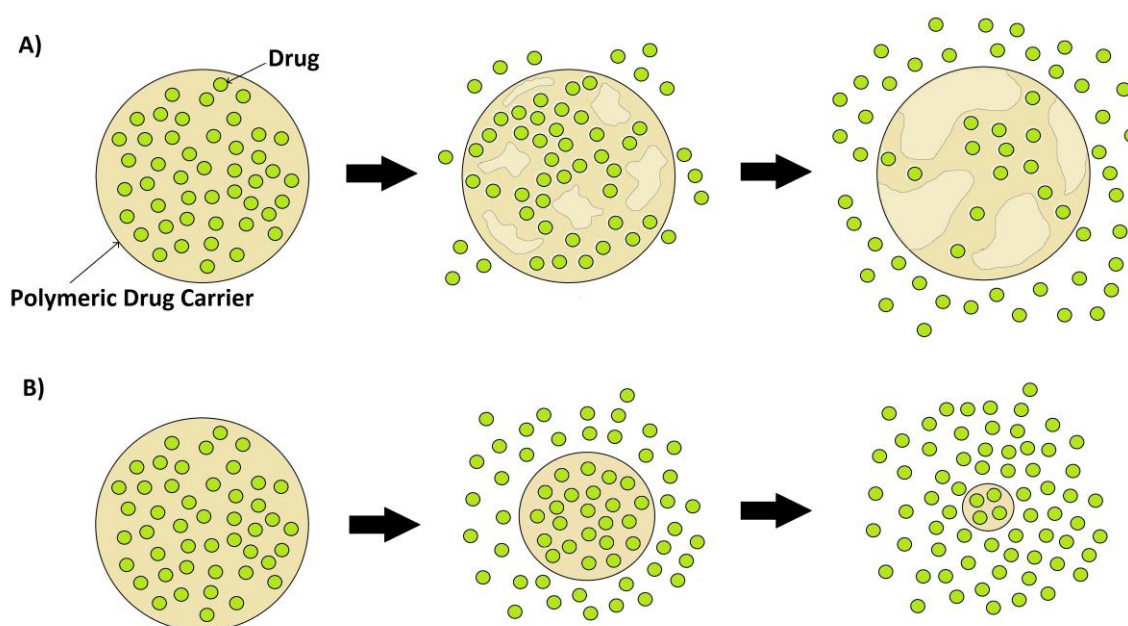
Figure 1.2. Degradation mechanisms of biodegradable polymeric drug carriers: A) bulk erosion, B) surface erosion.

Some carriers are designed to release the loaded drug only when exposed to external stimuli such as pH, temperature, reduction, enzymes, and light, preventing premature release of the encapsulated drug (Figure 1.3).[3] This results in an increased therapeutic efficacy of the drug and a decrease of potential toxicity to healthy cells.[9]
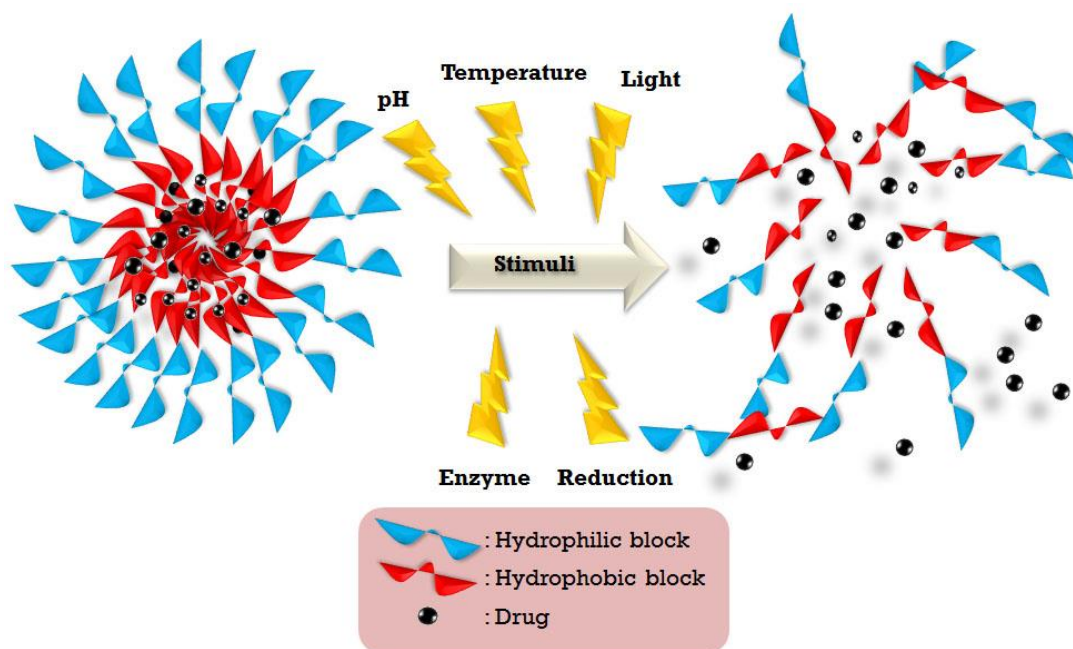
Figure 1.3. Schematic representation of stimuli-responsive drug release.

1.5 Stimuli-Responsive Polyester Drug Carriers

Polymeric drug carriers are able to enter tumor sites through passive targeting via the enhanced permeability and retention (EPR) effect. As a result of this phenomena, nanoparticles in the size range of 10 to 100 nm accumulate in tumor sites due to the presence of leaky vasculature.[3] In addition to utilizing this effect, polymeric drug carriers can be designed to respond either to a single or multiple stimuli by taking advantage of the difference in physiological environment between normal and tumor tissue. The difference in acidity between healthy and cancerous tissue allows for the development of pH-dependent release mechanisms.

For example, the pH of healthy tissue is 7.4 whereas the extracellular environment of the tumor tissue is 6.8 and intracellular endo/lysosomal pH is in the range of 4.0–6.5.[10] In the presence of acid-labile functional groups, drug carriers are cleaved in an acidic environment, releasing a drug

7

at the tumor site. Synthesis of a pH-responsive (mPEG-PLA)-curcumin prodrug and further self-assembly into a micellar system was investigated by Zhao and coworkers.[11] The drug, which was conjugated to the polymer via a pH-responsive acetal linkage, showed more than 45% release at pH 5 after 48 hours while less than 20% of curcumin was released from the micellar system at pH 7.4.[11]

The difference in concentration of glutathione (GSH) between healthy cells and cancer cells can also be used as stimuli. Tumor cells have an intracellular GSH concentration of ~2–10 mM; several times higher than the concentration in healthy cells.[10] The increased GSH concentration can cleave reduction-responsive disulfide bonds, allowing the release of the loaded cargo into the tumor site.[12] A reduction-responsive micellar drug delivery system based on disulfide bond-containing PEG-PLA amphiphilic block copolymers was developed by Shen and coworkers. In a reductive environment, the breaking of disulfide bonds caused the rapid release of doxorubicin (DOX). Up to 64% of DOX was released from PEG2000-PLA5000 micelles after 14 hours in the presence of the reducing agent dithiothreitol (DTT). In the absence of DTT, only 40% of DOX was released after 14 hours.[12]

Thermally responsive drug delivery systems typically consist of polymers featuring a lower critical solution temperature (LCST) and upper critical solution temperature (UCST). Above their LCST, the polymers undergo a phase transition, becoming insoluble in water.[13] Polymers with an LCST above normal physiological temperature (37 °C) are typically used in thermally responsive systems. These polymers are able to preserve their cargo in the body and undergo phase transition with the application of heat, leading to a burst release of drug in tumor tissue. A thermo-responsive monomer, γ-2-[2-(2-methoxyethoxy)ethoxy]ethoxy-ε-caprolactone (MEEECL), was introduced

by Stefan et al. and combined with octyloxy-ε-caprolactone (OCTCL) to create an amphiphilic block copolymer with a LCST of 38 °C.[14] The LCST could be adjusted in the range of 31–43 °C by replacing OCTCL with γ-(2-methoxyethoxy)-ε-caprolactone (MECL). The size of the resulting micelles increased from approximately 150 nm to 400 nm when the temperature exceeded the LCST of copolymer.[13] Moreover, they demonstrated (experimentally and computationally) the effect of varying the substituent in the γ-position of caprolactone monomers in the thermo-responsive behavior of a series of self-assembled micellar systems utilizing MEEECL as the hydrophilic block (Figure 1.4). The resulting amphiphillic diblock copolymers were found to have an LCST in the range of 36–39 °C.[15]

While polymer delivery systems that respond to a single stimulus have had a significant impact on the development of drug delivery technology, recent efforts have focused on systems that can respond to more than one stimulus. A dual pH- and redox-responsive system was reported by Ge and coworkers[16] in which copolymer prodrugs were encapsulated into PEG-b-PCL micelles. The copolymer prodrugs were prepared by the polymerization of pH-responsive 2-(piperidin-1-yl)ethyl methacrylate (PEMA) and reduction-responsive camptothecin (CPT, Sigma Prod. No C9911). Due to the protonation of PPEMA in acidic pH, the zeta potential of the micelles increased from -2 mV to +12 mV, resulting in an increase of the size of the micelles from 32.7 to 48.6 nm. 80% of CPT was released by the cleavage of the disulfide bonds in response to increased GSH concentration.
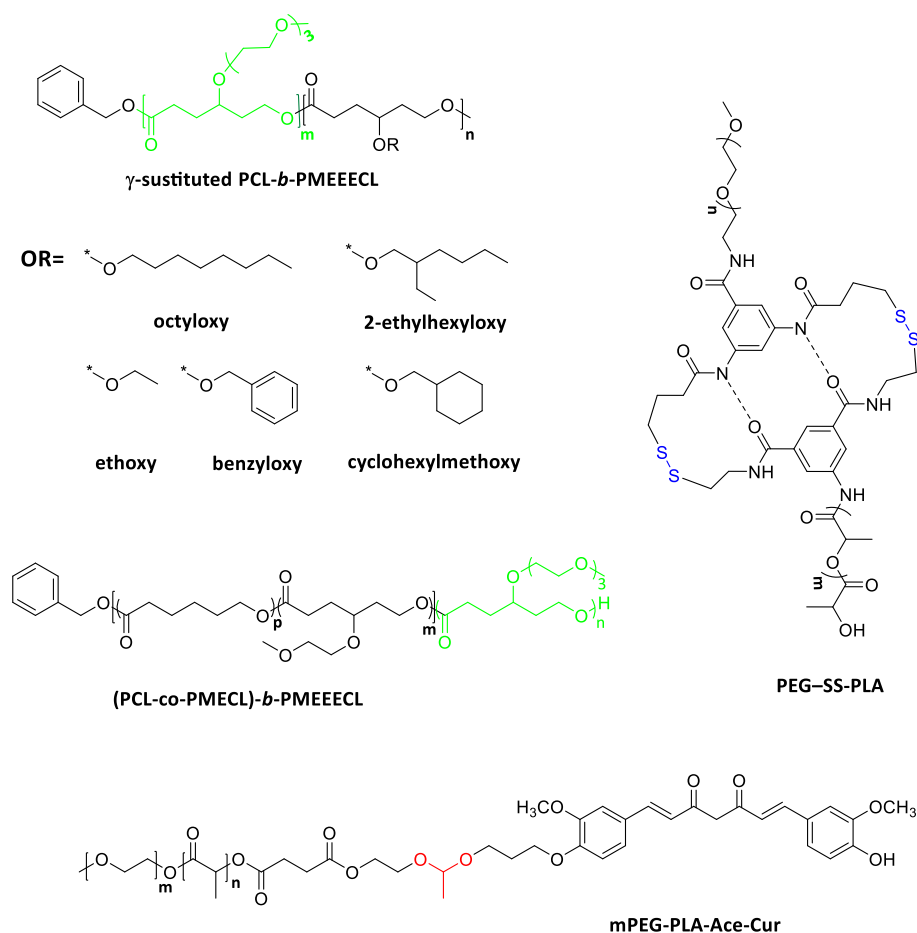
Figure 1.4. Single stimulus-responsive polyesters for drug delivery applications with responsive units highlighted (pH = red, temperature = green, and reduction = blue).

Thermo- and pH-responsive micelles designed by Chen and coworkers consist of a hydrophobic PCL segment and a thermo-responsive poly(N-isopropylacrylamide) (PNIPAAm) hydrophilic segment, which was copolymerized with a pH-sensitive β-alanine-functionalized monomer (βA).[17] The micelles were co-loaded with DOX and a photosensitizer, meso-tetraphenylchlorin. The LCST of this polymer decreased from 37 °C at pH 7.4 to 25.8 °C at pH 6.0, resulting in the release of the encapsulated drug in acidic conditions. Consequently, 70% and 40% of DOX was released in acidic and neutral environments, respectively.
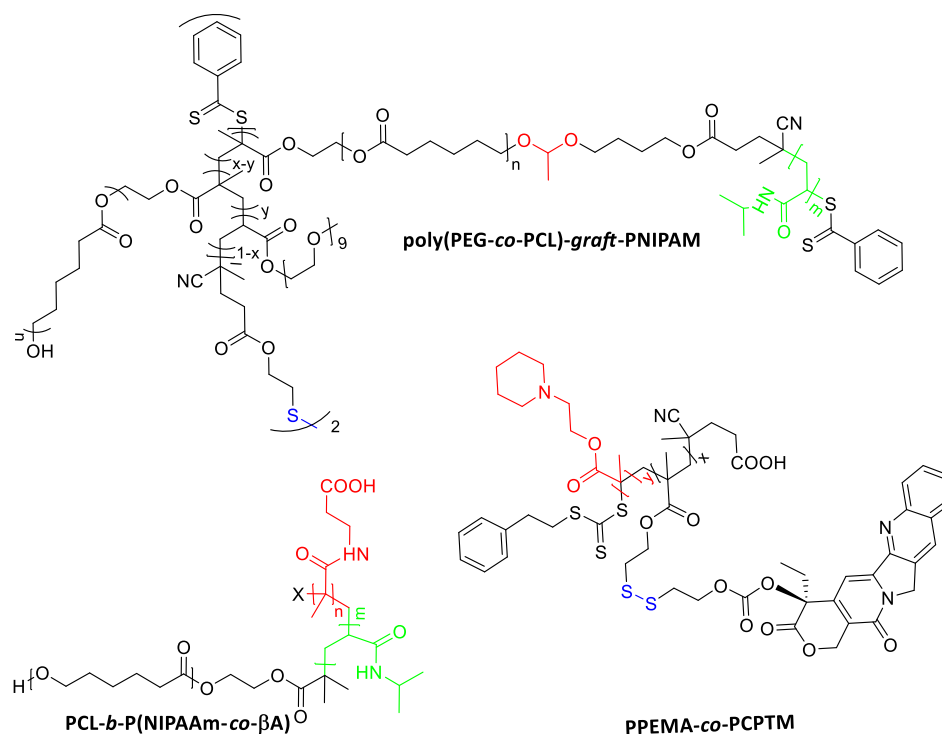
Figure 1.5. Multi-stimuli responsive polyesters for drug delivery applications with responsive units highlighted (pH = red, temperature = green, and reduction = blue).

Zhao and coworkers designed a multi-responsive, comb-like copolymer by grafting a copolymer of PEG, PCL, and a reduction responsive disulfide bond to a thermo-responsive PNIPAAm backbone via a pH-responsive acetal linkage (Figure 1.5).[10] This dual-cleavable, multi-responsive, graft copolymer aggregate demonstrated high DOX release after stimuli application. Cumulative DOX release was studied in different conditions, including neutral and acidic pH, elevated temperature, and in the presence or absence of DTT. A maximum release of 77.1 % was observed at 37 °C, pH 5.3, and in the presence of DTT, in contrast to only 36.1 % at 25 °C, pH 7.4, and without DTT. Although stimuli-responsive carriers increase the chance of accumulation in the targeted site, active targeting can be used to direct the drug delivery system to specific sites in the body.

1.6 Active Targeted Polyester Drug Carriers

Compared to passive targeting, targeted drug delivery allows for the delivery of encapsulated drugs to the targeted site, reducing the risk of toxicity to normal cells and allowing for the accumulation of drug in sufficient concentrations to eliminate tumor cells. A comparison of passive and active targeting is shown in Figure 1.6.
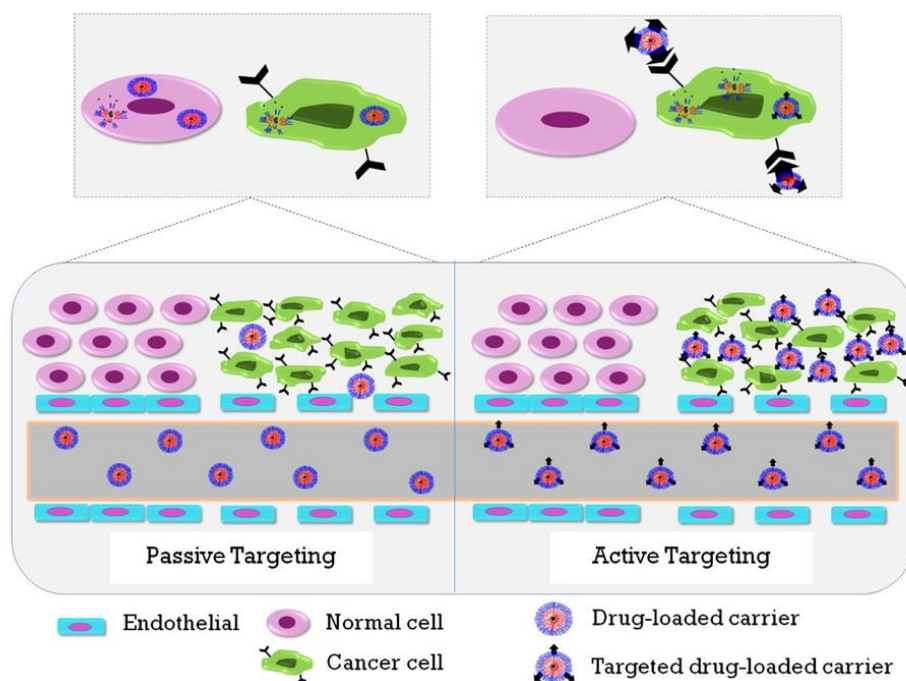
Figure 1.6. Graphical representation of passive versus active targeting.

Targeting moieties are typically attached to the polymer through end-group variation or conjugation along the polymer backbone. A wide spectrum of targeting moieties can be used, including antibodies, proteins, peptides, carbohydrates, vitamins, and nucleic acids.[3]

A biodegradable polymeric matrix with disulfide linkages (PEG-SS-PCL) from Zhong et al., was functionalized with cyclic arginine-glycine-aspartic acid (cRGD) peptide to form a cRGD/PEG-SS-PCL nanomicelle, which exhibited high affinity for αvß3 integrins. αvß3 integrins

are important biomarkers overexpressed on angiogenic tumor endothelial cells and malignant tumor cells, such as U87MG glioblastoma cells and B16 melanoma cells. These DOX-loaded, functionalized-nanomicelles showed a half-maximal inhibitory concentration (IC_{50}) of 6.36 µg/mL, 2.9-fold lower than that of the non-functionalized micelle (IC_{50}= 18.35 µg/mL). *In vivo* biodistribution was performed using U87MG tumor-bearing nude mice. Four hours post injection *ex vivo* DOX fluorescence imaging revealed that DOX delivered via cRGD/PEG-SS-PCL exhibited higher accumulation in the tumor (4.38% ID/g) in comparison to liver, heart, spleen, lung, and kidney tissue. In addition, this was also 2.2-fold higher than that of DOX delivered via PEG-SS-PCL (1.99% ID/g).[18]

Zhou and coworkers reported a dual-responsive polymer micelle generated from the self-assembly of a redox-responsive prodrug, a mPEG-SS-CPT and phenylboronic acid (PBA) functionalized enzyme-responsive copolymer, and PBA-PEG-4,4'-(diazene-1,2-diyl)benzoyl-PCL (PBA-PEG-Azo-PCL). PBA interacts with sialic acid, which is overexpressed in hepatoma carcinoma cells, enhancing in-vitro cellular uptake in HepG2 cells with the PBA-functionalized carrier. Moreover, strong fluorescence remained at the tumor site six hours post-injection in nude mice bearing H22 tumors; 1.84-fold higher than with the non-targeted micelle.[19]

Poly(poly(ethylene glycol)methacrylate)−poly(caprolactone)−poly(poly(ethylene glycol) methacrylate) (pPEGMA−PCL− pPEGMA) triblock copolymer was conjugated with DOX through an acid-labile hydrazone bond. This pH responsive system was then functionalized with folic acid and/or AS1411 aptamer, which specifically bind to folate and nucleolin receptors, respectively, that are overexpressed in cancer cells. Using fluorescence-activated cell sorting, the cellular uptake of this dual-targeted system in MCF-7 and PANC-1 cells was found to be 10- and

100-fold higher compared to single and non-targeted nanoparticles, respectively. Moreover, L929, a noncancerous cell line showed no DOX adverse effects.[20]

1.7 Conclusion

Due to their versatility, biodegradable aliphatic polyesters have been shown to be excellent candidates in a wide range of anti-cancer drug delivery applications. Stimuli-responsiveness and targeted release of anti-cancer drugs with polyester drug carriers has improved the therapeutic efficacy while reducing adverse side effects to healthy cells. The structural and functional diversity of aliphatic polyesters provides new opportunities for creating novel materials with enhanced performance with dramatic impact on the development of next generation drug delivery systems. Progress in the development of aliphatic polyesters for anticancer drug delivery applications will continue to advance from the laboratory to clinical trials, improving both treatment options and patient outcomes in cancer therapy.

1.8 References

1.   Jones, M.-C.; Leroux, J.-C. Eur. J. Pharm. Biopharm. 1999, 48(2), 101.

2.   Harrison, K. In Biomedical Polymers; Jenkins, M., Ed.; Woodhead Publishing Series in Biomaterials; Woodhead Publishing, 2007; pp 33–56.

3.   Washington, K. E.; Kularatne, R. N.; Karmegam, V.; Biewer, M. C.; Stefan, M. C. Wiley Interdiscip. Rev. Nanomed. Nanobiotechnol. 2016, 9(4), 1446.

4.   Coulembier, O.; Degée, P.; Hedrick, J. L.; Dubois, P. Prog. Polym. Sci. 2006, 31(8), 723.

5.   Winzenburg, G.; Schmidt, C.; Fuchs, S.; Kissel, T. Adv. Drug Deliv. Rev. 2004, 56(10), 1453.

6. Washington, K. E.; Kularatne, R. N.; Du, J.; Gillings, M. J.; Webb, J. C.; Doan, N. C.; Biewer, M. C.; Stefan, M. C. J. Polym. Sci. Part A Polym. Chem. 2016, 54(22), 3601.

7. De Jong, W. H.; Borm, P. J. A. Int. J. Nanomedicine 2008, 3(2), 133.

8. Uhrich, K. E.; Cannizzaro, S. M.; Langer, R. S.; Shakesheff, K. M. Chem. Rev. 1999, 99(11), 3181.

9. Yu, D.; Zou, G.; Cui, X.; Mao, Z.; Estrela-Lopis, I.; Donath, E.; Gao, C. J. Mater. Chem. B 2015, 3(45), 8865.

10. Liu, H.; Li, C.; Tang, D.; An, X.; Guo, Y.; Zhao, Y. J. Mater. Chem. B 2015, 3(19), 3959.

11. Li, M.; Gao, M.; Fu, Y.; Chen, C.; Meng, X.; Fan, A.; Kong, D.; Wang, Z.; Zhao, Y. Colloids Surf., B 2016, 140, 11.

12. Yang, Q.; Tan, L.; He, C.; Liu, B.; Xu, Y.; Zhu, Z.; Shao, Z.; Gong, B.; Shen, Y.-M. Acta Biomater. 2015, 17, 193.

13. Rainbolt, E. A.; Washington, K. E.; Biewer, M. C.; Stefan, M. C. J. Mater. Chem. B 2013, 1(47), 6532.

14. Cheng, Y.; Hao, J.; Lee, L. A.; Biewer, M. C.; Wang, Q.; Stefan, M. C. Biomacromolecules 2012, 13(7), 2163.

15. Hao, J.; Cheng, Y.; Ranatunga, R. J. K. U.; Senevirathne, S.; Biewer, M. C.; Nielsen, S. O.; Wang, Q.; Stefan, M. C. Macromolecules 2013, 46(12), 4829.

16. Huang, M.; Zhao, K.; Wang, L.; Lin, S.; Li, J.; Chen, J.; Zhao, C.; Ge, Z. ACS Appl. Mater. Interfaces 2016, 8(18), 11226.

17. Chen, C.-Y.; Wang, Y.-C.; Hung, C.-C. React. Funct. Polym. 2016, 98, 56.

18. Zhu, Y.; Zhang, J.; Meng, F.; Deng, C.; Cheng, R.; Feijen, J.; Zhong, Z. J. Control. Release 2016, 233, 29.

19. Zhang, L.; Wang, Y.; Zhang, X.; Wei, X.; Xiong, X.; Zhou, S. ACS Appl. Mater. Interfaces 2017, 9(4), 3388.

20. Lale, S. V; R. G., A.; Aravind, A.; Kumar, D. S.; Koul, V. Biomacromolecules 2014, 15(5), 1737.

CHAPTER 2

ENHANCED DOX LOADING IN BENZYL FUNCTIONALIZED-
POLYCAPROLACTONE MICELLES BASED ON STAR-POLYMER ARCHITECTURE

2.1   Abstract

The micellar self-assembly of functionalized polycaprolactone-based copolymer is widely explored in carrier-mediated doxorubicin delivery for effective cancer treatment. In this report, functionalized polycaprolactone-based block copolymers with controlled branching architecture are investigated.   Star-like copolymers, namely 4-arm and 6-arm poly(γ-benzyloxy-ε-caprolactone)-*b*-poly{γ-2-[2-(2-methoxyethoxy)   ethoxy]ethoxy-ε-caprolactone}   (PBCL-*b*-PMEEECL), were synthesized by *living* ring-opening polymerization (ROP) of [γ-(2-benzyloxy)-ε-caprolactone   with   {γ-2-[2-(2-methoxyethoxy)ethoxy]ethoxy-ε-caprolactone}   using multifunctional initiatiors. A systematic investigation of the effect of some branching points on polymer properties and on micellar carrier properties was carried out. The star-like PBCL-*b*-PMEEECL micelles displayed a better thermodynamic stability, reduction in size and enhanced doxorubicin encapsulation as compared to the linear PBCL-*b*-PMEEECL. Furthermore, the π–π stacking effect between the benzyl group of the hydrophobic PBCL core and the doxorubicin, the anti-cancer drug, also increased the stability and loading capacity of the micelles. The polymers displayed a tunable thermo-responsiveness in the range of 40-42 °C. When the DOX-loaded micelles are internalized by tumor cells, the shell of the polymeric micelles dehydrates upon heating (at temperature above its LCST), causing disassembling of the micelles and releasing of DOX into the nuclei of the tumor cells. Compared with DOX-loaded linear and 4-arm micelles, DOX-loaded 6-arm micelles exhibited higher anti-tumor activity *in-vitro*. Thus, the 6-arm benzyl

substituted polycaprolactone-based micellar systems are promising candidates for drug delivery applications.

2.2 Introduction

Aliphatic polyester materials, an important class of biocompatible and biodegradable polymers, are widely used in biomedical research for a broad array of demanding applications. Especially, it has been used in smart carrier development due to its remarkable biodegradability.[1–8] Aliphatic polyesters including poly(lactide)s (PLA), poly(caprolactone)s (PCL), poly(glycolide)s (PGA), poly(dioxanone)s (PDO), poly(butyrolactone)s (PBL), and poly(valerolactone)s (PVL) and their copolymers have been successfully employed in drug delivery applications. Owe to good mechanical properties and slow degradation rate, polycaprolactone-based drug delivery systems have been widely used compared to other polyesters.

Functional groups have been incorporated to tune the properties of PCLs to expand their application for drug delivery systems.[9–15] Pendent functional groups have been introduced along the PCL backbone by ring opening polymerization of functionalized ε-caprolactone monomer and /or post polymerization modification.[16] Polymerization of functional caprolactone(CL) substituted at α- or γ-position with functionality like halogen, hydroxy, carboxylic, acyloxy, allyl and amine have been reported to tune the PCL properties.[16–19]

Stefan et al has employed functional groups such as alkoxy-, benzyloxy-, and methoxyethoxy to improve the micellar properties including drug loading capacity, thermodynamic stability and kinetic stability.[12,20,21] Furthermore, PCLs can be chemically modified by coupling drugs, bioactive moieties and stimuli-responsive moieties. As such, functional groups, such as

17

doxorubicin (DOX), HDAC inhibitor and, paclitaxel have been incorporated in PCLs backbone to improve the drug loading and cellular accumulation.[15,22–24] Xiong et al. reported doxorubicin conjugated RGD-PEG-*b*-PCCL, (PEG-*b*-poly(α-carboxyl-ε-caprolactone)) and RGD4C-PEG-*b*-PCCL to selective delivery of DOX to tumor cells.[25,26] They showed that RGD-PEG-*b*-PCCL improves the degradation rate and cellular accumulation of dox in metastatic cancer cells.[25] Further, they reported that RGD4C-PEG-*b*-PCCL significantly enhances the cellular accumulation of DOX in DOX-resistance cancer cells.[26]

Stefan et al have reported, thermo-responsive functional moiety conjugated CL monomer, γ-2-[2-(2-methoxyethoxy)ethoxy] ethoxy-ε-caprolactone (ME3CL).[27–29] Furthermore, a few amphiphilic block copolymers from (ME3CL) as thermo-responsive hydrophilic block and various functional group conjugated PCL as hydrophobic block to improve the micellar properties.[12,30,31] The thermo-responsibility of the block copolymers was tuned by varying the composition of hydrophilic/hydrophobic units and pendent groups of the hydrophobic PCL unit. The lower critical solution temperature (LCST) of PME3CL-*b*-PME1CL (PME3CL-*b*-γ-2-[2-(2-methoxyethoxy)-ε-caprolactone (ME1CL)) could be tuned in range of 31–43 °C, by varying the ratios of PME3CL and PME1CL.[28]

Cisplatin grafted PEG-*b*-P[carboxylic acid caprolactone]s have been reported using post-polymerization chemical modification of PCL.[32,33] The self-assembly of these block copolymers achieved a cisplatin loading > 12 mol%.[32,33] He at el, synthesized a dual-responsive amphiphilic graft copolymer P(OPD-*co*-CL)-*g*-PNIPAM, poly(2-oxepane-1,5-dione-*co*-ε-caprolactone)-*g*-poly(N-isopropylacrylamide)) through post-polymerization of PCL and investigated its pH and

thermoresponsivity of this core–shell micelle assembly.[34] The acid cleavable hydrazone bond and the PNIPAM unit offer the pH-responsivity and the thermo-responsivity, respectively.

Stimuli-responsive polyesters offer great promise in the development of smart drug carriers by releasing their cargo in response to specific stimuli. The stimulus can be either endogenous and/or exogenous.[18,19] The endogenous stimuli, which is an inherent property of pathological or physiological site, include variation in pH, enzyme concentration, hormone level or redox gradients. Meanwhile, endogenous stimuli, which is applied externally, includes changes in temperature, magnetic field or light. Responding to the desired stimulus the smart polymers go through a specific protonation, a molecular conformational alternation or a hydrolytic cleavage. [18,19]

Polymeric micelles offer great promise in drug delivery application and have been extensively studied for delivering poor water-soluble drugs, such as doxorubicin, to the pathological cells. Also, these polymeric micelles help to protect the healthy cells against toxic side effects of drugs by encapsulating the drugs inside the hydrophobic core. However, the low drug loading remains an obstacle for the effective use of polymer micellar drug carriers in cancer treatment.

Herein, we developed a series of stimuli-responsive micellar drug carriers based on linear and star-like benzyl functionalized polycaprolactone, where poly(γ-benzyloxy-ε-caprolactone) (PBCL) was used as a hydrophobic block and poly{γ-2-[2-(2-methoxyethoxy)ethoxy]ethoxy-ε-caprolactone} (PMEECL) as a hydrophilic block. It was hypothesized that the star polymer could enhance the polymer properties and DOX loading capacity and efficiency, due to the higher density of the functional groups in the core forming segment allowing increased hydrophobic interactions. The effect of branching architecture on polymer properties was investigated by comparing their

CMCs, micelle sizes, thermodynamic stabilities, drug loading capacities, and thermo-induced drug release of DOX. The benzyl substituted polycaprolactone (PBCL), the hydrophobic unit, was used to develop the micellar core to encapsulate doxorubicin, a hydrophobic anti-cancer drug. Additionally, the incorporation of a benzyl functionalities along the backbone of the hydrophobic polycaprolactone block might support in enhancing the DOX loading, due to its ability of forming π-π stacking interaction with encapsulated doxorubicin.[20] The oligo (ethylene glycol) substituted polycaprolactone (PMEEECL) offers not only the hydrophilicity but also thermo-responsibility to the micelles. Thermo-responsive polymeric micelles release its encapsulated drug to the pathological cells in a controlled way upon temperature variation.

2.3   Experimental

2.3.1   Materials

All commercially available chemicals and solvents were purchased from Sigma Aldrich or Fisher Scientific and were used without further purification unless otherwise noted. Benzyl alcohol and Sn(Oct)$_2$ were purified through vacuum distillation prior to use and stored in glove box. Toluene was dried over sodium/benzophenone ketyl and freshly distilled prior to use. All polymerization reactions were conducted under purified nitrogen. The polymerization glassware and syringes were dried at 120 °C for at least 24 hours before use and cooled in a desiccator prior to use.

2.3.2 Analysis

^{1}H NMR spectra of the synthesized polymers were recorded on a 500 MHz Bruker AVANCE IIITM spectrometer at 25 °C using deuterated chloroform as the solvent. Number average molecular weights and polydispersity indices of the synthesized polymers were determined by size exclusion chromatography (SEC) using a Viscotec VE 3580 system equipped with Viscotek columns (T6000M), connected to the refractive index (RI), low angle light scattering (LALS), right angle light scattering (RALS), and viscosity detectors. HPLC grade THF was used as the eluent (1 mL min^{-1}) at 30 °C with GPC max as the sample module and triple point calibration was based on polystyrene standards. Dynamic light scattering (DLS) measurement was performed using a Malvern Zetasizer instrument using a 4 mW He–Ne laser (633 nm) and an avalanche photodiode (APD) detector. The scattered light was detected at an angle of 173° at 25 °C. The absorbance spectra were recorded using an Agilent 8453 UV-vis spectrometer. Transmittance measurements were performed using a temperature controlled Cary5000 UV-vis spectrometer equipped with temperature controlled multi-cell holders. Cytotoxicity and cellular uptake measurements were performed with a BioTek Cytation 3 cell imaging multi-mode reader. TEM images were performed on a Tecnai G2 Spirit Biotwin microscope operated at 120 keV and images were analyzed using Gatan Digital Micrograph software. Copper mesh grids were treated with 1 mg mL^{-1} polymer micelle solution for 2 minutes and staining with 2% phosphotungstic acid for 30 seconds.

2.3.3 Synthetic Procedure

Monomer Synthesis

The substituted caprolactone monomers, γ-2-[2-(2-methoxyethoxy)ethoxy] ethoxy-3-caprolactone (MEEECL) and γ-benzyl-ε-caprolactone (BCL), were prepared according to a previously reported method, as shown in Scheme 2.1.[12]

R= M1/ MEEECL

M2/ BCL
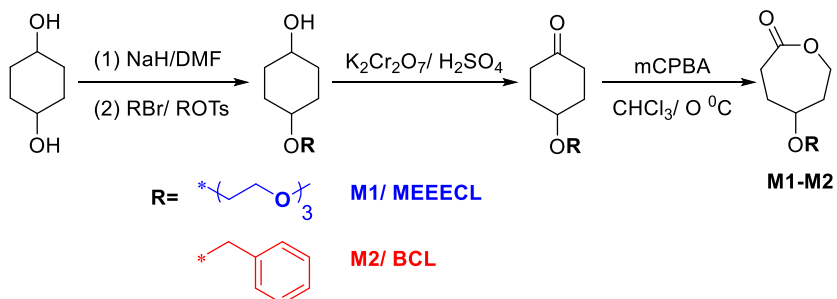
Scheme 2.1. Synthesis of Functionalized ε-caprolactone monomers, γ-benzyloxy-ε-caprolactone (M1/BCL) and γ-2-[2-(2-methoxyethoxy)ethoxy]ethoxy-ε-caprolactone(M2/ MEEECL).

Polymer Synthesis

Synthesis of Linear poly(γ-benzyloxy-ε-caprolactone)-*b*-poly{γ-2-[2-(2-methoxy-ethoxy)ethoxy]ethoxy-ε-caprolactone} (Linear PBCL-*b*-PMEEECL, Linear)

Inside a nitrogen-filled glove box, dried BCL (244 mg, 1.11×10^{-3} mol), benzyl alcohol (2.50 mg, 1.39×10^{-5} mol) and Sn(Oct)$_2$ (5.98 mg, 1.39×10^{-5} mol) in 0.4 mL dry toluene were added to an oven-dried 10 mL Schlenk flask and sealed. The reaction flask was heated in a thermostat-controlled oil bath at 110 °C. The monomer consumption was monitored using GC/MS and ^{1}H NMR. After BCL was consumed, dried MEEECL (303 mg, 1.11×10^{-3} mol) in 0.2 mL of toluene was added to the reaction flask under nitrogen and the reaction was left for 12 hours. After the MEEECL was consumed, the reaction was precipitated in cold hexane. The polymer was filtered

and dried under vacuum to yield a clear gel-like polymer (0.45g, 75.4%). ^{1}H NMR (500 MHz, CDCl$_3$): δH 1.82 (m,8H), 2.34 (m,4H), 3.37 (s,3H),3.45-3.64 (b,14H),4.15(b, 4H), 4.45 (m,2H), 7.29(b,5H). ^{1}H-NMR spectrum of the polymer is given in Figure 2.1

Similar molar composition (BCL/MEEECL at 50:50) was targeted and similar polymerization procedure was used to synthesize 4-arm poly(γ-benzyloxy-ε-caprolactone)-*b*-poly{γ-2-[2-(2-methoxy-ethoxy)ethoxy]ethoxy-ε-caprolactone} (**4-arm**, yield-62.1%, 19800 g mol^{-1}, PDI-1.32) and 6-arm poly(γ-benzyloxy-ε-caprolactone)-*b*-poly{γ-2-[2-(2-methoxy-ethoxy)ethoxy]ethoxy-ε-caprolactone} (**6-arm**, yield-69.7%, 23700 g mol^{-1}, PDI-1.66) using pentaerythritol and myo-inositol, respectively.

Molar ratios of 1:4.50:50 and 1:6.50:50 of initiator, Sn(Oct)$_2$, BCL and MEEECL were used to synthesize 4- and 6-arm polymer, respectively. ^{1}H-NMR spectra of the polymers are given in Figure 2.2 and 2.3.

2.3.4   Preparation of Empty Polymeric Micelles

Empty polymeric micelles were prepared according to the previously reported method.[30] Solvent evaporation method was used to prepare empty polymeric micelles. Briefly, the 2 mL of polymer in 2 mL of THF and added dropwise to deionized water (4 mL) with rapid stirring. The polymer was stirred vigorously in a 20 mL vial opened to the atmosphere over 3 hours. The resulting suspension was filtered using a nylon syringe filter (0.22 μm) to obtain an empty polymer micellar solution (1 mg mL^{-1}), N=6.

2.3.5 Preparation of DOX- Loaded Polymeric micelles

DOX-loaded polymeric micelles were prepared according to the previously reported method.[30] DOX· HCl was mixed with THF and neutralized with 3 equivalents of triethylamine. Polymer (4 mg) in THF (2 mL) and mixed with the neutralized DOX solution at a weight ratio of 5:1. The solution of polymer/DOX in THF was added dropwise to deionized water (4 mL) with rapid stirring, and THF was evaporated. The DOX-loaded micelle suspension was filtered with a nylon syringe filter (0.22 μm) to remove the non-encapsulated drug. The final concentration of the DOX-loaded micelles was 1 mg mL^{-1}, N=6.

2.3.6 Determination of Drug-Loading Capacity and Drug-Loading Efficiency

Spectrometric technique was used to determine the drug-loading capacity (wt% DLC) and drug-loading efficiency (wt% DLE). 1 mL of DOX-Loaded polymeric micelle solution was mixed with DMSO in a 1:1 volume ratio and the DOX concentration was determined by measuring absorbance at 485 nm. The weight of the drug entrapped in the micelles was determined by a calibration curve of DOX in DMSO/DI H$_2$O at 485 nm.

The DLC and DLE of dox-loaded micelles were calculated using following equations:

$$wt\% \, DLC = \frac{Weight \, t \, of \, encapuslated \, drug}{Weight \, of \, the \, polymer \, added} \times 100$$

$$wt\% \, DLE = \frac{Weight \, of \, encapuslated \, drug}{Weight \, of \, the \, drug \, added} \times 100$$

2.3.7   Determination of LCST

3 mg of polymer was dissolved in 10 mL of deionized water to prepare a 0.3 wt% polymer suspension. At 600 nm, the %transmittance was measured using a UV-vis spectrophotometer equipped with temperature controlled multi-cell holders by gradually heating the polymer suspension. The point of 50% drop in transmittance was taken as LCST of the polymer solution.

2.3.8   Critical Micelle Concentration (CMC) Measurements

CMC of the polymer was determined by fluorescence technique using pyrene as the fluorescence probe. [29,30] Briefly, a series of polymer samples with various concentrations were prepared and mixed with 6.0×10^{-5} M pyrene in THF. Each polymer/pyrene solutions were added dropwise into deionized water (10 mL) to obtain a final polymer concentration of 1×10^{-5} to 1 gL^{-1}. The resulting solutions were stirred for 4 hours to evaporate THF. At 25 °C, the fluorescence spectra of each samples were recorded on a fluorescence spectrometer using the emission wavelength of 390 nm. The first inflection point on a plot of the intensity ratio of the pyrene excitation peaks at 337.5 and 334.5 nm against the logarithm of the copolymer concentration (C) of the samples was taken to be the CMC.

2.3.9   Hydrodynamic Diameter and Size Distribution

Hydrodynamic diameters (Dh) and size distribution of the empty and the DOX-loaded micelles were determined by dynamic light scattering (DLS). Solutions of empty and DOX-loaded micelles (1 mg mL^{-1}) were prepared as mentioned above and the measurements were recorded at 25 °C, N=3.

2.3.10 *In Vitro* DOX Release

DOX-loaded polymer micellar solutions (1 mg mL^{-1}) were prepared as mentioned above. Polymer micellar solution (4 mL) was added to Snakeskin dialysis bag (3500 Da molecular weight cutoff) and immersed in 10 mL of PBS (pH 7.4). 2 mL of aliquots were withdrawn at 0, 4, 8, 12, 24 and 48 hours and were replaced with the equal volume of PBS (pH 7.4). The aliquots withdrawn were mixed with DMSO in a volume ratio of 1:1 and the UV-Vis spectra were measured. The amount of DOX release was calculated using a calibration plot of free DOX in DMSO/DI mixture (volume ratio of 1:1). (N=3).

2.3.11 Biological Studies

HeLa cells were grown on RPMI-1640 medium with L-glutamine and sodium bicarbonate supplemented with 10% FBS and 1% penicillin-Streptomycin. The cells were grown at 37 °C in a humidified atmosphere with the addition of 5% CO_2.

2.3.12 Cytotoxicity Studies

Cytotoxicity studies were performed according to the previously reported method.[30] Cell viability was assessed in HeLa cell line. HeLa cells were seeded (5000 cells/well) in 96-well plates with 100 μL of growth medium. The HeLa cells were incubated at 37 °C in a humidified atmosphere with 5% CO_2 for 24 hours for attachment. After the cells were adhered, the medium was removed, washed 100 μL of PBS, and replaced with 100 μL of fresh growth medium. Post attachment cells were treated with 100 μL of pH 7.4 phosphate buffer (control); Solutions of empty micelles, DOX-loaded micelles and free DOX were prepared in PBS at a series of concentrations

and added to the cells and incubated at 37 °C for another 24 hours. After 24 hours, cytotoxicity evaluation was done using CellTiter Blue assay.

2.3.13 Cellular Uptake Studies

Cellular uptake studies were performed according to the previously reported method.[30] HeLa cells were grown in a 35 mm glass bottom imaging dishes (250 000 cells/ dish) with 2 mL of growth media and incubated in a humidified atmosphere with 5% CO_2 for 24 hours at 37 °C. After 24 hours, the cell culture medium was removed, the cells were washed with 2 mL of PBS, replaced with 2 mL of growth medium and 1 mL of the DOX-loaded micelles (0.25 mg mL^{-1}) prepared in PBS and incubated for 4 hours at 37 °C in a humidified atmosphere with 5% CO_2. After 4 hours of incubation, the cells were washed with fresh PBS (3×2 mL, pH 7.4). The cells were fixed with 4% paraformaldehyde, washed with PBS (3×2 mL), and the nuclei were counterstained with DAPI. Images were recorded using a BioTek Cytation3 Cell Imaging Multi-Mode Reader.

2.3.14 IC$_{50}$ determination:

The IC$_{50}$, the drug concentration at 50% growth inhibition, was determined by dose-response curve. Mean % cell viability (N=12) over a concentration range was plotted using the Software GraphPad PRISM and the IC$_{50}$ value was assessed using regression analysis of the PRISM program.

2.3.15 Statistical Analysis

The mean and standard deviation (SD) were determined for all *in-vitro* data and expressed as the mean ± standard deviation (mean±SD). One-way analysis of variance (one-way ANOVA) was

performed using Microsoft Office to evaluate the differences between experimental groups. Statistical significance was assumed at $P<0.01$. Multi-factor analysis of variance (Multi-factor ANOVA) was performed using Minitab 2018.

2.4 Results and Discussion

2.4.1   Block copolymer synthesis

In a previous study from our group, a series of linear substituted polycaprolactone-based amphiphilic diblock copolymers were reported and their micellar properties such as size, thermodynamic stability, thermo responsivity and drug loading capacity were investigated.[12] Further studies have been continued to improve the drug loading capacity and stability, focusing on star-like substituted and unsubstituted polycaprolactone-based block copolymers. Micelles obtained from 4-arm PEEECL-*b*- PCL and 4- and 6-arm PEEECL-*b*-PECL diblock copolymers showed drug loading capacities of 1.14 wt% 2.06 wt% and 2.63 wt%, respectively.[21,22] The DOX loading content of the star-like copolymers was shown to be higher than their corresponding linear polymer, PEEECL-*b*-PCL (0.77 wt%) and PEEECL-*b*-PECL (2.05 wt %). [21,22]

In this report, the synthesis of linear and star-like poly(γ-benzyloxy-ε-caprolactone)-*b*-poly{γ-2-[2-(2-methoxyethoxy)ethoxy]ethoxy-ε-caprolactone} (PBCL-*b*-PMEEECL) were reported. To understand the effects of polymer architecture on drug loading capacity, stability and size of the polymeric micelles, two star-like block copolymers were used that are 4-arm and 6-arm PBCL-*b*-PMEEECL. To synthesize linear and star-like PBCL-*b*-PMEEECL polymers, tin-catalyzed ring opening polymerization was carried out using the benzyl alcohol and multifunctional alcohols as initiators, respectively. Briefly, coordination-insertion ring opening polymerization of BCL were

28

carried out at 110 °C to generate the hydrophobic segment. Upon complete consumption of BCL, the second monomer, MEEECL, was added to generate the hydrophilic block. According to the previously reported literature, linear PBCL-*b*-PMEEECL was synthesized using benzyl alcohol as initiator, while 4-armed pentaerythritol and 6-armed myo-inositol, multifunctional initiators, were used to synthesize 4- and 6- arm PBCL-*b*-PMEEECL, respectively. The synthesis of the polymers is presented in Scheme 2.2 and ^{1}H NMR spectra are given in Figure 2.1, 2.2 and 2.3.
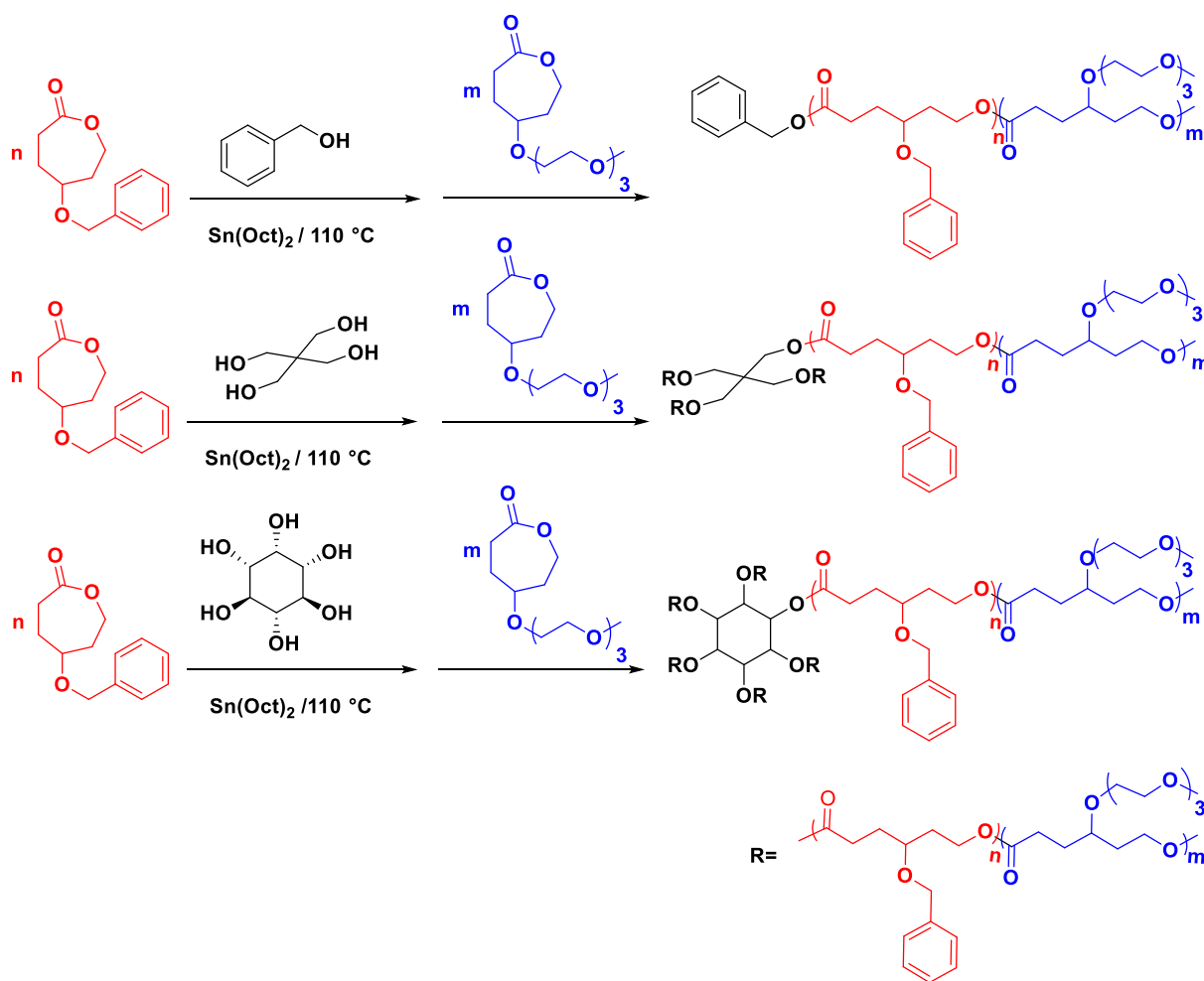
Scheme 2.2. Synthesis of linear, 4- arm and 6-arm PBCL-b-PMEEECL amphiphilic block copolymers.
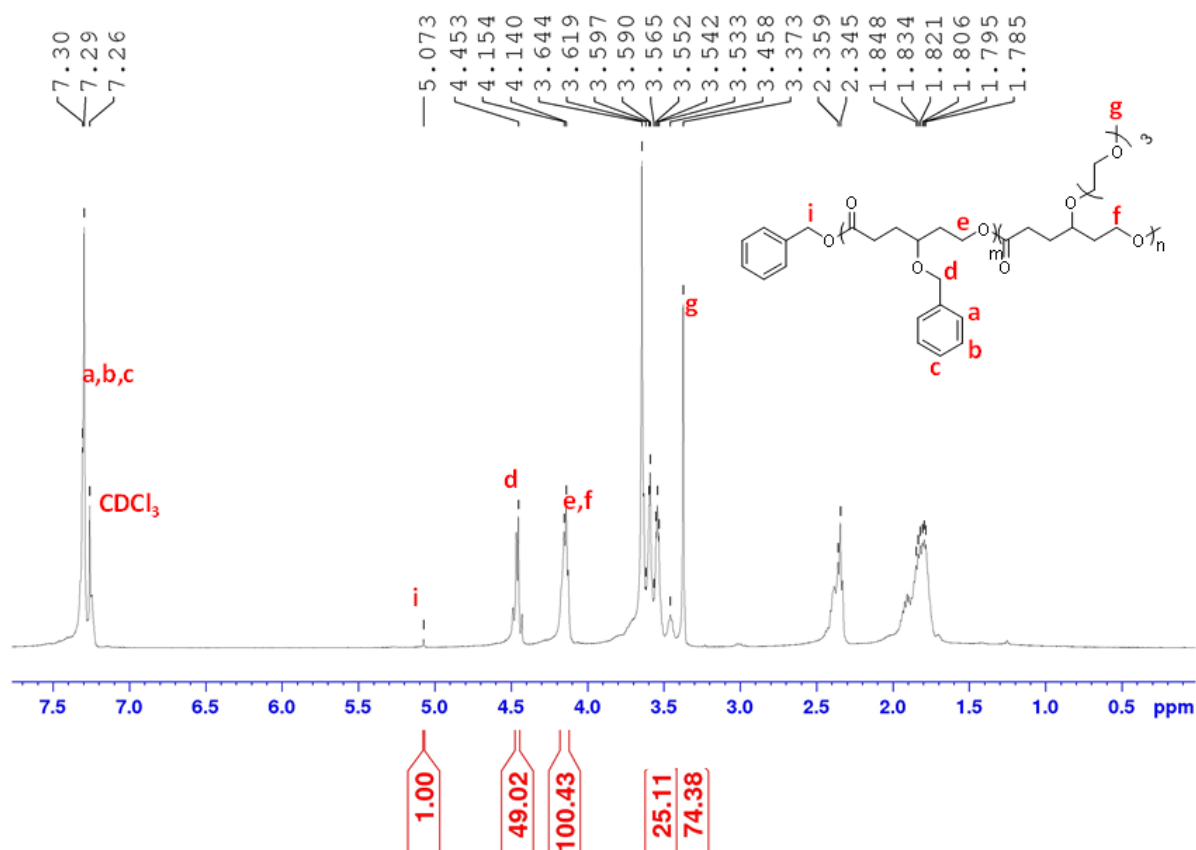
Figure 2.1. ¹H NMR spectrum of linear poly(γ-benzyloxy-ε-caprolactone)-*b*-poly{γ-2-[2-(2-methoxyethoxy)ethoxy]ethoxy-ε-caprolactone} (Linear PBCL-*b*-PMEEECL).

Similar molar composition (BCL/MEEECL at 50:50) was targeted and similar polymerization procedure was used to synthesize 4-arm poly(γ-benzyloxy-ε-caprolactone)-*b*-poly{γ-2-[2-(2-methoxy-ethoxy)ethoxy]ethoxy-ε-caprolactone} **(4-arm)** and 6-arm poly(γ-benzyloxy-ε-caprolactone)-*b*-poly{γ-2-[2-(2-methoxy-ethoxy)ethoxy]ethoxy- ε -caprolactone} **(6-arm)** using pentaerythritol and myo-inositol, respectively. Molar ratios of 1:4.50:50 and 1:6.50:50 of initiator, Sn(Oct)₂, BCL and MEEECL were used to synthesize 4- and 6-arm polymer, respectively.
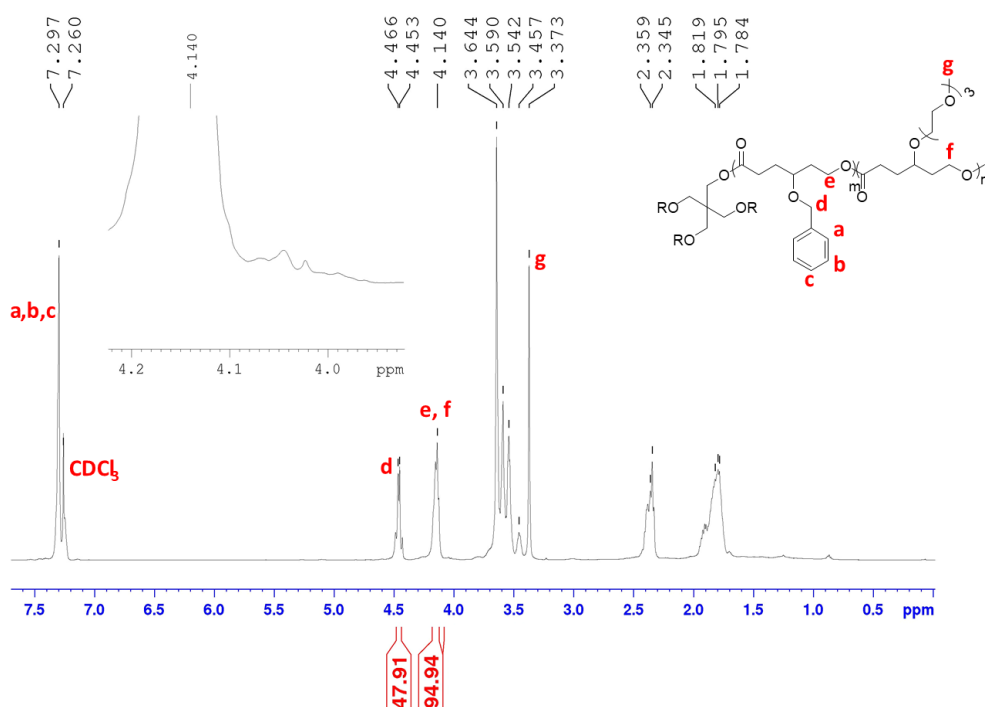
Figure 2.2. ¹H NMR spectrum of 4-arm poly(γ-benzyloxy-ε-caprolactone)-*b*-poly{γ-2-[2-(2-methoxyethoxy)ethoxy]ethoxy-ε-caprolactone} (4-arm PBCL-*b*-PMEEECL).
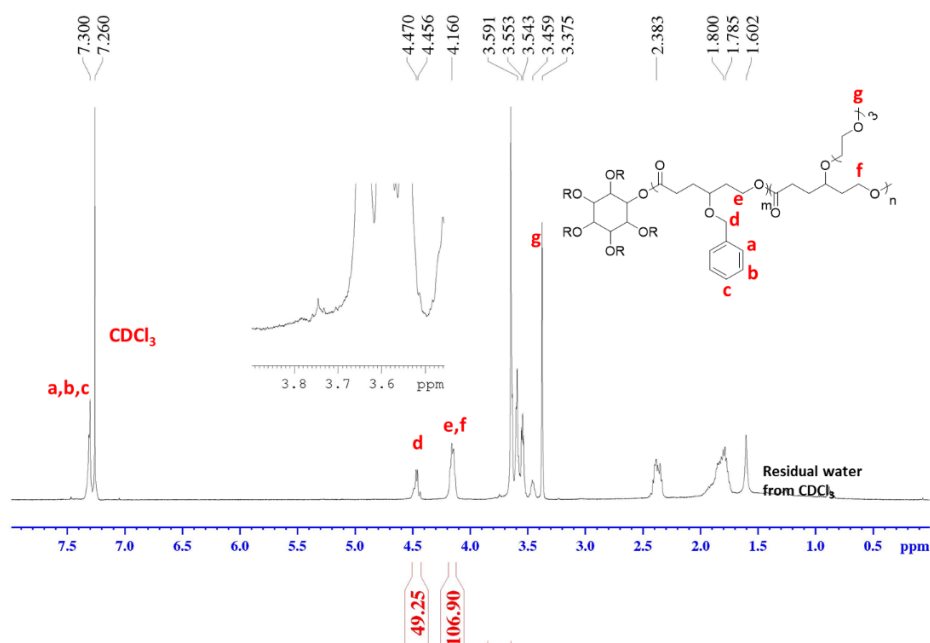
Figure 2.3. ¹H NMR spectrum of 6-arm poly(γ-benzyloxy-ε-caprolactone)-*b*-poly{γ-2-[2-(2-methoxyethoxy)ethoxy]ethoxy-ε-caprolactone} (6-arm PBCL-*b*-PMEEECL).

Block copolymers with 50 mol % PMEEECL and 50 mol% PBCL units were targeted to achieve a comparable molecular weight in all three amphiphilic block copolymers. The molecular weight and molar compositions of all three polymers are shown in Table 2.1. The results confirm that the synthesized polymers have comparable molar compositions.

Table 2.1. Summary of block copolymer compositions and molecular weight

	M_n^a (g mol^{-1})	PDI	Mol % BCL[b]	Mol % MEEECL[b]
Linear	26300	1.27	49.0	51.0
4-arm	19800	1.32	47.9	52.1
6-arm	23700	1.66	49.2	50.8

[a] Calculated from size exclusion chromatography. [b] Calculated from by ^{1}H NMR spectroscopy.

The Size Exclusion Chromatography (SEC) traces obtained for all three polymers exhibit monomodal distributions, demonstrating the development of block copolymers with the addition of the second caprolactone monomer, MEEECL (Figure 2.4).
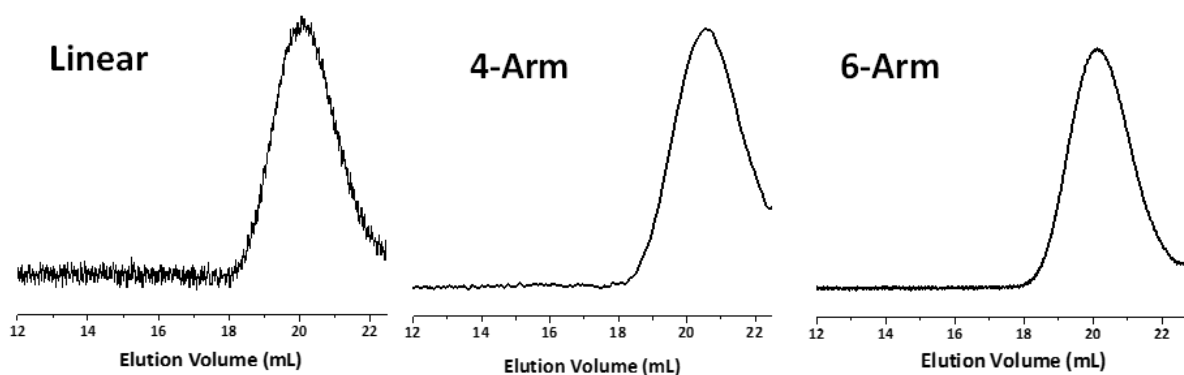
Figure 2.4. SEC trace of Linear, 4-arm and 6-arm PBCL-*b*-PMEEECL.

2.4.2 Self-assembly and Thermo-responsibility of Block copolymers

The amphiphilic diblock copolymers self-assembled into micelles in aqueous media above the critical micellar concentration (CMC). The solvent-polarity dependent fluorescent of the pyrene probe is used to study the CMC values of the amphiphilic block copolymers.[23,24] The pyrene excitation spectrum displays a peak shift (from 334.5 nm to 337.5 nm), when the environmental polarity changes, from hydrophilic to hydrophobic.[12,23] The ratio of intensities of the peaks ($I_{337.5}/I_{334.5}$) were obtained to determine the CMC values. The CMC value of the linear polymeric micelles, 1.23×10^{-3} gL^{-1}, was comparable with previously reported values.[12] The 4- and 6- arm polymeric micelles reach CMC values of 2.70×10^{-4} gL^{-1} and 9.19×10^{-5} gL^{-1}, respectively.

The CMC value is a key factor to determine the thermodynamic stability of micelles, the lower the CMC value, the better the thermodynamic stability. In comparison with the linear polymer, significantly lower CMC values were obtained for 4- and 6-arm amphiphilic block copolymers indicating that the star-like polymeric micelles have improved thermodynamic stability. Higher density of benzyl functionality in the hydrophobic core enhances the intermolecular and intramolecular hydrophobic−hydrophobic interaction. The resultant interaction increases the thermodynamic stability of the micelles.

A thermo-responsiveness was expected for PBCL-*b*-PMEEECL copolymers due to the presence of PMEEECL block, which was reported as a thermo-responsive unit.[12] At room temperature, thermoresponsive polymer is soluble in water, which forms a clear solution. However, a phase transition happens upon heating the polymer solution, which forms a cloudy solution the dehydration and precipitation of the polymer. Thermosensitive copolymer, PBCL-*b*-PMEEECL, undergo reversible phase transitions in response to temperature variation.
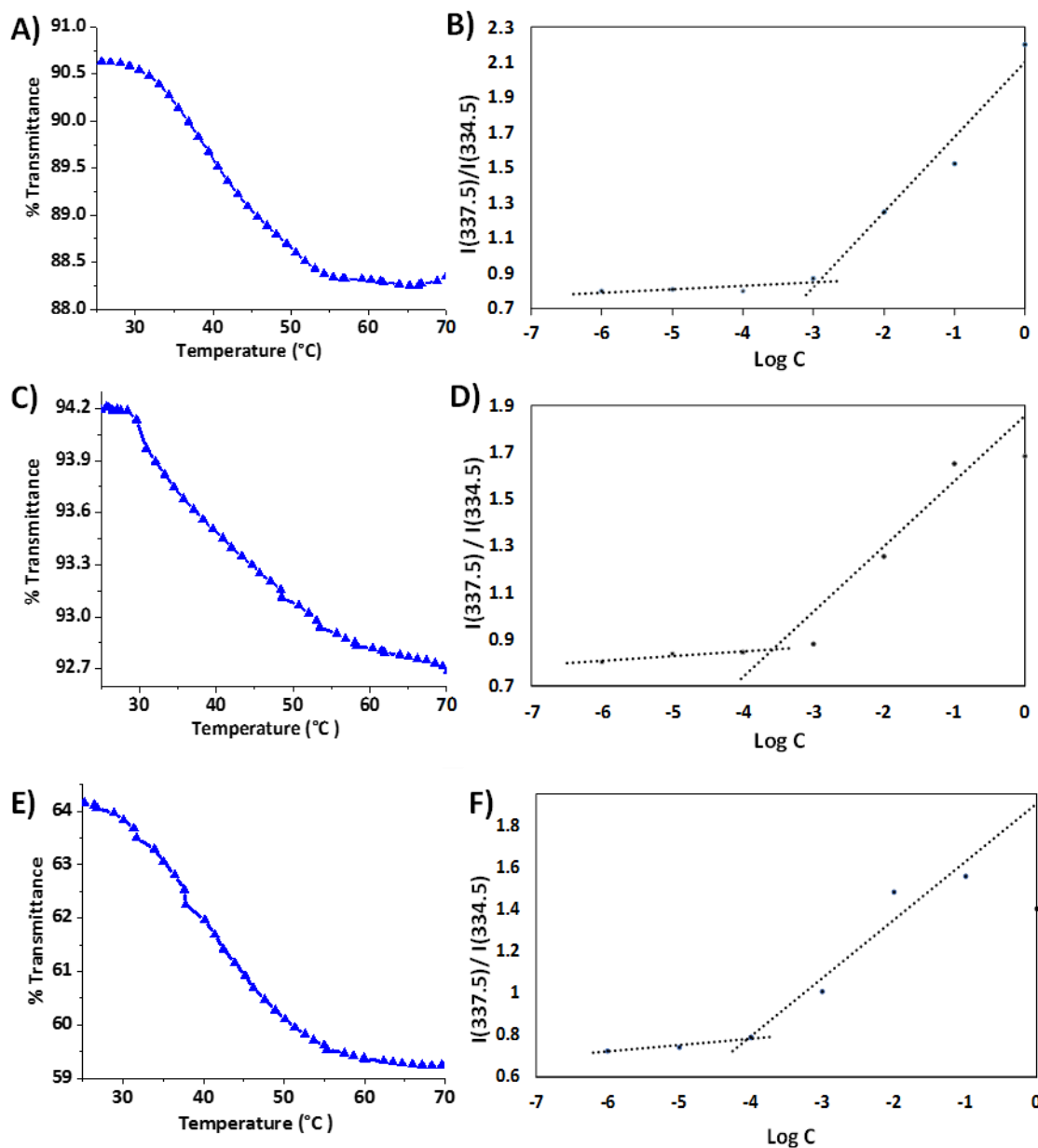
Figure 2.5. Determination of LCST and CMC of block copolymers; Linear (A, B), 4-arm (C, D) and 6-arm (E, F) polymers, respectively.

The temperature-dependent transmittance of the thermoresponsive polymer was used to determine the lower critical solution temperature (LCST). When the polymer solution was heated above its LCST, a drop-in transmittance was observed. The LCST was taken at the point at which

50% drop in transmittance (the midpoint between the maximum %T and minimum %T) was observed (Figure 2.5). A sharp transition in transmittance was observed in all three polymers. Theses polymers displayed a comparable LCST due the incorporation of comparable mol% of PMEEECL unit in the block copolymer. The polymers displayed LCSTs in the range of 40-42 °C (Table 2.2) and are in the useful range for *in vivo* drug delivery applications. At physiological temperature (37 °C), drug-loaded polymeric micelles circulate in the bloodstream in a highly stable form. The drug release, however, can occur is expected by applying an external temperature above its LCST value.

2.4.3   Size and morphology of micelles

Dynamic light scattering (DLS) was employed to evaluate the hydrodynamic diameter (Dh) and polydispersity of the self-assembled polymeric micelles. The hydrodynamic diameter of empty micelles prepared from linear, 4-arm and 6-arm were about 144 nm, 85 nm, and 52 nm respectively, with micelle dispersity indices of 0.095, 0.101, 0.114 (Figure 2.6, Table 2.2). The results showed that the size of the micelles obtained from star-like polymers were much smaller as compared to those formed from linear polymeric micelles. TEM analysis was performed to study the morphology of the polymer micelles. The TEM images confirms that the polymers self-assemble into spherical micelles in aqueous medium and the sizes of the micelles estimated from TEM analysis were comparable to the micelle sizes determined by DLS.
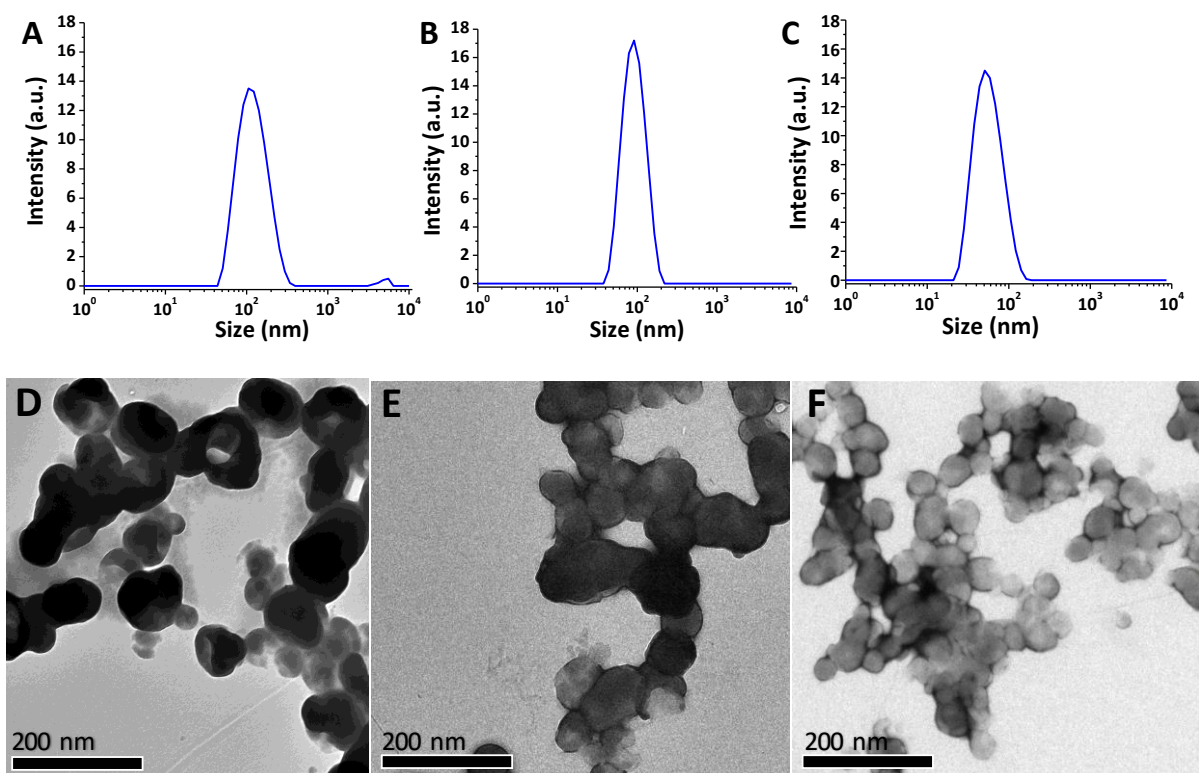
Figure 2.6. Size distribution (Dh) and TEM images obtained for empty polymer micelles; Linear (A, D), 4-arm (B, E), and 6-arm (C, F), respectively.

Table 2.2. Summary of DOX-loaded polymer micelle properties

Polymer	CMC[a] (g L^{-1})	LCST[b] (°C)	Dh[c] (nm)	Size dispersity
Linear	1.23×10^{-3}	40.29	108.2±1.6	0.194±1.6
4-arm	2.70×10^{-4}	40.80	85.30±0.7	0.101±0.05
6-arm	9.19×10^{-5}	41.20	52.14±0.3	0.114±0.02

[a] Determined with UV-vis spectroscopy at 485 nm. [b] Hydrodynamic diameter and [d] size dispersity of DOX- loaded polymer micelles determined from DLS, at 25 °C.

2.4.4 Doxorubicin encapsulation

Previously reported linear PMEEECL-b-PBCL copolymer achieved 2.35 wt% doxorubicin (DOX) loading, where polymer: DOX feed weight ratio of 10:1 was used.[25] To further enhance the drug loading capacity, polymer: DOX feed weight ratio of 5:1 was targeted. As can be seen from Table 2.3 and Figure 2.7, the drug loading capacities (DLC) and encapsulation efficiencies (EE) were significantly higher in 4- and 6-arm star-like polymers than linear polymer micelles. This considerable improvement was attributed to the higher density of benzyl substituent in the core-forming segment of the star polymers. Also, the incorporation of the aromatic ring substituent increases drug loading compared to that of nonaromatic substituent, due to the π-π stacking formed between the aromatic groups of the encapsulated drug molecules and the core unit.
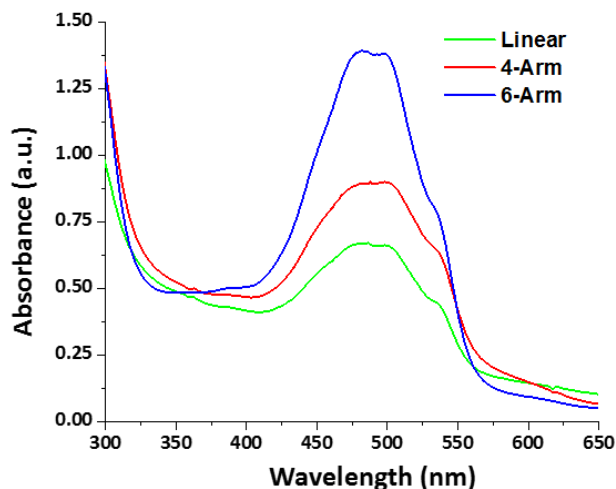
Figure 2.7. Absorbance spectra of DOX-loaded polymer micelles.

The micelle sizes were determined after dox loading and are summarized in Figure 2.8 and Table 2.3. the DOX-micelles exhibited narrow poly dispersity, indicating the formation of uniform micelles. The DOX-loaded micelles showed hydrodynamic diameters larger than the size the empty micelles, due to the encapsulation of DOX. The dox micelles still retained its size within

the range appropriate for passive targeting using the EPR effect. Polymeric micelle drug carriers with size range from 10 to 200 nm prevents elimination in kidneys and allows for accumulation in cancer cells via enhanced permeation and retention (EPR) effect. [26–28]
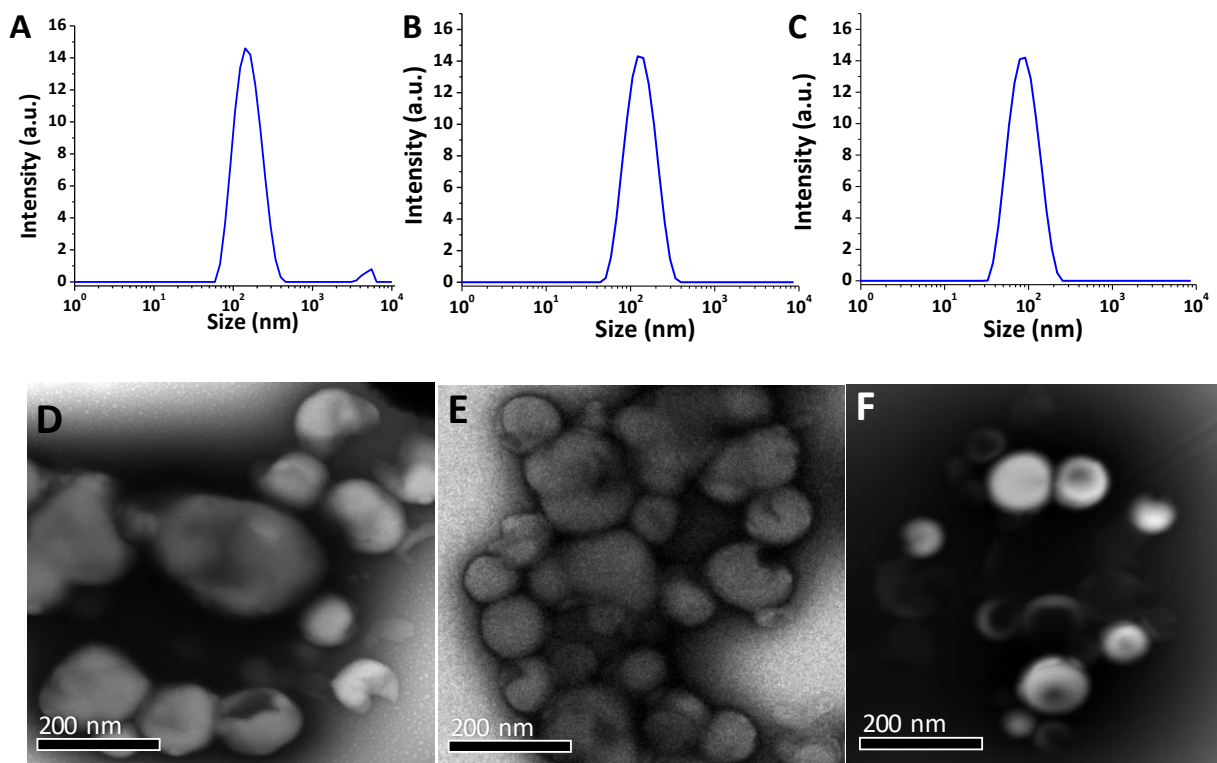
Figure 2.8. Size distribution (Dh) and TEM images (scale bar=200 nm) obtained for DOX-loaded polymer micelles; Linear (A, D), 4-arm (B, E), and 6-arm (C, F), respectively.

Table 2.3. Summary of DOX-loaded polymer micelle properties

Polymer	DLC[a] (wt%)	EE[a] (wt%)	Dh^{DOX} [b] (nm)	Size dispersity[b]
Linear	5.14±0.93	25.70±4.64	145.4± 1.0	0.18±0.06
4-arm	8.21±0.39	41.06±1.95	114.4 ± 2.6	0.14±0.01
6-arm	12.58±0.72	62.90±3.60	81.56 ± 0.7	0.13±0.03

[a] Determined with UV-vis spectroscopy at 485 nm. [b] Hydrodynamic diameter and [d] size dispersity of DOX- loaded polymer micelles determined from DLS, at 25 °C.

2.4.5 *In-vitro* DOX Release

Cumulative DOX release studies were performed using DOX-loaded linear, 4-arm and 6-arm polymer micelles in PBS (pH 7.4). The samples were incubated at physiological temperature (37 °C) and temperature above LCST (42 °C), separately. As shown in Figure 2.9, all three polymer micelles showed significantly higher DOX release at 42 °C compared to that of release at 37 °C. This confirms that at temperature above LCST, the micellar shell is deformed and faster DOX release is achieved. DOX release of ~56% for linear polymer micelles was obtained at 42 °C, which is shown to be higher than 4-arm (47%) and 6-arm polymer micelles (44 %) at 42 °C. The higher density of the benzyl groups in the star-like polymer micellar core resulted in enhanced π-π interaction between the benzyl groups of the polymer backbone and the aromatic group of the DOX. The enhanced interaction diminishes the DOX release from the star-like polymer micelles compared to linear polymer micelles.
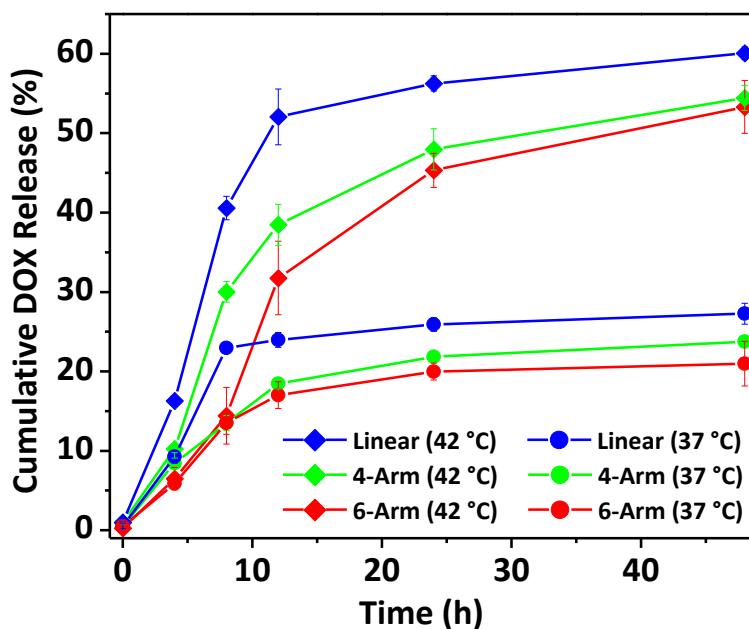
Figure 2.9. In-vitro DOX release for the DOX-loaded linear, 4-arm and 6-arm polymer micelles at 37 °C and 42 °C in PBS.

2.4.6 *In-vitro* Cytotoxicity and Cellular Uptake of DOX Loaded micelles

The cytotoxicity effect of DOX-loaded polymeric micelles compared to that of free DOX and empty polymeric micelles was determined using HeLa cell lines as model tumor cells (Figure 2.10). To test the cytotoxic effect of polymer alone, the HeLa cells were treated with the empty polymeric micelles (the micelles without DOX encapsulation) and incubated for 24 hours. It was observed no obvious cytotoxicity against HeLa cells and confirms that the polymer alone was ineffective in killing cancer cells in-vitro at all tested concentrations.
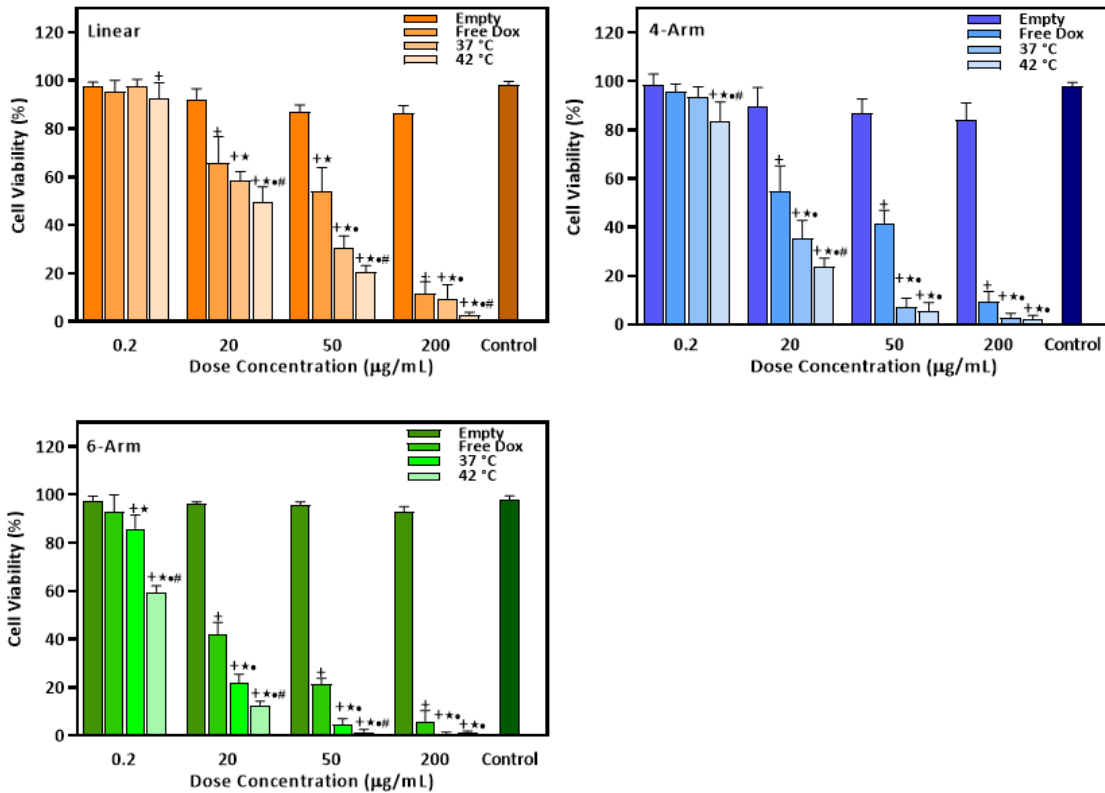
Figure 2.10. Effect of empty micelles, free DOX and DOX-loaded micelles on viability of HeLa cells.

Data is expressed as mean ± SE and three independent experiments made in twelve replicates. $+p < 0.01$, significant differences of empty micelles, free DOX, DOX-loaded micelles (37 °C) and DOX-loaded micelles (42 °C) vs control (Cells only); ★$p < 0.01$, significant differences of free DOX, DOX-loaded micelles (37 °C) and DOX-loaded micelles (42 °C) vs empty micelles; •$p < 0.01$, significant differences of DOX-loaded micelles (37 °C) and DOX-loaded micelles (42 °C) vs free DOX; #$p < 0.01$

40

The cytotoxicity of DOX-loaded polymeric micelles were tested in HeLa cells at various concentrations. The results showed that the DOX-loaded 6-arm micelles were highly toxic to tumor cells compared to other two DOX-loaded polymer micelles, due to the higher DOX loading capacity obtained for the 6-arm polymeric micelles. The effect of temperature-dependent release of DOX on HeLa cells was studied at both at physiological temperature (37 °C) and at a temperature above the LCST of the polymer (42 °C). HeLa cells were treated with DOX-loaded polymeric micelles and incubated for 24 hours at 37 °C and 42 °C, separately. At all the tested concentrations, the incubation of DOX-loaded micelles with HeLa cells at 42 °C significantly increased the cytotoxicity of DOX-loaded micelles against HeLa cells compared to those incubated at physiological temperature (37 °C), as shown in Figure 2.10. This confirms the higher drug release at temperature above LCST of the polymers (42 °C).

IC_{50} values of DOX-loaded micelles against HeLa cells were determined at 37 °C and 42 °C and results were shown in Figure 2.11 and Table 2.4. IC_{50} values of the DOX- loaded linear, 4-arm and 6-arm micelles from the dose−response curve were 20.18, 8.19, and 6.96 µg/mL, respectively at 37 °C. By contrast, the IC_{50} values were 18.98, 3.24, 0.39 µg/ml for DOX-loaded linear, 4-arm and 6-arm micelles, respectively, at 42 °C. According to the results, the IC_{50} values of DOX-loaded linear, 4-arm and 6-arm micelles against HeLa cells at 37 °C were approximately 1.1-, 2.5- and 17.8-fold, respectively, higher than the IC_{50} value of the corresponding DOX-loaded polymers incubated at 42 °C. Moreover, the IC_{50} values of DOX-loaded linear, 4-arm and 6-arm micelles against HeLa cells at 37 °C were nearly 2.2-, 5.5- and 6.5-fold, respectively, lower than the IC_{50} value of the previously reported benzyl substituted PCL-*b*-PEG micelles (45.0 µg/mL). [24]
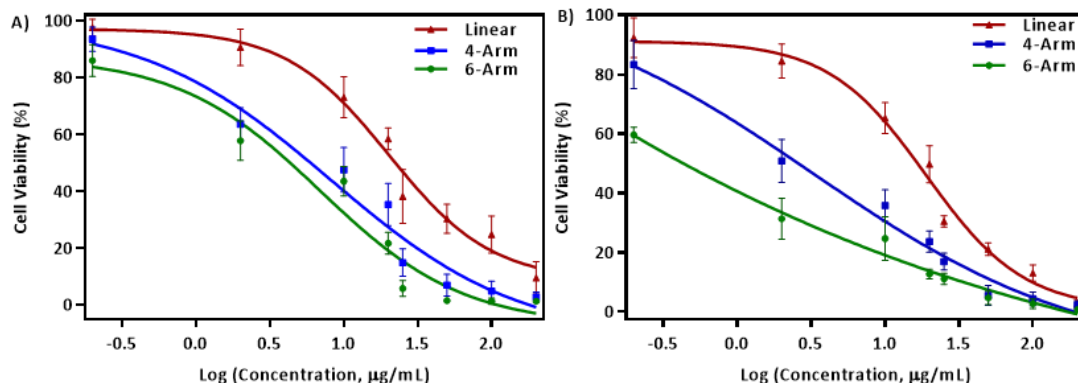
Figure 2.11. Dose response curve for the DOX loaded polymeric micelles at A) 37 °C, and b) 42 °C, respectively.

Table 2.4. IC $_{50}$ values of DOX-loaded polymer micelles

Polymer	IC$_{50}$ at 37 °C (µg/mL)	IC$_{50}$ at 42 °C (µg/mL)
Linear	20.18 ± 0.04	18.98 ± 0.02
4-arm	8.19 ± 0.07	3.24 ± 0.05
6-arm	6.96 ± 0.05	0.39 ± 0.03

The IC$_{50}$ values for DOX-loaded polymeric micelles were determined against HeLa cell line are means of twelve independent experiments, (n=12, mean $\pm$ SD).

The DOX-loaded micelles have higher cytotoxicity against HeLa cells when incubated at temperature above LCST, as evidenced by its low IC$_{50}$. This improved antitumor activity was an outcome of the enhanced drug release at temperatures above LCST, as mentioned previously. At both temperatures, the IC$_{50}$ values of DOX-loaded 6-arm polymeric micelles against HeLa cells were significantly lower than that for DOX-loaded linear and 4- arm polymeric micelles. This lower IC$_{50}$ values is due to the increased cytotoxicity and enhanced cellular uptake by tumor cells. The DOX-loaded micelles have higher cytotoxicity against HeLa cells when incubated at temperature above LCST, as evidenced by its low IC$_{50}$. This improved antitumor activity was an

outcome of the enhanced drug release at temperatures above LCST, as mentioned previously in this chapter.

The *in-vitro* accumulation of DOX-Loaded micelles in HeLa cells were evaluated by taking benefit of the DOX fluorescence. After incubation of HeLa cells with DOX-Loaded micelles for 4 hours, the cell nuclei were counterstained with DAPI and imaged. Figure 2.12 illustrates the results of DOX-loaded micelles utilizing DAPI stain with HeLa cells for visualization of cell nuclei. The stronger red fluorescence in the nuclei was observed in the tumor cells that was co-cultured with the DOX loaded polymeric micelles. This may be due to the delivery of the DOX loaded micelles into the cells due to the endocytosis.
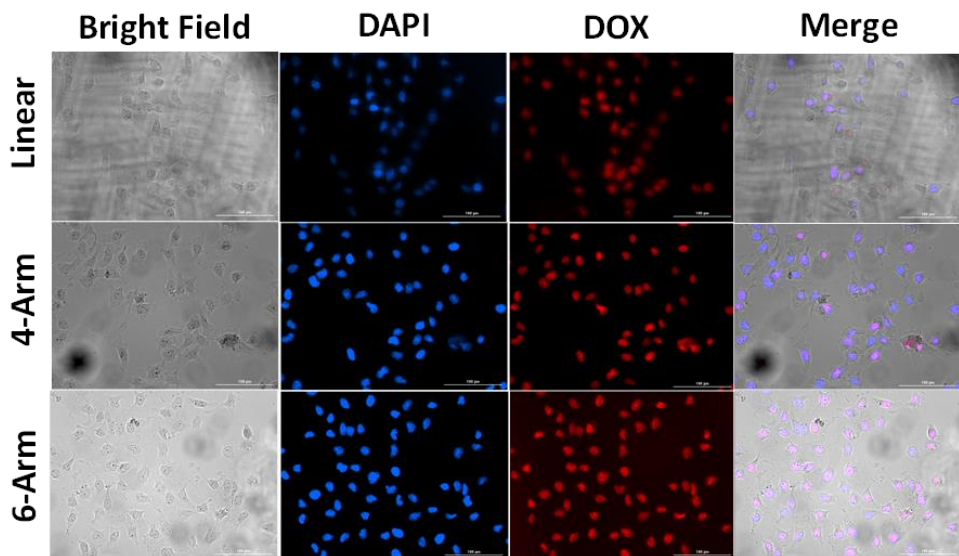
Figure 2.12. Cellular uptake of DOX-loaded polymeric micelles by HeLa cells, (scale bar= 100 µm).

2.4.7 Statistical Analysis

The ANOVA was setup with twelve repetitions per condition selected. Three polymer types at eight different concentration levels and two temperature levels were used in the analysis and

cytotoxicity was measured as the dependent variable. Experiment design is summarized in the Table 2.5.

….. Collected data were analyzed using MiniTab 2018 with a confidence level of 95%. ANOVA results are shown in Table 2.5. The ANOVA model consisted of number of polymer arms, temperature and concentration as the independent variables. The p value for all three variables is less than 0.05. Therefore, it can be concluded that there is a significant difference in % cell viability due to number of polymer arms, temperature and concentration, independently.

Table 2.5. Summary of ANOVA experiment setup and results

Factor Information

Factor	Type	Levels	Values
Polymer Arm	Fixed	3	1, 4, 6
Temperature	Fixed	2	37, 42
Concentration	Fixed	8	0.2, 2.0, 10.0, 20.0, 25.0, 50.0, 100.0, 200.0

Analysis of Variance

Source	DF	Adj SS	Adj MS	F-Value	P-Value
Polymer Arm	2	67721	33860.3	524.29	0.000
Temperature	1	8773	8773.4	135.85	0.000
Concentration	7	431897	61699.6	955.35	0.000
Error	565	36490	64.6		
Lack-of-Fit	37	23959	647.5	27.29	0.000
Pure Error	528	12531	23.7		
Total	575	544881			

Model Summary

S	R-sq	R-sq(adj)	R-sq(pred)
8.03639	93.30%	93.18%	93.04%

Further, the model summary results (Table 2.5) shows that 93.04% of the effects can be modelled via the selected independent variables. Main Effect Plots from multi-factor ANOVA is shown in Figure 2.13(A) and interaction plots are shown in Figure 2.13 (B).
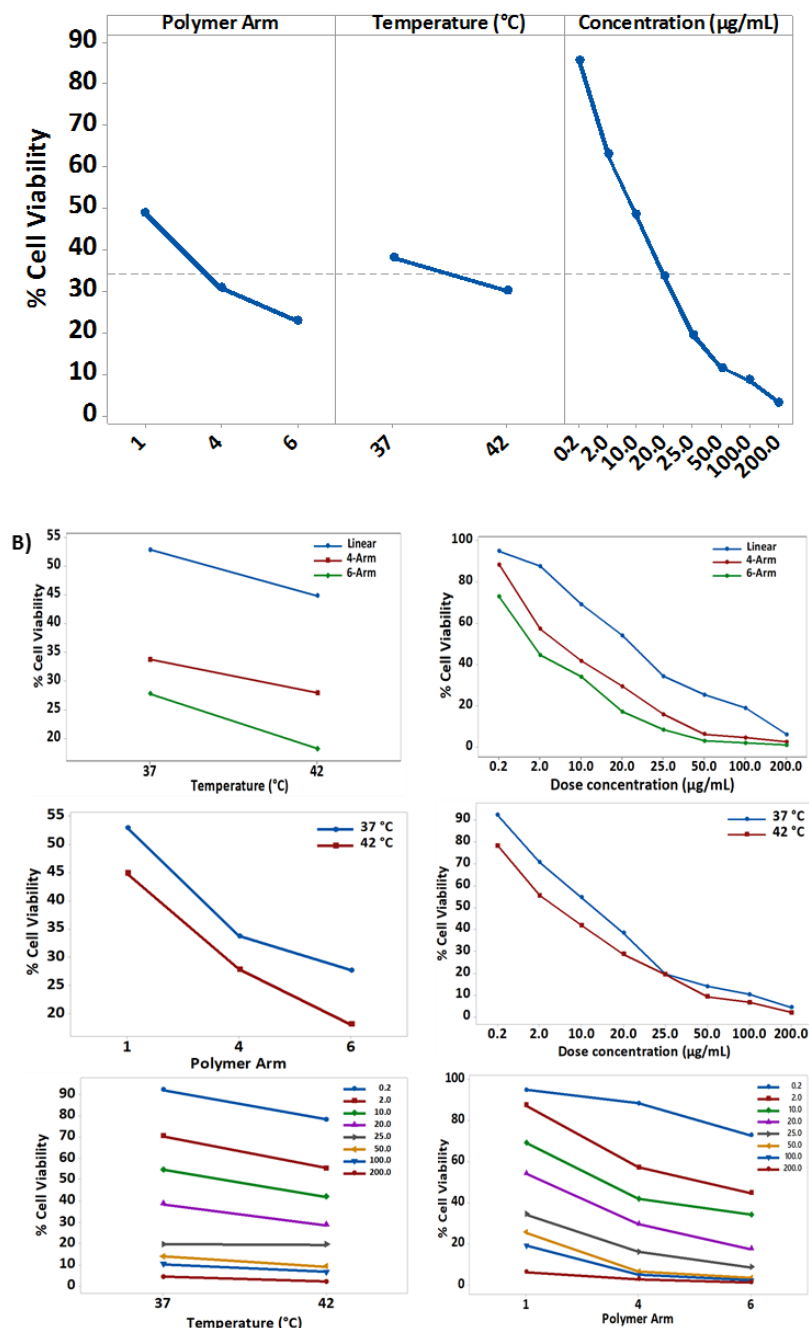
Figure 2.13. A) Main effect plot and B) interaction plot for the polymer arm, temperature and dose concentration on the % cell viability of HeLa cells.

Main effects plot clearly shows that all three independent variables are contributing towards the reduction in mean % Cell viability (i.e. higher concentration, higher number of polymer arms, higher temperature). Furthermore, the main effects plot show that the concentration has a greater effect on the mean of % cell viability followed by number of polymer arms. Temperature has less effect on mean % cell viability compared to the other two independent variables. The interaction plot shows that there is no noticeable interaction between the three variables. Further the interaction plot supports the conclusions made from the main effect plots.

2.5 Conclusions

Considering the polymer architecture, the star-like polymer-based micelles showed significant improvement in size reduction, stability and drug loading due to the higher density of functionality in the core. Comparatively, the 6-arm copolymer structure enables the development of thermodynamically more stable and compact micelles with enhanced doxorubicin encapsulation. Remarkably, the DOX-loaded polymeric micelles exhibited superiority of cytotoxicity in HeLa cells against free DOX. This study suggests that compared to linear micellar drug carrier, the star-like polymer micellar drug carrier with the enhanced doxorubicin encapsulation are promising drug carriers in effective cancer treatment.

2.6 References

1. Chandra, R., Rustgi, R. Prog. Polym. Sci., 1998, 23, 1273–1335.

2. Nair, L. S., Laurencin, C. T. Prog. Polym. Sci., 2007, 32, 762–798.

3. Albertsson, A.-C., Varma, I. K. In Degradable Aliphatic Polyesters Springer Berlin Heidelberg, Berlin, Heidelberg 2002; pp. 1–40.

4. Vert, M. Biomacromolecules, 2005, 6, 538–546.

5. Zia, K. M., Noreen, A., Zuber, M., Tabasum, S., Mujahid, M. Int. J. Biol. Macromol., 2016, 82, 1028–1040.

6. Dash, T. K., Konkimalla, V. B. J. Control. Release, 2012, 158, 15–33.

7. Dash, T. K., Konkimalla, V. B. Mol. Pharm., 2012, 9, 2365–2379.

8. Oh, J. K. Soft Matter, 2011, 7, 5096–5108.

9. Katz, J. S., Eisenbrown, K. A., Johnston, E. D., Kamat, N. P., Rawson, J., Therien, M. J., Burdick, J. A., Hammer, D. A. Soft Matter, 2012, 8, 10853–10862.

10. Chang, L., Deng, L., Wang, W., Lv, Z., Hu, F., Dong, A., Zhang, J. Biomacromolecules, 2012, 13, 3301–3310.

11. Surnar, B., Jayakannan, M. Biomacromolecules, 2013, 14, 4377–4387.

12. Hao, J., Cheng, Y., Ranatunga, R. J. K. U., Senevirathne, S., Biewer, M. C., Nielsen, S. O., Wang, Q., Stefan, M. C. Macromolecules, 2013, 46, 4829–4838.

13. Chen, W., Zou, Y., Jia, J., Meng, F., Cheng, R., Deng, C., Feijen, J., Zhong, Z. Macromolecules, 2013, 46, 699–707.

14. Mahmud, A., Patel, S., Molavi, O., Choi, P., Samuel, J., Lavasanifar, A. Biomacromolecules, 2009, 10, 471–478.

15. Senevirathne, S. A., Washington, K. E., Miller, J. B., Biewer, M. C., Oupicky, D., Siegwart, D. J., Stefan, M. C. J. Mater. Chem. B, 2017, 5, 2106–2114.

16. Hao, J., A. Rainbolt, E., Washington, K., C. Biewer, M., Stefan, M. Curr. Org. Chem., 2013, Accepted.

17. Habnouni, S. El, Darcos, V., Coudane, J. Macromol. Rapid Commun., 30, 165–169.

18. Truong, T. T., Thai, S. H., Nguyen, H. T., Vuong, V.-D., Nguyen, L.-T. T. J. Polym. Sci. Part A Polym. Chem., 55, 928–939.

19. Washington, K. E., Kularatne, R. N., Biewer, M. C., Stefan, M. C. ACS Biomater. Sci. Eng., 2018, 4, 997–1004.

20. Cheng, Y., Hao, J., Lee, L. A., Biewer, M. C., Wang, Q., Stefan, M. C. Biomacromolecules, 2012, 13, 2163–2173

21. Hao, J., Granowski, P. C., Stefan, M. C. Macromol. Rapid Commun., 33, 1294–1299.

22. Shahin, M., Lavasanifar, A. Int. J. Pharm., 2010, 389, 213–222.

23. Senevirathne, S. A., Boonsith, S., Oupicky, D., Biewer, M. C., Stefan, M. C. Polym. Chem., 2015, 6, 2386–2389.

24. Kularatne, R. N., Washington, K. E., Bulumulla, C., Calubaquib, E. L., Biewer, M. C., Oupicky, D., Stefan, M. C. Biomacromolecules, 2018, 19, 1082–1089.

25. Xiong, X.-B., Mahmud, A., Uluda\ug, H., Lavasanifar, A. Pharm. Res., 2008, 25, 2555–2566.

26. Xiong, X.-B., Ma, Z., Lai, R., Lavasanifar, A. Biomaterials, 2010, 31, 757–768.

27. Rainbolt, E. A., Miller, J. B., Washington, K. E., Senevirathne, S. A., Biewer, M. C., Siegwart, D. J., Stefan, M. C. J. Mater. Chem. B, 2015.

28. Rainbolt, E. A., Washington, K. E., Biewer, M. C., Stefan, M. C. J. Mater. Chem. B, 2013, 1, 6532–6537.

29. Hao, J., Cheng, Y., Ranatunga, R. J. K. U., Senevirathne, S., Biewer, M. C., Nielsen, S. O., Wang, Q., Stefan, M. C. Macromolecules, 2013, 46, 4829–4838.

30. Washington, K. E., Kularatne, R. N., Du, J., Ren, Y., Gillings, M. J., Geng, C. X., Biewer, M. C., Stefan, M. C. J. Mater. Chem. B, 2017.

31. Washington, K. E., Kularatne, R. N., Du, J., Gillings, M. J., Webb, J. C., Doan, N. C., Biewer, M. C., Stefan, M. C. J. Polymer Sci. Part A Polym. Chem., 2016, 54, 3601–3608.

32. Surnar, B., Subash, P. P., Jayakannan, M. Zeitschrift für Anorg. und Allg. Chemie, 640, 1119–1126.

33. Shahin, M., Safaei-Nikouei, N., Lavasanifar, A. J. Drug Target., 2014, 22, 629–637.

34. He, Y., Zhang, Y., Xiao, Y., Lang, M. Colloids Surfaces B Biointerfaces, 2010, 80, 145–154.

35. Mura, S., Nicolas, J., Couvreur, P. Nat. Mater., 2013.

36. Liu, D., Yang, F., Xiong, F., Gu, N. Theranostics, 2016.

37. Shi, Y., van Steenbergen, M. J., Teunissen, E. A., Novo, L., Gradmann, S., Baldus, M., van Nostrum, C. F., Hennink, W. E. Biomacromolecules, 2013, 14, 1826–1837.

38. Kalyanasundaram, K., Thomas, J. K. J. Phys. Chem., 1977, 81, 2176–2180.

39. Aguiar, J., Carpena, P., Molina-Bolívar, J. A., Ruiz, C. C. J. Colloid Interface Sci., 2003, 258, 116–122

40. Wang, H., Xu, F., Wang, Y., Liu, X., Jin, Q., Xu, J.-P. Polym. Chem., 2013, 4, 3012–3019.

41. Sano, K., Nakajima, T., Choyke, P. L., Kobayashi, H. ACS Nano, 2013, 7, 717–724.

42. Ahmad, Z., Shah, A., Siddiq, M., Kraatz, H.-B. RSC Adv., 2014, 4, 17028–17038.

43. Hao, J., Servello, J., Sista, P., Biewer, M. C., Stefan, M. C. J. Mater. Chem., 2011.

44. Ray, G. B., Chakraborty, I., Moulik, S. P. J. Colloid Interface Sci., 2006, 294, 248–254.

CHAPTER 3

STAR POLYMER MICELLAR SYSTEM FOR CO-DELIVERY OF DOXORUBICIN AND RESVERATROL

3.1 Abstract

Active clinical application of doxorubicin (DOX) is limited by DOX-resistance in tumor cells and serious toxicity to normal tissues caused by off-target DOX delivery. The use of a polymeric micellar drug delivery system has shown potential for enhanced drug delivery at the tumor site. Additionally, the co-delivery of drugs with synergistic therapeutic effect has become the emerging strategy to treat drug resistant tumors. In this work we aimed at reporting; (1) preparation of DOX- and resveratrol (RSV) co-encapsulated polymeric micelles formulated with linear and 6-arm star-like copolymer poly(γ-benzyloxy-ε-caprolactone)-*b*-poly{γ-2-[2-(2-methoxy-ethoxy)ethoxy]ethoxy-ε-caprolactone(PBCL-*b*-PMEEECL); (2) improvement in the DOX-loading capacity and DOX-loading efficiency by the co-encapsulation, due to the interaction between DOX and RSV; (3) enhanced cytotoxic effect to tumor cells *in-vitro* due to the higher DOX encapsulation of co-encapsulated polymeric micelles. The co-delivery of DOX and RSV using polymeric micelles has resulted in increased drug-loading and enhanced cytotoxic effect. The developed multi-drug loaded micellar drug delivery system has potential benefits in cancer therapy by minimizing associated toxic side effects and expands the therapeutic window.

3.2 Introduction

Doxorubicin (DOX), an anthracycline antibiotic, is a Food and Drug Administration (FDA)-approved chemotherapeutic drug with a wide spectrum of antitumor activity.[1] It has been

recognized as a potent anti-cancer drug and used to treat a wide range of tumor types including Hodgkin's and non-Hodgkin's lymphoma, lung, ovarian, breast, pediatric, gastric, thyroid, and sarcoma cancers. [2,3] However, the development of dose-limited toxicity and DOX- resistance result in treatment failure and limit the therapeutic efficacy. Considering these major drawbacks, significant effort has been made on developing alternative approaches for efficient DOX delivery for successful cancer treatment.

The non-specific site delivery of DOX results in serious multidirectional cytotoxic effects to the normal tissues including kidney, liver and brain tissues; resulting in the major adverse effect of cardiomyopathy. [4,5,6] Many researches have been conducted to minimize the toxic side effects, focusing on delivery of doxorubicin using site-specific drug delivery systems such as macromolecular conjugation,[7–9] liposomes,[10-12] polymersomes,[13–15] polymer micelles,[16,17,26–29,18–25] nanoparticles[30-32] and hydrogels. [33–35] The emergence of these nano-carriers provides the potential to securely encapsulate and deliver doxorubicin specifically at the tumor sites through enhanced permeation and retention (EPR) effect or by active targeting that reduce the toxic side effects to the healthy cells.[32]

DOX-resistance exists in wide range of tumor types due to the over-expression of ATP-binding cassette (ABC), a protein super-family, on the tumor cell membrane.[12,36,37] The main function of ABC transporters is active transport of a wide variety of compounds, including complex lipids, simple ions, and xenobiotics, across the cell membrane.[38] P-glycoprotein (P-gp), multidrug resistance protein 1 (MRP-1) and breast cancer resistance protein (BCRP) are mainly associated with the drug resistance in tumor cells.[36,39] In tumor cells, drug-resistant proteins recognize the rapid internalization of anti-cancer drugs and move them out of the cells.[38]

In recent years, many strategies have been proposed to avoid DOX resistance and thereby enhance the therapeutic efficiency of DOX (Figure 3.1.). One of the methods includes co-administration of DOX. The delivery of DOX with another chemotherapeutic drug which has different antitumor mechanism.[40–43] One example of these drugs is Resveratrol (RSV), a plant-derived polyphenol anti-cancer drug (Figure 3.1.).[44] When co-administrated with DOX, RSV hinders P-gp activity and thereby enhances the intracellular accumulation of the DOX. Furthermore, recent studies show that RSV is associated with the reduction of doxorubicin induce cardiac toxicity and fibrosis.[45,46] However, RSV has poor bioavailability and water solubility, rapid metabolism and short plasma half life time in human.[47–49] Therefore, using free DOX along with free RSV cannot be considered as an effective method for cancer treatment. This challenge has been overcome by co-loading DOX and RSV in a nanocarrier, which enables simultaneous delivery of DOX and RSV into the same tumor cells.

Doxorubicin   **Resveratrol**
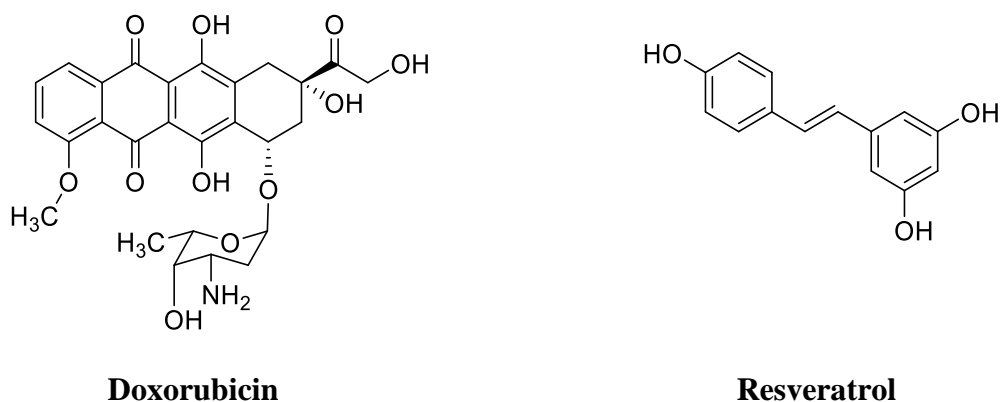
Figure 3.1. Chemical structures of drugs used.

In the previous chapter, we reported the synthesis and characterization of thermoresponsive linear and star-like amphiphilic diblock copolymer using poly(γ-benzyloxy-ε-caprolactone)-*b*-poly{γ-2-[2-(2-methoxy-ethoxy)ethoxy]ethoxy-ε-caprolactone(PBCL-*b*-PMEEECL). A significant

increase in DOX-loading capacity and cytotoxicity effect against HeLa cells was achieved using 6-arm star-like (PBCL-*b*-PMEEECL). In this study, DOX and RSV were co-encapsulated in linear and 6-arm star-like (PBCL-*b*-PMEEECL) polymeric micelles to further increase the drug loading capacity, due to interaction between DOX and RSV. The anti-tumor activity of DOX and RSV-loaded polymer micelles on HeLa cells were investigated in-vitro. An increase in the concentration of DOX and RSV in tumor cells were expected, due to the higher drug loading capacity.

3.3 Experimental

3.3.1   Materials

Commercially available chemicals and solvents were purchased from Sigma Aldrich or Fisher Scientific and were used without further purification unless otherwise noted. Benzyl alcohol and Sn(Oct)$_2$ were purified by high vacuum distillation before use and stored in glove box. Toluene were dried over sodium/benzophenone ketyl and freshly distilled prior to use. Polymerization reactions were performed under purified nitrogen. The polymerization glassware and syringes were dried at 120 °C for at least 24 hours and cooled in a desiccator before use.

3.3.2   Analysis

^{1}H NMR spectra of the polymers were recorded on a 500 MHz Bruker AVANCE IIITM spectrometer at 25 °C using deuterated chloroform as the solvent. Number average molecular weights and polydispersity indices of the synthesized polymers were determined by size exclusion chromatography (SEC) using a Viscotec VE 3580 system equipped with Viscotek columns (T6000M), connected to the refractive index (RI), low angle light scattering (LALS), right angle

light scattering (RALS), and viscosity detectors. HPLC grade THF was used as the eluent (1 mL min^{-1}) at 30 °C with GPC max as the sample module and triple point calibration with polystyrene standards. Dynamic light scattering (DLS) measurement was performed using a Malvern Zetasizer instrument using a 4 mW He–Ne laser (633 nm) and an avalanche photodiode (APD) detector. The scattered light was detected at an angle of 173° at 25 °C. The absorbance spectra were recorded using an Agilent 8453 UV-vis spectrometer. Transmittance measurements were performed using a temperature controlled Cary5000 UV-vis spectrometer equipped with temperature controlled multi-cell holders. Cytotoxicity and cellular uptake analysis were performed with a BioTek Cytation 3 cell imaging multi-mode reader. TEM images were performed on a Tecnai G2 Spirit Biotwin microscope operated at 120 keV. The TEM images were examined using Gatan Digital Micrograph software. Copper mesh grids were treated with 1 mg mL^{-1} polymer micelle solution for 2 minutes and staining with 2% phosphotungstic acid for 30 seconds.

3.3.3 Preparation of Empty Polymeric Micelles

Empty polymeric micelles were prepared according to the previously reported method.[28] Empty polymeric micelles were obtained using solvent evaporation technique. 6 mg of polymer was dissolved in THF (3 mL) to prepare a 2 mg mL^{-1} polymer solution and added dropwise to deionized water (6 mL) with rapid stirring. THF was evaporated by vigorous stirring for 3 hours. After 3 hours, resulted suspension was filtered using a nylon syringe filter (0.22 μm) to get an empty polymer micelle solution. The concentration of the final empty polymer micelle solution was 1 mg mL^{-1}.

3.3.4 Preparation of DOX- Loaded Polymeric micelles

DOX, RSV and combination of DOX and RSV-loaded polymeric micelles were prepared according to the previously reported method.[28] Briefly, DOX **.** HCl was mixed with THF and neutralized with 3 equivalents of triethylamine to prepare a 1 mg mL^{-1} stock DOX solution. RSV was dissolved in THF to prepare a 1 mg mL^{-1} of RSV stock solution. 6 mL of polymer in THF (2 mg mL^{-1}) was mixed with appropriate molar ratios of DOX and RSV stock solution. The polymer/drug solution was added drop wise to deionized water (6 mL) with rapid stirring, and THF was evaporated by vigorous stirring. The resulting solution was filtered using a nylon syringe filter (0.22 μm) to remove the non-encapsulated drug. The concentration of the final drug-loaded polymer micelle solution was 1 mg mL^{-1}.

3.3.5 Hydrodynamic Diameter and Size Distribution

Hydrodynamic diameters (Dh) and size distribution of the empty and the drug-loaded micelles were determined by dynamic light scattering (DLS). Solutions of empty and drug-loaded micelles (1 mg mL^{-1}) were prepared as mentioned above and the measurements were recorded at 25 °C, N=3.

3.3.6 *In Vitro* DOX Release

DOX-and RSV-loaded polymer micellar solutions (1 mg mL^{-1}) were prepared as mentioned above. Drug-loaded polymer micellar solution (4 mL) was added to Snakeskin dialysis bag (3500 Da molecular weight cutoff) and immersed in 10 mL of PBS (pH 7.4). An aliquot (2 mL) were withdrawn at 0, 4, 8, 12, 24 and 48 hours and were replaced with the equal volume of PBS (pH 7.4). The aliquots withdrawn were mixed with DMSO in a volume ratio of 1:1 and the UV-Vis

spectra were obtained. The amount of DOX release was analyzed by a calibration plot for free DOX and RSV in DMSO/DI mixture (volume ratio of 1:1). (N=3).

3.3.7   Biological Studies

HeLa cells were grown in Dulbecco's Modified Eagle's medium (DMEM) containing 10% fetal bovine serum (FBS) and 1% penicillin-Streptomycin. The cells were incubated at 37 °C in a humidified atmosphere with the addition of 5% CO_2.

3.3.8   Cytotoxicity Studies for Empty polymeric micelles

Cytotoxicity assay was performed according to the previously reported method.[28] A cell density of 5000 cells/well were grown onto 96-well plates with 100 µL of DMEM growth medium and incubated for 24 hours at 37 °C in an atmosphere that contained 5% CO_2. After the cells were adhered in 24 hours, growth medium was removed from the cells and washed with 100 µL of fresh PBS. Empty micellar stock solution with a concentration of 1 mg mL^{-1} was diluted with PBS to prepare a series of empty micelles with different concentration. 100 µL of empty polymer micelle solutions and 100 µL of growth medium were added to each well and incubated for another 24 hours at 37 °C. After 24 hours of incubation, the cell viability assay was evaluated by the CellTiter-Blue assay according to the protocol recommended by manufacture (N = 12).

3.3.9   Cytotoxicity Studies for Drug-loaded polymeric micelles

Cytotoxicity assay was performed according to the previously reported method.[28] A cell density of 5000 cells/ well were grown onto 96-well plates with 100 mL of DMEM growth

medium and incubated for 24 hours at 37°C in an atmosphere that contained 5% CO_2. After the cells were adhered in 24 hours, medium was removed from the wells and the cells were washed with 100 µL of PBS (pH 7.4). DOX-loaded micelle stock solution (1 mg mL$^{-1)}$ was diluted with PBS to prepare concentrations ranging from 0.02 to 0.2 mg mL^{-1}. 100 µL of empty polymer micelle solutions added to each well along with 100 µL of growth medium and incubated for another 24 hours at 37 °C. After 24 hours of incubation, the cell viability assay was evaluated by the CellTiter-Blue assay according to the protocol recommended by manufacture (N = 12).

The above procedure was repeated for RSV-loaded, combination of DOX and RSV-loaded micelles with a range of concentration.

3.3.10 Cytotoxicity Studies for Free drugs

Cytotoxicity assay was performed according to the previously reported method.[28] The amounts needed to prepare the stock solutions of free DOX, free RSV and combination free DOX and RSV were calculated according to the DLCs of DOX-, RSV- and combination of DOX and RSV- loaded of micelles, respectively. The sample dilution was done by diluting the stock solutions with PBS, matching the concentration of corresponding drug-loaded polymeric micelles. Cytotoxicity assay of free drug was performed, according to the above described procedure. The cell viability assay was evaluated by the CellTiter-Blue assay according to the protocol recommended by manufacture (N = 12).

3.3.11 Cellular Uptake Studies

Cellular uptake study was performed according to the previously reported method.[28] A cell density of 250 000 HeLa cells were seeded in 35 mm clear bottom imaging dishes along with 2 mL growth media and incubated for 24 hours at 37 °C in a humidified atmosphere with 5% CO_2. After cells were adhered in 24 hours, 1 mL of DOX and RSV-loaded micelles in PBS (0.25 mg mL^{-1}) was added to each well along with fresh growth media (2 mL) and incubated for 2 hours at 37 °C. After 2 hours, the growth media was removed from the wells, cells were washed with PBS (3×2 mL, pH 7.4) and fixed with 4% freshly prepared paraformaldehyde (1 mL) and incubated for 10 min at room temperature. After incubation, the cells were washed with PBS (3×2 mL) and treated with 1 mL of Triton X-100. The treated cells incubated at room temperature for 2 min. After 2 minutes, the cells were washed with PBS (4×2 mL), and the nucleus were counterstained with DAPI. Cell were imaged with a BioTek Cytation3 Cell Imaging Multi-Mode Reader. The fluorescence of DOX and RSV were imaged using 590 nm and 528 nm emission filters, respectively.

3.3.12 IC$_{50}$ determination

The IC$_{50}$, the drug concentration at 50% growth inhibition, of combination of DOX and RSV-loaded polymer micelles was determined by dose-response curve. Mean %cell viability (N=12) over a concentration range (0.2, 2.0, 10.0, 20.0, 25.0, 50.0, 100.0, 200.0 µg/mL) was plotted using the Software GraphPad PRISM and the IC$_{50}$ value was assessed using regression analysis of the PRISM program.

3.3.13 Statistical Analysis

The mean and standard deviation (SD) were determined for all *in-vitro* data and expressed as the mean ± standard deviation. One-way analysis of variance (one-way ANOVA) was performed using Microsoft Office to evaluate the differences between experimental groups and p Value of less than 0.01 was considered as statistically significant. Multi-factor analysis of variance (Multi-factor ANOVA) was performed using Minitab 2018.

3.4 Results and Discussion

3.4.1 Block copolymer synthesis

In our previous chapter, linear and star-like (4-arm and 6-arm) thermo-responsive benzyl substituted polycaprolactone-based amphiphilic diblock copolymers, PBCL-*b*-PMEEECL, were reported and their micellar properties such as size, thermodynamic stability, thermo responsivity, and drug loading capacity were investigated. *In-vitro* biological studies were done to investigate the DOX-loaded polymer micellar cytotoxicity against HeLa cells and micelle uptake by HeLa cells.

As the previous report in the chapter 2, micelles obtained from linear, 4-arm and 6-arm PBCL-*b*-PMEEECL diblock copolymers showed drug loading capacities of 5.14 wt% 8.21 wt% and 12.58 wt%, respectively. The DOX loading content of the star-like copolymers was shown to be higher than their corresponding linear polymer, PBCL-*b*- PMEEECL.

In this report, further improvement in the drug loading has been expected in the linear and star-like PBCL-*b*-PMEEECL using combination drug loading strategy. The synthesis of linear and star-like poly(γ-benzyloxy-ε-caprolactone)-*b*-poly{γ-2-[2-(2-methoxyethoxy)ethoxy]ethoxy-ε-

caprolactone} (PBCL-*b*-PMEEECL), polymer properties and micellar properties were reported in Chapter 2. The synthesis and properties of the polymers are presented in Scheme 3.1 and Table 3.1. The drug loading capacities of linear and 6-arm PBCL-*b*-PMEEECL and micellar properties were compared.
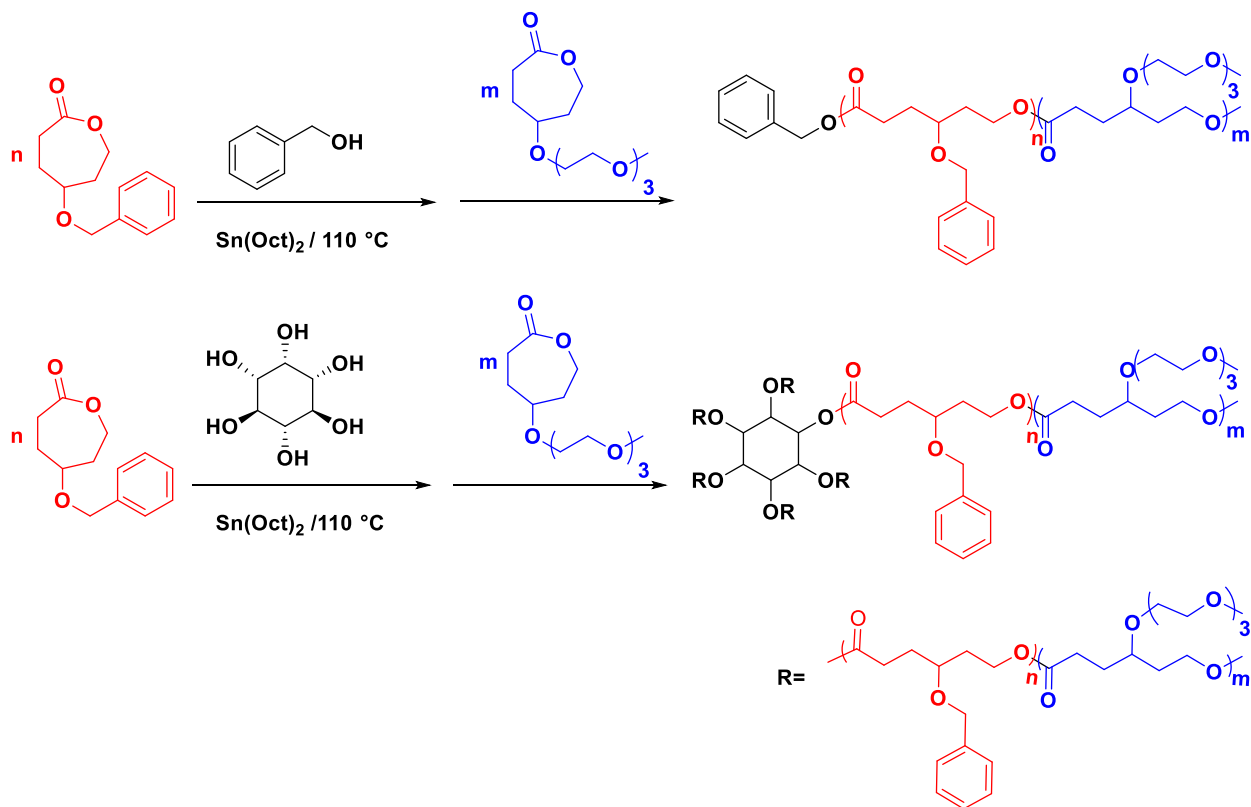
Scheme 3.1. Synthesis of linear and 6-arm PBCL-*b*-PMEEECL amphiphilic block copolymers.

Table 3.1. Summary of block copolymer compositions and molecular weight

	M_n^a (g mol^{-1})	PDI	Mol % BCL[b]	Mol % MEEECL[b]
Linear	26300	1.27	49.0	51.0
6-arm	23700	1.66	46.1	53.9

[a] Calculated from size exclusion chromatography. [b] Calculated from by ^{1}H NMR spectroscopy.

60

3.4.2 Thermo-responsivity of the polymer

As discussed in chapter 2, the linear and 6-arm PBCL-*b*-PMEEECL show thermoresponsivess, due to the incorporation of thermoresponsive PMEEECL block.[17,19,23–25,28,29] At room temperature, linear and 6-arm PBCL-*b*-PMEEECL dissolve in water to form a clear solution. Upon heating, PBCL-*b*-PMEEECL precipitates out from the solution to form a cloudy solution. Change in transmittance occurs with increasing temperature, due to the phase transition. The change in % transmittance *vs* temperature was plotted. The temperature where 50% drop in transmittance was observed was used as the LCST point. The linear and 6-arm polymers showing LCST of 40.3 °C and 41.2 °C, respectively (Figure 3.2). The mol% of PMEEECL incorporated in the linear and 6-arm polymers were comparable, therefore the LCSTs of polymers were comparable. The range of 40-42 °C is useful for *in vivo* drug delivery applications. At physiological temperature (37 °C) the encapsulated drugs are not released. When an external temperature above its LCST value is applied, the encapsulated drugs are released.
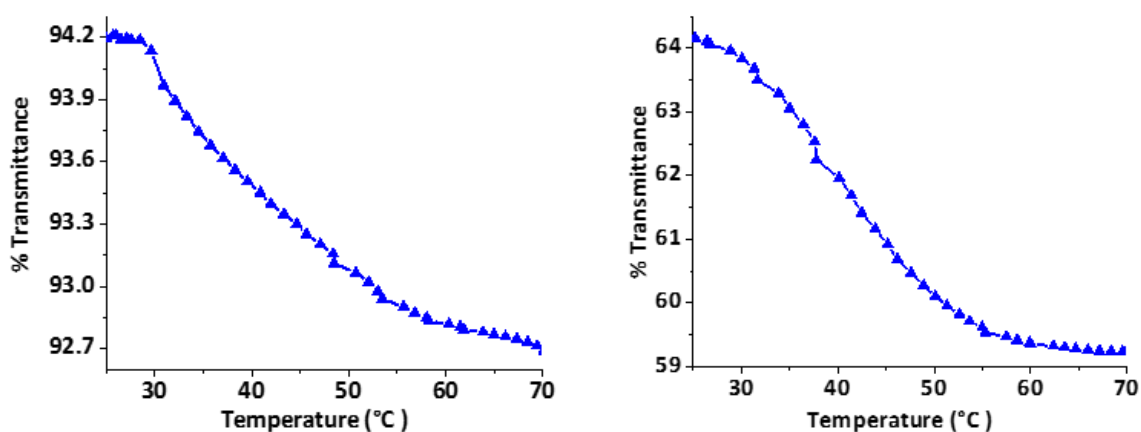
Figure 3.2. Determination of LCST; Linear (A), and 6-arm (B) polymers, respectively.

3.4.3 Size and Morphology of micelles

Dynamic light scattering (DLS) was used to determine the hydrodynamic diameter (Dh) and polydispersity of the linear and star polymeric micelles. The hydrodynamic diameter of empty and DOX and RSV-loaded micelles are given in Figure 3.3 and Table 3.2. The drug-loaded linear and 6-arm micelles exhibited sizes of 150.2 and 98.2 nm, respectively. The polymer micelles prepared from 6-arm polymer is smaller in size compared to the liner polymer micelles. The results showed that the size of the DOX and RSV loaded polymer micelles were larger compared to the empty polymeric micelles. Increase in the micellar size confirms the encapsulation of drugs inside the polymer micelles.
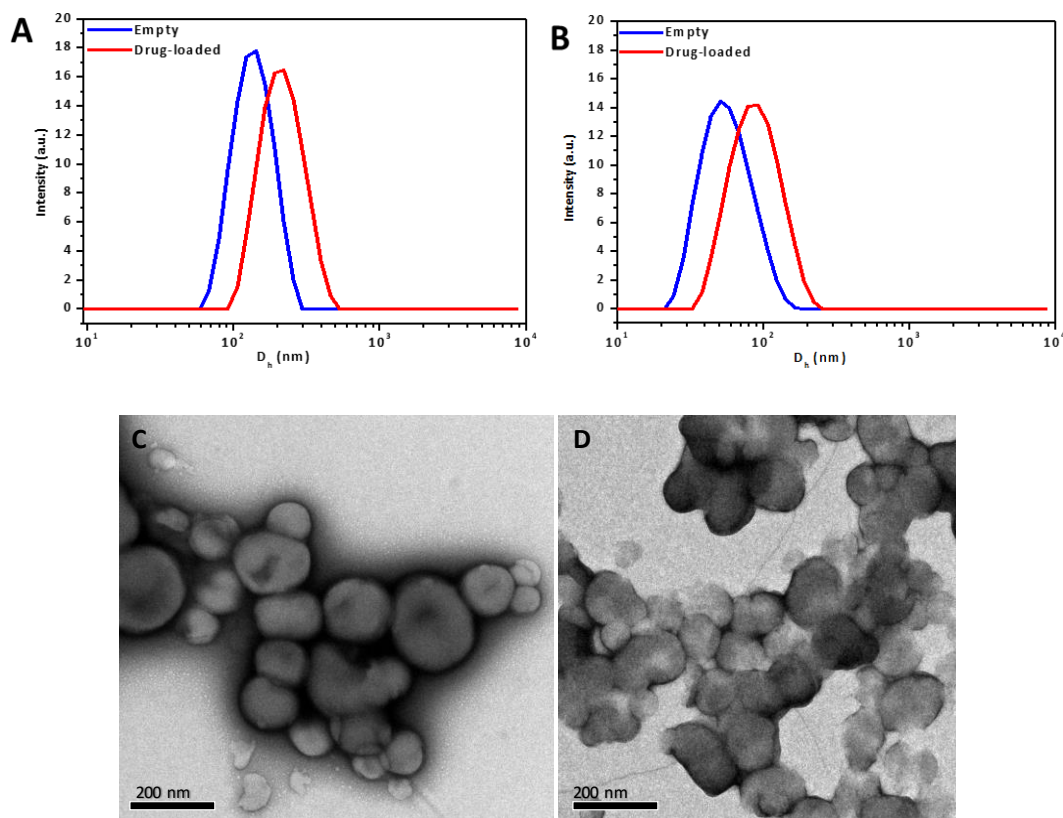
Figure 3.3. Size distribution (Dh) for empty and drug-loaded polymer micelles; A) Linear, and B) 6-arm; TEM images obtained for drug-loaded polymer micelles; C) Linear, and D) 6-arm.

Table 3.2. Summary of empty and drug-loaded polymer micelle properties

Polymer	Dh ^{empty} (nm)	Size dispersity	Dh ^{Loaded} (nm)	Size dispersity
Linear	108.2±1.6	0.194±0.01	151.5±1.9	0.28±0.25
6-arm	52.14±0.3	0.114±0.02	94.32±2.2	0.23±0.02

Morphology of the polymer micelles was obtained using TEM analysis (Figure 3.3). The TEM images confirms that the linear and star polymers self-assemble into spherical micelles in aqueous medium. The size distribution of the micelles determined from TEM is comparable to the micelle sizes determined by DLS.

3.4.4 Determination of Drug-Loading Capacity and Encapsulation Efficiency

Drug-loading capacity (wt% DLC) and encapsulation efficiency (wt% EE) were determined using UV-vis absorbance spectra by diluting the drug-loaded polymeric micelle solution with DMSO in a 1:1 volume ratio. The absorbance of the samples was measured at 485 nm for DOX and 320 nm for RSV and fitted to a standard calibration curve for DOX and RSV in DMSO/DI water.

The DLC and EE of drug-loaded micelles were calculated using following equations:

$$wt\% \, DLC = \frac{Weight \; t \; of \; encapuslated \; drug}{Weight \; of \; the \; polymer \; added} \times 100$$

$$wt\% \, EE = \frac{Weight \; of \; encapuslated \; drug}{Weight \; of \; the \; drug \; added} \times 100$$

To compare the DOX loading with our previous work, the combination drug loading in linear and star polymer was performed using the same polymer ratio (polymer/DOX at 5:1). Furthermore, molar ratios of DOX and RSV was systematically changed to study the effect of feed molar ratios of DOX and RSV on DOX loading (Figure 3.4 and Table 3.3-3.6). First, feed ratios of DOX was varied while keeping the molar ratios of RSV and polymer constant. The feed molar ratio of DOX was varied in the following ratios, [polymer]: [DOX]: [RSV] at 5:1:1, 5:2:1, 5:3:1 and 5:4:1. The results have shown that the DOX loading gradually increases in both polymer type, when the feed molar ratio of DOX was increased from 1 to 2 (Table 3.3 and 3.5). However, further increase in DOX feed ratio decreases the DLC and EE of the polymer. The lowest DLC and EE were observed at 5:4:1 feed ratio. At this feed ratio, DOX precipitates out of the solution and reduces the DLC and EE to 9.8% and 12.25 % in 6-arm star polymer and 4.37% and 5.46% in linear polymer. Overall, the star polymeric micelles showed a high encapsulation efficiency (> 93%) at DOX and RSV feed molar ratios of 1:1.

In a previous study from our group, DOX and RSV-loaded micelles were prepared using linear substituted and unsubstituted polycaprolactone-based amphiphilic diblock copolymers to improve the drug loading capacity.[21] Micelles obtained from PEG-*b*- PCL and PEG-*b*-PBCL diblock copolymers showed drug loading capacities of 4.74 wt% and 8.77 wt%.[21] The DOX loading content of the linear and star-like PMEEECL-*b*-PBCL copolymers were shown to be higher than PEG-*b*-PBCL and PEG-*b*- PCL.
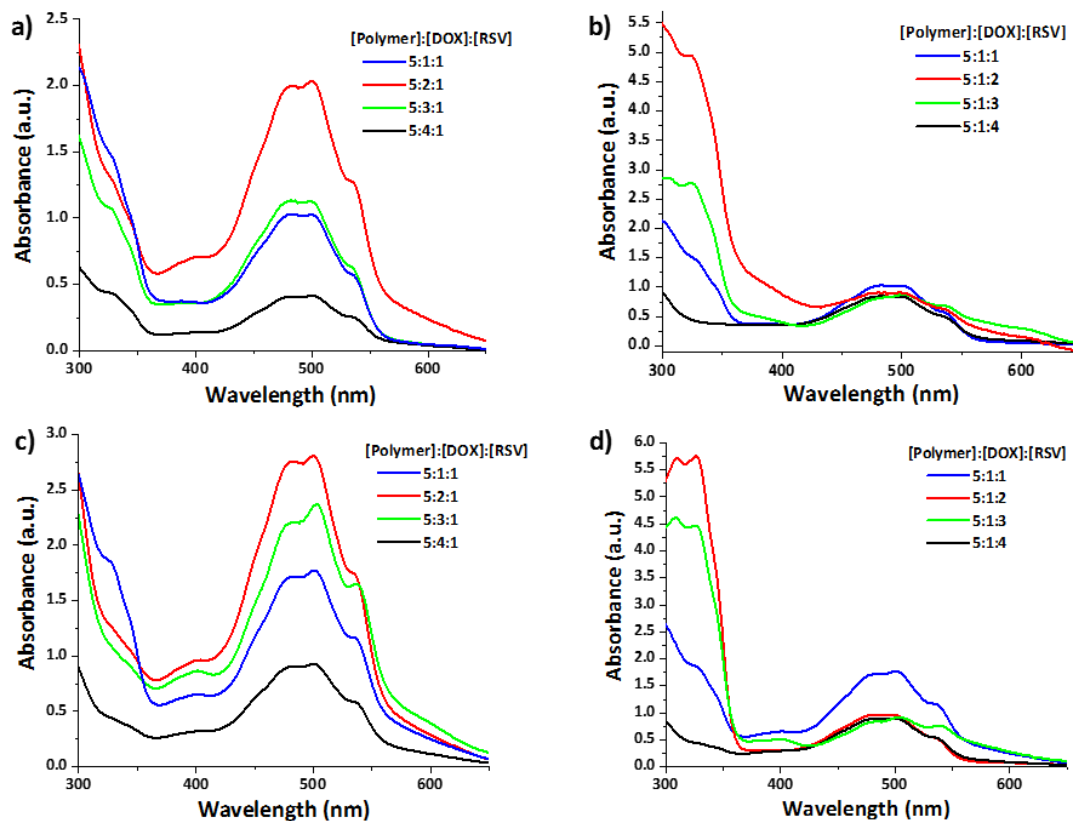
Figure 3.4. Absorbance spectra of DOX and RSV-loaded polymer micelles varying feed ratios of DOX and RSV. a) DOX and b) RSV variation in linear polymer, and c) DOX and d) RSV variation in 6-arm star polymer.

Finally, feed ratio of RSV was varied from [polymer]:[DOX]:[RSV] of 5:1:1 to [polymer]:[DOX]:[RSV] 5:1:4, while keeping the feed ratios of DOX and polymer constant (Table 3.4 and 3.6). The highest RSV loading capacity and encapsulation efficiency was found at [6-arm polymer]: [DOX]: [RSV] ratio of 5:1:2, which showed DLC and EE of 9.12 % and 22.81%, respectively. Linear polymer has shown a highest DLC and EE of 8.00% and 20.00%, respectively, at [polymer]: [DOX]: [RSV] ratio of 5:1:2. Further increase in feed ratio of RSV decreases the DLC and EE, due to the precipitation of RSV. Considering the DOX content in the linear and star polymers, [polymer]: [DOX]: [RSV] ratio of 5:1:1 was used in the biological study.

Table 3.3. Drug loading in Linear PBCL-*b*-PMEEEL varying the DOX feed ratios

Feed Ratio [Polymer]: [DOX]: [RSV]	DLC ^{RSV} (%)	EE ^{RSV} (%)	DLC ^{DOX} (%)	EE ^{DOX} (%)
5:1:1	2.54	12.69	11.20	55.98
5:2:1	2.25	11.23	21.61	54.02
5:3:1	1.78	8.88	12.36	20.60
5:4:1	0.72	3.58	4.37	5.46

Table 3.4. Drug loading in Linear PBCL-*b*- PMEEEL varying the RSV feed ratios

Feed Ratio [Polymer]: [DOX]: [RSV]	DLC ^{RSV} (%)	EE ^{RSV} (%)	DLC ^{DOX} (%)	EE ^{DOX} (%)
5:1:1	2.54	12.69	11.20	55.98
5:1:2	8.00	20.00	9.86	49.29
5:1:3	4.45	0.07	9.11	45.54
5:1:4	0.77	0.96	9.31	46.57

Table 3.5. Drug loading in 6-arm star PBCL-*b*- PMEEEL varying the DOX feed ratios

Feed Ratio [Polymer]: [DOX]: [RSV]	DLC ^{RSV} (%)	EE ^{RSV} (%)	DLC ^{DOX} (%)	EE ^{DOX} (%)
5:1:1	3.06	15.28	18.60	93.02
5:2:1	2.21	11.07	29.94	74.85
5:3:1	1.94	9.71	23.89	39.82
5:4:1	0.76	3.78	9.80	12.25

Table 3.6. Drug loading in 6-arm star PBCL-*b*- PMEEEL varying the RSV feed ratios

Feed Ratio [Polymer]: [DOX]: [RSV]	DLC ^{RSV} (%)	EE ^{RSV} (%)	DLC ^{DOX} (%)	EE ^{DOX} (%)
5:1:1	3.09	15.44	18.60	93.02
5:1:2	9.12	22.81	10.48	52.39
5:1:3	7.18	11.97	9.03	45.16
5:1:4	0.75	0.94	9.51	47.55

As reported in Chapter 2, DLC and EE of DOX were found to be 5.14% and 25.70% in linear polymer and 12.58% and 62.90% in 6-arm star polymer, when using feed ratio of polymer: DOX at 5:1. In this study, DLC and EE of DOX were found to be 11.20% and 55.98% in linear polymer and 18.60% and 93.02% in 6-arm star polymer, when using feed ratio of polymer :DOX: RSV at 5:1:1. This results suggested that the RSV encapsulation in multi-drug-loaded linear and star polymer micelles increases the drug loading capacity and encapsulation efficiency of DOX, compared to DOX-loaded linear and 6-arm star polymer, at the same feed ratio [polymer]:[DOX]=5:1. This increase could be attributed to the interaction between RSV and DOX, such as π-π stacking and hydrogen bonding. Additionally, π-π stacking between the aromatic groups of the drugs and benzyl groups of the polymer backbone supports in enhancing the DOX and RSV loading. The highest DOX and RSV loading were found in 6-arm star polymer, due to the higher density of benzyl functionality in the hydrophobic core.

3.4.5 *In vitro* Drug Release

In Vitro DOX release studies were evaluated using DOX and RSV- loaded linear and 6-arm polymer micelles in PBS (pH 7.4) and presented in figure 3.5. The polymer micellar solutions were incubated at physiological temperature (37 °C) and temperature above LCST (42 °C), separately. At temperature above LCST (42 °C), DOX and RSV-loaded polymer micelles released higher amount of DOX compared to that of amount of DOX released at 37 °C. The temperature above LCST, the shell of the polymer micelles is deformed that resulted in faster DOX release. At 42 °C, ~72% of DOX was released from the linear polymer micelles, which is higher than the DOX release from the 6-arm polymer micelles (60 %) incubated at 42 °C. The higher density of

the benzyl functional groups in the 6-arm polymer micellar core enhances the π-π interaction between the benzyl groups of the polymer backbone and the aromatic group of the DOX. The enhanced π-π interaction weakens the DOX release from the 6-arm polymer micelles compared to linear polymer micelles.
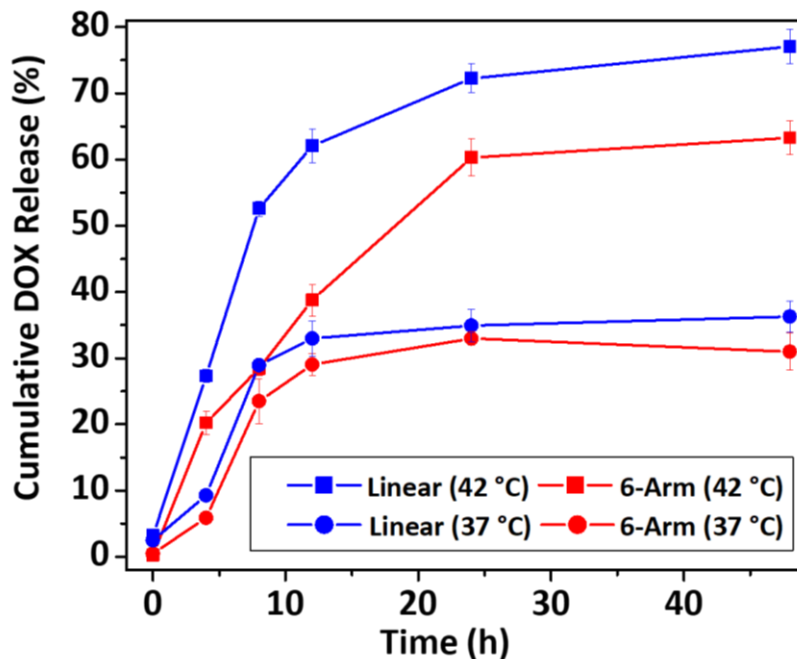
Figure 3.5. *In-vitro* DOX release for the DOX-and RSV-loaded linear and 6-arm polymer micelles at 37 °C and 42 °C in PBS.

3.4.6　*In vitro* **Cytotoxicity Studies**

The cytotoxicity effect of empty, RSV, and combination drug (DOX and RSV)-loaded micelles were examined by CellTiter-blue assay in HeLa cells with cells only as a control (Figure 3.6). The cytotoxicity effect of RSV-loaded and combination drug-loaded micelles were compared with free RSV and combination of free RSV and DOX, respectively, at the same experimental condition.

The amount of free drugs used in the study was determined according to the drug-loading capacity of the drug- loaded polymer micelles.
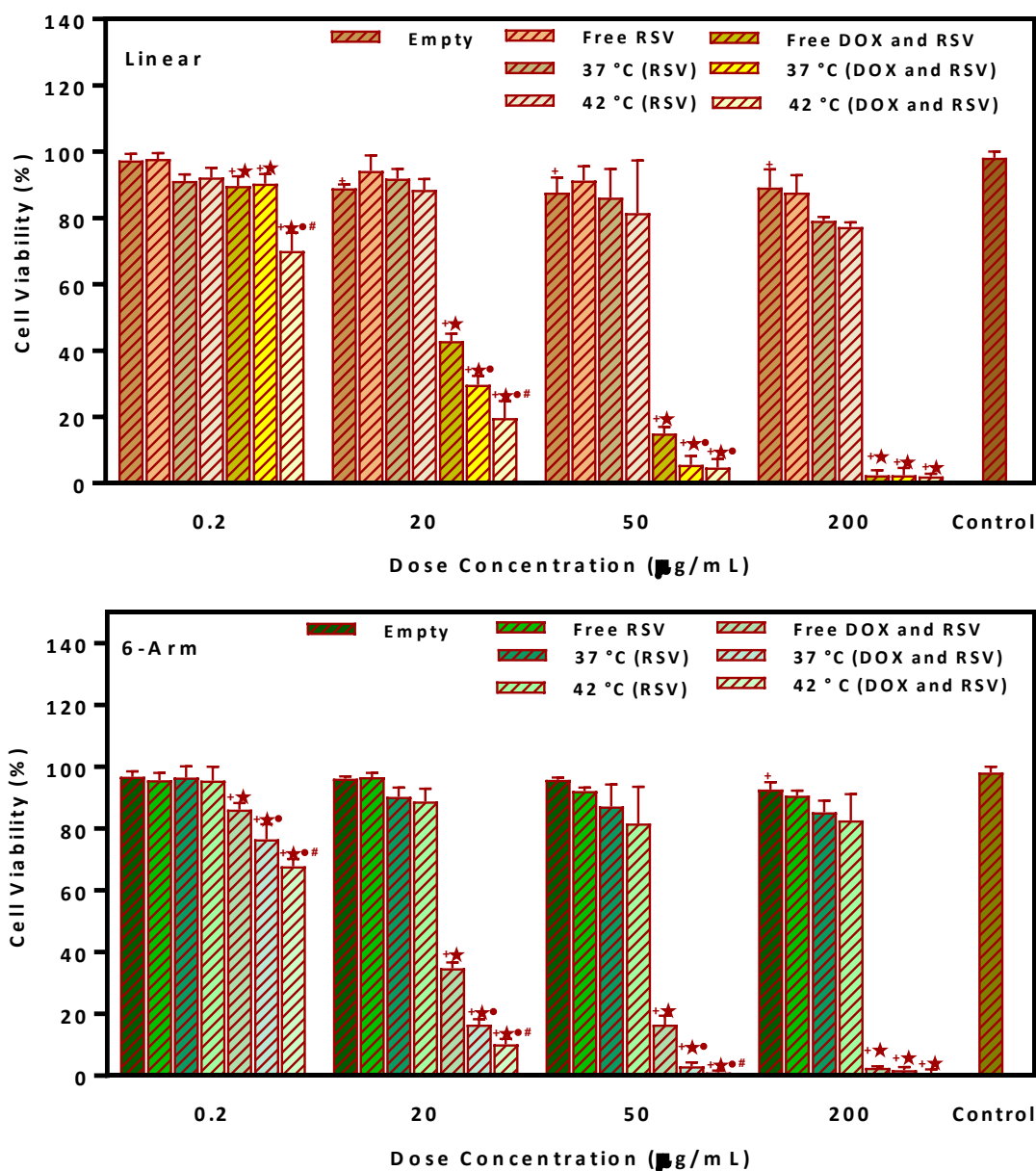
Figure 3.6. Cytotoxic effect of empty micelles, free drugs, and drug-loaded micelles.

Data is expressed as mean ± SE and two independent experiments made in twelve replicates. +p < 0.01, Significant differences of empty micelles, free DOX and RSV, DOX and RSV-loaded micelles (37 °C) and DOX and RSV-loaded micelles (42 °C) vs control (Cells only); ★p < 0.01, Significant differences of free DOX and RSV, DOX and RSV-loaded micelles (37 °C) and DOX and RSV-loaded micelles (42 °C) vs empty micelles; •p < 0.01, Significant differences of DOX and RSV-loaded micelles (37 °C) and DOX and RSV-loaded micelles (42 °C) vs free DOX and RSV; #p < 0.01, Significant differences of DOX and RSV-loaded micelles (37 °C) vs DOX and RSV-loaded micelles (42 °C).

As shown in Figure 3.6, empty micelles have shown no cytotoxicity effect against HeLa cells, at all tested concentrations. Additionally, at both temperatures, RSV-loaded micelles and free RSV treated HeLa cells have shown less cytotoxic effect, at all tested concentrations.

The combination drug-loaded linear and 6-arm star polymer micelles exhibited higher cytotoxicity compared to the equivalent amount of free DOX and RSV mixture. Furthermore, DOX and RSV-loaded 6-arm polymer micelles were more active in inhibiting tumor cell proliferation than the DOX and RSV-loaded linear polymer micelles at both temperatures (37 °C and 42 °C) (Figure 3.4), due to the higher DOX content in the 6-arm polymer micelles. When comparing our previous DOX-loading studies using linear and star-like PBCL-*b*-PMEEECL polymers, the DOX and RSV-loaded polymer micelles have the highest loading of DOX that result in enhanced cytotoxicity to the tumor cells.

Furthermore, higher cytotoxicity effect in HeLa cells were expected at 42 ° C due to higher drug release compared to at 37 °C. To test this hypothesis, HeLa cells were treated with DOX and RSV-loaded micelles and incubated at physiological temperature (37 °C) and a temperature above the lower critical solution temperature (42 °C). Significantly lower cell viability was observed from cells incubated at 42 °C as compared to cells incubated at 37 °C, supporting the concept that the higher release of DOX from polymer micelles incubated at temperature above the LCST.

Dose response curves and the IC_{50} (half maximal inhibitory concentration) values of combination drug-loaded linear and 6-arm star polymer micelles in HeLa cells were summarized in Figure 3.7 and Table 3.7. According to the data obtained, DOX and RSV-loaded 6-arm star polymer micelles showed IC_{50} values of 5.33 and 0.299 µg/mL, at 37 °C and 42 °C, respectively,

which was much lower than those of DOX and RSV-loaded linear polymer micelles. More DOX was released at temperature above the LCST, therefore cytotoxicity against HeLa cells were higher at 42 °C compared to the cells incubated at 37 °C. The temperature-dependent DOX release resulting in lower IC_{50} values at 42 °C. Moreover, these IC_{50} values are lower than the our previously report. DOX-loaded 6-arm star micelles (6.96 and 0.39 µg/mL, at 37 °C and 42 °C, respectively) and DOX-loaded linear micelles (20.18 and 18.98 µg/mL, at 37 °C and 42 °C, respectively). The enhanced cytotoxicity of combination-loaded star polymer is attributed to the improved drug-loading through interaction between DOX and RSV, and the synergistic therapeutic effect of DOX and RSV
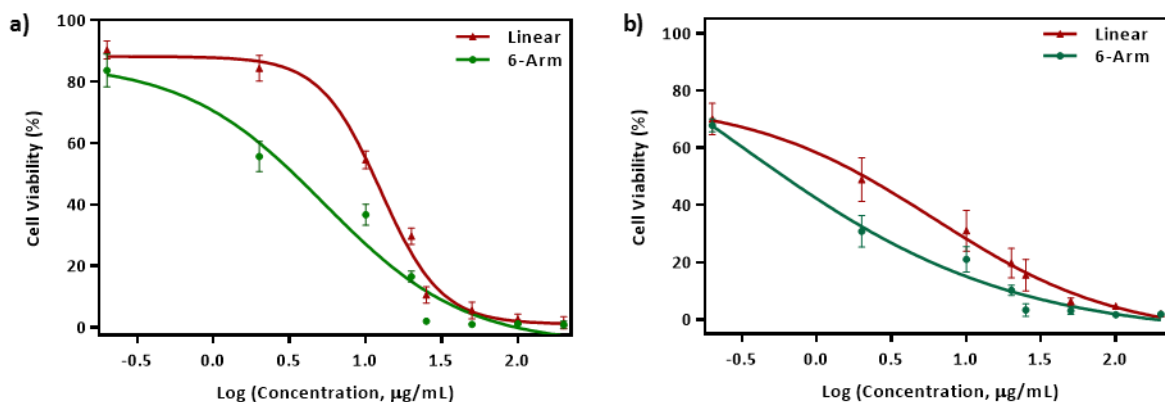

Figure 3.7. Dose response curve for the DOX and RSV-loaded polymeric micelles at a) 37 °C, and b) 42 °C, respectively.

Table 3.7. IC_{50} values of DOX and RSV-loaded polymer micelles

Polymer	IC_{50} at 37 °C (µg/mL)	IC_{50} at 42 °C (µg/mL)
Linear	12.52±0.09	5.33±0.02
6-arm	6.045±0.7	0.299±0.07

3.4.7 Cellular Uptake Studies

As shown in Figure 3.8, when DOX and RSV- loaded linear and star polymer micelles were cultured with HeLa cells, DOX red fluorescence and RSV green florescence were localized in the nucleus, which confirms that the DOX and RSV-loaded polymeric micelles were taken into the tumor cells via endocytosis process. A large amount of DOX red fluorescence accumulated in the cells, which were cultured with DOX and RSV-loaded star polymer micelles. This may due to the higher DOX content in the star polymer micelles and led to a higher cytotoxicity in HeLa cells. The amount of RES green florescence of linear and star polymers treated cells were comparable, due to the comparable RSV loading in polymers.
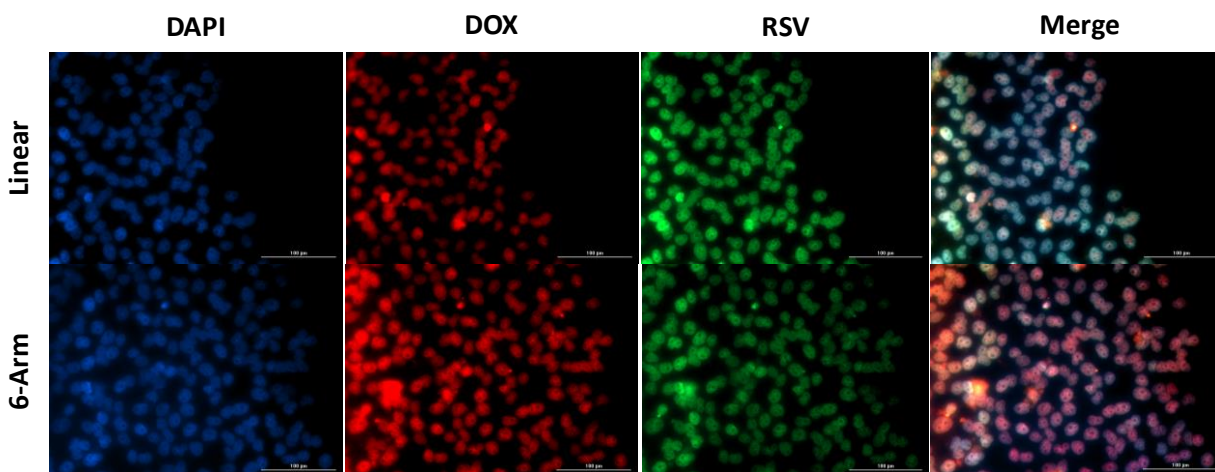

Figure 3.8. Cellular uptake of DOX and RSV-loaded polymeric micelles by HeLa cells, (scale bar = 100 μm).

3.4.8 Statistical Analysis

The following experiment was setup with 12 repetitions per condition selected. Two polymer types at eight different concentration levels and two temperature levels were used in the analysis.

Cytotoxicity was measured as the dependent variable. Experiment design is summarized in the table below in Table 3.8.

Table 3.8. Factor Information of the Multi-Factor ANOVA

Factor	Type	Levels	Values
Polymer arm	Fixed	2	1, 6
Temperature	Fixed	2	37, 42
Concentration	Fixed	8	0.2, 2.0, 10.0, 20.0, 25.0, 50.0, 100.0, 200.0

Summary of Analysis of Variance

Source	DF	Adj SS	Adj MS	F-Value	P-Value
Polymer arm	1	3666	3666.3	58.85	0.000
Temperature	1	3614	3614.0	58.01	0.000
Concentration	7	135422	19346.1	310.53	0.000
Error	182	11339	62.3		
Lack-of-Fit	22	9348	424.9	34.15	0.000
Pure Error	160	1991	12.4		
Total	191	154041			

Model Summary

S	R-sq	R-sq(adj)	R-sq(pred)
7.89307	92.64%	92.28%	91.81%

   Collected data were analyzed using MiniTab 2018 with a confidence level of 95%. ANOVA results are shown below. The ANOVA model consisted of Number of Polymer arms, Temperature and Concentration as the independent variables. The p value for all three variables is less than 0.05. Therefore, we can conclude that there is a significant difference in %cell viability due to number of polymer arms, temperature and concentration, independently. Further the model

summary results below show that 92.28% of the effects can be modelled via the selected independent variables.

The main effects and interaction plots from multifactor ANOVA are shown in Figure 3.9 and 3.10. The main effect plot illustrates that the all three variables are contributing towards the reduction mean % cell viability. The main effect plot shows that all three variables have a significant effect on cell viability.
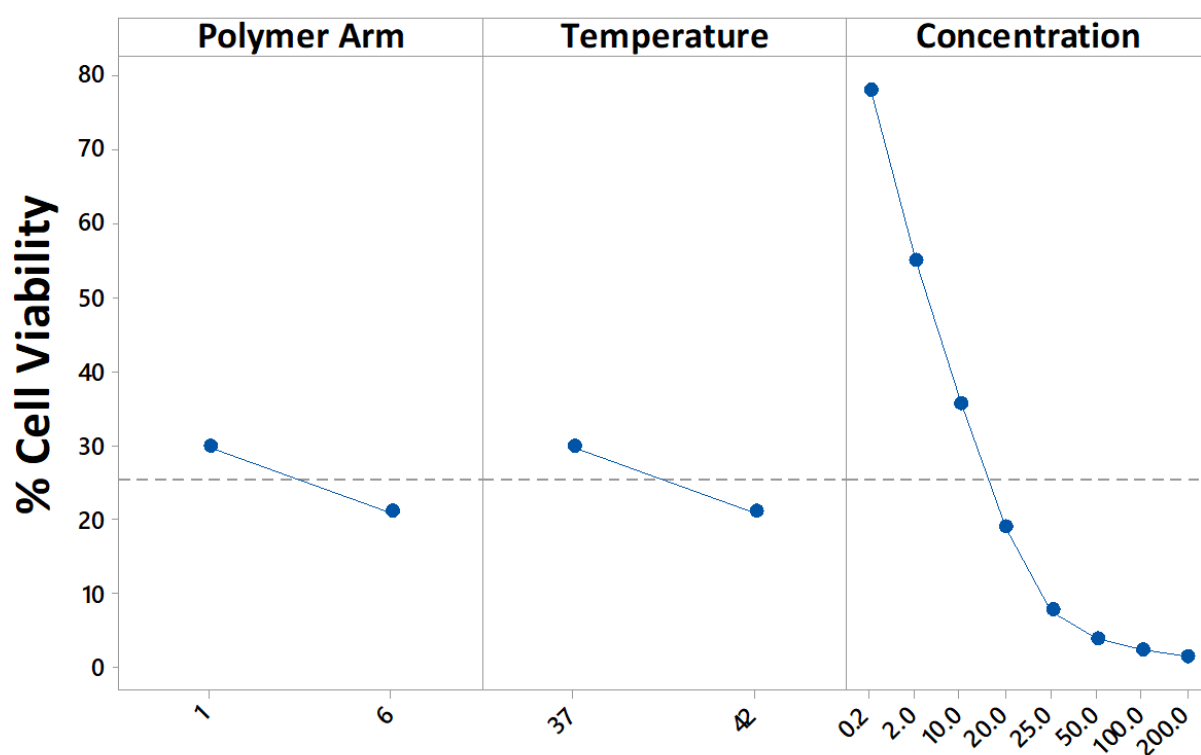
Figure 3.9. Main effect plot for the polymer arms, temperature and dose concentration.
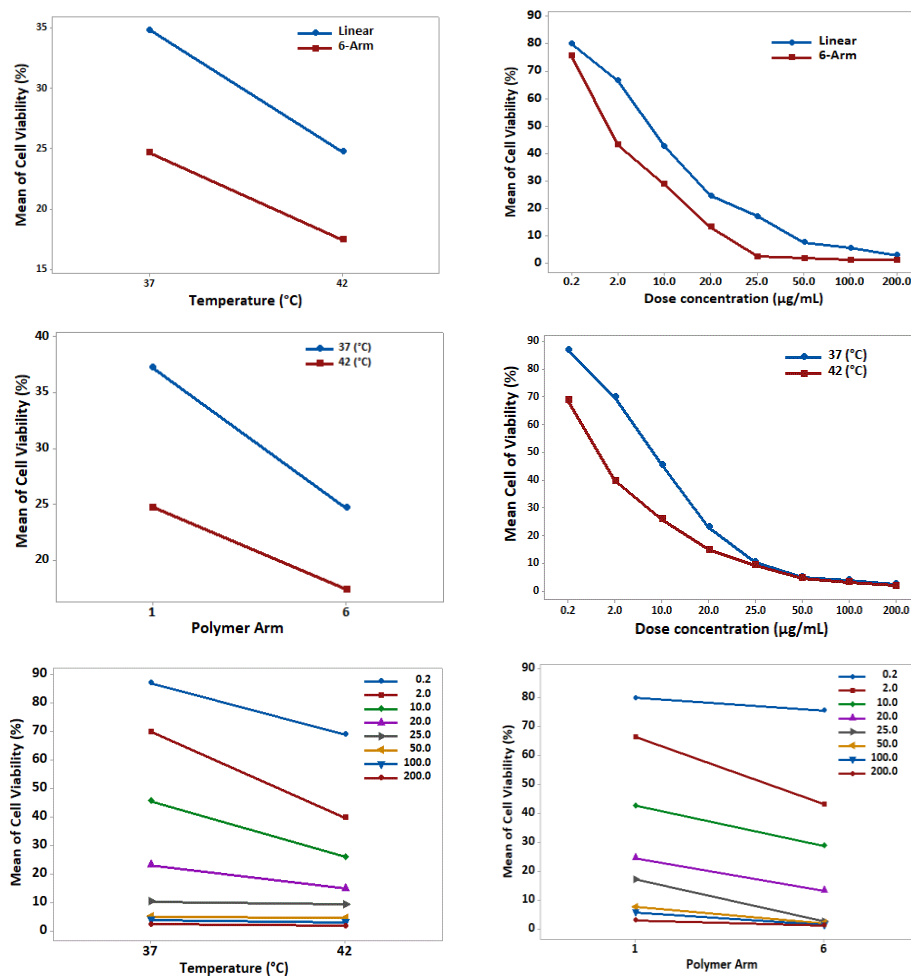
Figure 3.10. Interaction plots for the polymer arms, temperature and dose concentration.

3.5 Conclusion

In this study, multi-drug-loaded linear and star polymer polymeric micellar drug carriers were successfully developed by co-encapsulating Doxorubicin and Resveratrol drug pair in a single carrier for improving the chemotherapeutic effect for cancer therapy. The combination drug loading strategy showed a significant improvement in DOX loading over the previously reported DOX loading in same polymer micelles. The enhanced drug loading in the micelles is attributed

favorable to π-π stacking and hydrophobic interactions between the polymer and drug pair. The combined delivery of DOX and RSV exhibited a much lower IC_{50} value than that of the DOX only-loaded micelles, suggesting a desirable in-vitro anti-tumor effect. Furthermore, the 6-arm polymer micellar carrier shows a significant improvement in drug loading and cytotoxicity effect over liner polymer micellar carriers. Overall, combined drug loaded polymeric micelles are a promising candidate for anti-cancer therapy.

Acknowledgment

3.6 References

1. Carvalho, C., Santos, R., Cardoso, S., Correia, S., Oliveira, P., Santos, M., Moreira, P. Curr. Med. Chem., 2009.

2. Weiss, R. B., Sarosy, G., Clagett-Carr, K., Russo, M., Leyland-Jones, B. Cancer Chemother. Pharmacol., 1986, 18, 185–197.

3. Cortés-Funes, H., Coronado, C. Cardiovasc. Toxicol., 2007, 7, 56–60.

4. Chatterjee, K., Zhang, J., Honbo, N., Karliner, J. S. Cardiology, 2010.

5. Tacar, O., Sriamornsak, P., Dass, C. R. J. Pharm. Pharmacol., 65, 157–170.

6. Cappetta, D., Rossi, F., Piegari, E., Quaini, F., Berrino, L., Urbanek, K., Angelis, A. De Pharmacol. Res., 2018, 127, 4–14.

7. Etrych, T., Strohalm, J., Chytil, P., Černoch, P., Starovoytova, L., Pechar, M., Ulbrich, K. Eur. J. Pharm. Sci., 2011, 42, 527–539.

8. Pechar, M., Braunová, A., Ulbrich, K., Jelínková, M., Ríhová, B. J. Bioact. Compat. Polym., 2005, 20, 319–341.

9.   Veronese, F. M., Schiavon, O., Pasut, G., Mendichi, R., Andersson, L., Tsirk, A., Ford, J., Wu, G., Kneller, S., Davies, J., Duncan, R. Bioconjug. Chem., 2005, 16, 775–784.

10.   Ferreira, D. dos S., Faria, S. D., Lopes, S. C. de A., Teixeira, C. S., Malachias, A., Magalhï¿½es-Paniago, R., de Souza Filho, J. D., Oliveira de Jesus Pinto, B. L., Guimarï¿½es, A. R., Caravan, P., Ferreira, L. A. M., Alves, R. J., Oliveira, M. C. Int. J. Nanomedicine, 2016.

11.   dos Santos Ferreira, D., Jesus de Oliveira Pinto, B. L., Kumar, V., Cardoso, V. N., Fernandes, S. O., Souza, C. M., Cassali, G. D., Moore, A., Sosnovik, D. E., Farrar, C. T., Leite, E. A., Alves, R. J., de Oliveira, M. C., Guimarães, A. R., Caravan, P. Nanomedicine Nanotechnology, Biol. Med., 2017.

12.   Füredi, A., Szebényi, K., Tóth, S., Cserepes, M., Hámori, L., Nagy, V., Karai, E., Vajdovich, P., Imre, T., Szabó, P., Szüts, D., Tóvári, J., Szakács, G. J. Control. Release, 2017, 261, 287–296.

13.   Zhu, D., Wu, S., Hu, C., Chen, Z., Wang, H., Fan, F., Qin, Y., Wang, C., Sun, H., Leng, X., Kong, D., Zhang, L. Acta Biomater., 2017, 58, 399–412.

14.   Li, M., Lv, S., Tang, Z., Song, W., Yu, H., Sun, H., Liu, H., Chen, X. Macromol. Biosci., 13, 1150–1162.

15.   Xu, J., Zhao, Q., Jin, Y., Qiu, L. Nanomedicine Nanotechnology, Biol. Med., 2014, 10, 349–358.

16.   Washington, K. E., Kularatne, R. N., Du, J., Gillings, M. J., Webb, J. C., Doan, N. C., Biewer, M. C., Stefan, M. C. J. Polym. Sci. Part A Polym. Chem., 2016, 54, 3601–3608.

17.   Hao, J., Cheng, Y., Ranatunga, R. J. K. U., Senevirathne, S., Biewer, M. C., Nielsen, S. O., Wang, Q., Stefan, M. C. Macromolecules, 2013, 46, 4829–4838.

18.   Cheng, Y., Hao, J., Lee, L. A., Biewer, M. C., Wang, Q., Stefan, M. C. Biomacromolecules, 2012, 13, 2163–2173.

19.   Hao, J., Cheng, Y., Ranatunga, R. J. K. U., Senevirathne, S., Biewer, M. C., Nielsen, S. O., Wang, Q., Stefan, M. C. Macromolecules, 2013, 46, 4829–4838.

20.   Washington, K. E., Kularatne, R. N., Karmegam, V., Biewer, M. C., Stefan, M. C. In Stimuli Responsive Polymeric Nanocarriers for Drug Delivery Applications, Volume 1, A. S. H. Makhlouf, and N. Y. Abu-Thabit, Eds.; Woodhead Publishing 2018; pp. 501–529.

21. Rainbolt, E. A., Washington, K. E., Biewer, M. C., Stefan, M. C. J. Mater. Chem. B, 2013, 1, 6532–6537.

22. Senevirathne, S. A., Boonsith, S., Oupicky, D., Biewer, M. C., Stefan, M. C. Polym. Chem., 2015, 6, 2386–2389.

23. Hao, J., Servello, J., Sista, P., Biewer, M. C., Stefan, M. C. J. Mater. Chem., 2011.

24. Washington, K. E., Kularatne, R. N., Du, J., Ren, Y., Gillings, M. J., Geng, C. X., Biewer, M. C., Stefan, M. C. J. Mater. Chem. B, 2017.

25. Washington, K. E., Kularatne, R. N., Du, J., Gillings, M. J., Webb, J. C., Doan, N. C., Biewer, M. C., Stefan, M. C. J. Polymer Sci. Part A Polym. Chem., 2016, 54, 3601–3608.

26. Senevirathne, S. A., Washington, K. E., Miller, J. B., Biewer, M. C., Oupicky, D., Siegwart, D. J., Stefan, M. C. J. Mater. Chem. B, 2017, 5, 2106–2114.

27. Rainbolt, E. A., Washington, K. E., Biewer, M. C., Stefan, M. C. J. Mater. Chem. B, 2013, 1, 6532–6537.

28. Washington, K. E., Kularatne, R. N., Karmegam, V., Biewer, M. C., Stefan, M. C. Wiley Interdiscip. Rev. Nanomedicine Nanobiotechnology, 2016, n/a--n/a.

29. Washington, K. E., Kularatne, R. N., Biewer, M. C., Stefan, M. C. ACS Biomater. Sci. Eng., 2018, 4, 997–1004.

30. Zhang, B., Cheng, G., Zheng, M., Han, J., Wang, B., Li, M., Chen, J., Xiao, T., Zhang, J., Cai, L., Li, S., Fan, X. Drug Deliv., 2018, 25, 461–471.

31. Betancourt, T., Brown, B., Brannon-Peppas, L. Nanomedicine, 2007, 2, 219–232.

32. Kularatne, R. N., Washington, K. E., Bulumulla, C., Calubaquib, E. L., Biewer, M. C., Oupicky, D., Stefan, M. C. Biomacromolecules, 2018, 19, 1082–1089.

33. Dadsetan, M., Liu, Z., Pumberger, M., Giraldo, C. V., Ruesink, T., Lu, L., Yaszemski, M. J. Biomaterials, 2010, 31, 8051–8062.

34. Wang, C., Zhang, G., Liu, G., Hu, J., Liu, S. J. Control. Release, 2017, 259, 149–159.

35. Kozlovskaya, V., Chen, J., Tedjo, C., Liang, X., Campos-Gomez, J., Oh, J., Saeed, M., Lungu, C. T., Kharlampieva, E. J. Mater. Chem. B, 2014, 2, 2494–2507.

36. Zhao, Y., Huan, M. L., Liu, M., Cheng, Y., Sun, Y., Cui, H., Liu, D. Z., Mei, Q. B., Zhou, S. Y. Sci. Rep., 2016.

37. Kunjachan, S., Rychlik, B., Storm, G., Kiessling, F., Lammers, T. Adv. Drug Deliv. Rev., 2013, 65, 1852–1865.

38. Ambudkar, S. V, Kim, I.-W., Sauna, Z. E. Eur. J. Pharm. Sci., 2006, 27, 392–400.

39. Greenberg, R. M. Parasitol. Int., 2013, 62, 647–653.

40. Hu, C.-M. J., Zhang, L. Biochem. Pharmacol., 2012, 83, 1104–1111.

41. Kim, T. H., Shin, Y. J., Won, A. J., Lee, B. M., Choi, W. S., Jung, J. H., Chung, H. Y., Kim, H. S. Biochim. Biophys. Acta - Gen. Subj., 2014, 1840, 615–625.

42. Wang, S., Chen, R., Morott, J., Repka, M. A., Wang, Y., Chen, M. Expert Opin. Drug Deliv., 2015, 12, 361–373.

43. Wang, J., Ma, W., Tu, P. Macromol. Biosci., 15, 1252–1261.

44. Kasiotis, K. M., Pratsinis, H., Kletsas, D., Haroutounian, S. A. Food Chem. Toxicol., 2013, 61, 112–120.

45. Arafa, M. H., Mohammad, N. S., Atteia, H. H., Abd-Elaziz, H. R. J. Physiol. Biochem., 2014.

46. Dolinsky, V. W., Jones, K. E., Sidhu, R. S., Haykowsky, M., Czubryt, M. P., Gordon, T., Dyck, J. R. B. J. Physiol., 590, 2783–2799.

47. Wenzel, E., Somoza, V. Mol. Nutr. Food Res., 49, 472–481.

48. Greer, A. K., Madadi, N. R., Bratton, S. M., Eddy, S. D., Mazerska, Z., Hendrickson, H. P., Crooks, P. A., Radominska-Pandya, A. Chem. Res. Toxicol., 2014, 27, 536–545.

49. Walle, T., Hsieh, F., DeLegge, M. H., Oatis, J. E., Walle, U. K. Drug Metab. Dispos., 2004, 32, 1377–1382.

CHAPTER 4

SYNTHESIS AND OPTO-ELECTRONIC PROPERTIES OF FUNCTIONALIZED

PYRIMIDINE-BASED CONJUGATED POLYMERS

Authors: Vasanthy Karmegam, Chinthaka M. Udamulle Gedara, Michael C. Biewer,
Mihaela C. Stefan

The Department of Chemistry and Biochemistry, BE26

The University of Texas at Dallas

800 West Campbell Road

Richardson, Texas 75080-3021

4.1 Abstract

Side chain engineering has been used for tuning the opto-electronic properties of organic semiconductors. In this work, a series of novel pyrimidine-based donor-acceptor (D-A) conjugated polymers functionalized with electron-withdrawing or -donating side chains were synthesized. The opto-electronic properties of the pyrimidine D-A conjugated polymers were investigated focusing on the dependence on the electron withdrawing strength of the acceptor moiety, while maintaining the same donor moiety. Fine-tuning of the energy levels was achieved by introducing electron donating (alkoxy (-OR) and alkylthio (-SR)) or electron withdrawing (alkylsulfinyl (-SOR) and alkylsulfonyl (-SO2R)) side chains onto the acceptor moiety. The effects of side chain modification have been investigated through DFT calculations, UV−vis analysis and electrochemical measurements.

4.2 Introduction

Organic semiconductors have attracted much attention in recent years as promising materials for flexible, low-cost, and light-weight electronic devices. To date, various organic electronics applications, including organic photovoltaics (OPVs), field-effect transistors (FETs), light-emitting diodes, and electrochromic devices have been developed.[1–6] Organic field-effect transistors (OFETs) have promising applications in the field of flexible electronics with the discovery of the first OFET using polythiophene in the 1980's.[7] Research on p-type semiconducting polymers has shown tremendous improvement, with charge-carrier mobility values exceeding 10 $cm^2V^{-1}s^{-1}$ in conjugated small molecules or polymer-based OFETs.[8–13] Single-crystal-based OFETs have been reported with electron mobility values over 10 $cm^2V^{-1}s^{-1}$

using a solution processing technique.[14,15] Meanwhile, a power conversion efficiency >10% has been reported in conjugated polymer-based solar cells in recent years.[16]

The incorporation of flexible side chains to the polymer backbone has a significant effect on the solubility of the donor-acceptor (D-A) conjugated polymers, which is crucial in the fabrication of solution-processed devices. A good solution-processability facilitate the fabrication of inexpensive, low temperature and large-area devices.[17] Moreover, the side chain engineering of the D-A conjugated polymers has been widely investigated in order to tune the polymer molecular conformation, molecular packing, electron affinity and thin film morphology, thereby influencing the device performance.[1] In recent years, more effort has been dedicated to incorporating numerous flexible side chain substituents on polymer backbone to improve device performance in an efficient way. Based on the chemical composition, the flexible side chains are classified mainly as alkyl, hybrid, oligoether, fluoroalkyl and latently reactive side chains.[18] Among these categories, our research mainly focuses on hybrid side chain that is further sub grouped, namely as electron donating, electron withdrawing and conjugated groups, depending on the bridging position of the functionalized side chain on the conjugated polymer backbone.[18] A variety of electron-donating and electron-withdrawing side chains are attached to conjugated polymers not only to improve the solution processability but also finely tune the optical and electronic properties of the conjugated polymer. Electron-donating side chains, such as alkoxy (-OR),[19–22] alkylthio (-SR)[19,22–24] and alkylamino (−NHR and −NRR′)[25] have been widely investigated. Simultaneously, acetyl (−COR),[26] esters (−COOR),[21] amides (−CONHR),[27] boron (−BR2),[28] and sulfonyl (−SO3R)[29] groups have been explored as an electron-withdrawing substituent.

Recently, D-A conjugated polymers made of combinations of electron rich donor (D) moieties, and electron deficient acceptor (A) moieties have been extensively reported. Incorporating electron-deficient heteroaryl moieties, such as aromatic diimides, halogenated aromatic diimides, and cyano and/or carbonyl aromatic ring, into the polymer backbone reduces the LUMO level and thus facilitates electron injection and transport.[30–33] Among these moieties, polymer incorporating electron deficient pyrimidine and its derivatives as the electron-accepting unit possess high reactivity and potential for substituent modification. With evolving cross-coupling strategies and other polymerization techniques, many pyrimidine-based D−A conjugated polymers having good optical and electronic properties have been reported with potential applications in various fields.[20,34,35]
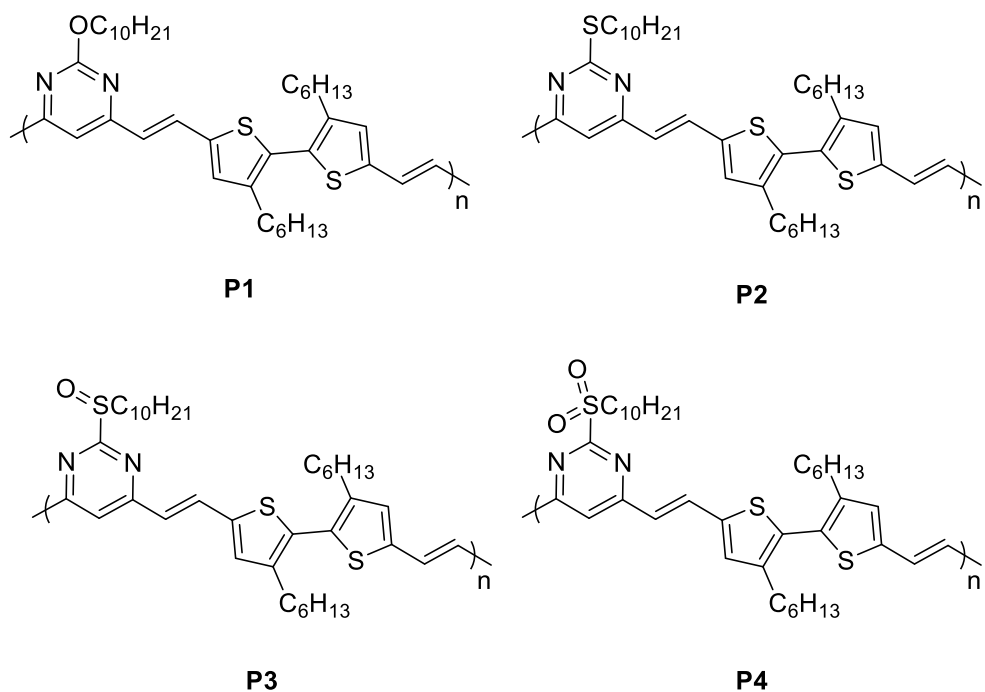

Figure 4.1. The scheme of polymers: poly[2-(decyloxy)-4-(2-(3,3'-dihexyl-5'-vinyl-2,2'-bithiophen-5-yl)vinyl)-6- vinylpyrimidine] (P1), poly[2-(decylthio)-4,6-dimethylpyrimidine] (P2), poly[2-(decylsulfinyl)-4,6-dimethylpyrimidine] (P3) and poly[2-(decylsulfonyl)-4,6-dimethylpyrimidine] (P4).

Previously, our group reported a series of pyrimidine-based D-A conjugated polymers varying donor moiety, while maintaining the same acceptor moiety and studied their opto-electronic properties.[20,35] As a continuation, we report here, the synthesis of another series of pyrimidine-based D-A copolymers varying the acceptor moiety, while retaining the same donor moiety, to investigate the optoelectronic properties of the polymers (Figure 4.1). The optoelectronic properties have been tuned by changing the electron withdrawing strength of the acceptor unit, which is strongly dependent on the electron -donating or -withdrawing the power of the side chain.

4.3 Experimental

4.3.1 Materials

2-Chloro-4,6-dimethylpyrimidine was purchased from AK Scientific, Inc. and all the other chemicals were purchased from Aldrich and Fisher chemicals and were used without further purification unless otherwise noted. Tetrahydrofuran (THF) and toluene were dried over sodium/benzophenone ketyl and freshly distilled prior to use.

4.3.2 Methods

^{1}H NMR spectra were recorded on a 500 MHz Bruker AVANCE IIITM spectrometer at 25 °C using deuterated chloroform as the solvent. Multiplicities were denoted as: s(singlet), d(doublet), t(triplet), q(quartet) and m(multiplet). Number average molecular weights of the polymers were determined by size exclusion chromatography (SEC) using a Viscotec VE 3580 system equipped with CLM3009 columns, refractive index detector and UV detectors (254 nm laser). HPLC grade THF was used as the eluent (1 mL min^{-1}) at 30 °C with GPC max as the sample module and

84

calibration was based on polystyrene standards. The UV-Visible spectra of the polymer solution and thin film were recorded using an Agilent 8453 UV-vis spectrometer with 1 cm path length cuvettes. Thin films were obtained by drop casting the polymer solutions on glass microscope slides. Cyclic voltammograms were obtained with BAS CV-50W voltammetric analyzer with the platinum disk, platinum wire, and Ag/Ag^+ as working, auxiliary and reference electrodes, respectively. Electrochemical grade tetrabutylammonium perchlorate (0.1 M) in acetonitrile was used as the electrolytic solution. All electrochemical shifts were standardized to the ferrocene redox couple at 0.474 V. GC-MS was obtained on an Agilent 6890-5973 apparatus equipped with Hewlett-Packard fused with silica capillary column cross-linked with 5% phenylmethylsiloxane. Helium was used as the carrier gas (1 mL min^{-1}). High-resolution mass spectra (HRMS) was recorded with Shimadzu LCMS-IT-TOF Mass Spectrometer using a Shim-pack XR-ODS column. The sample was dissolved in CHCl3, and 15 µL sample was injected. The theoretical calculation was conducted at B3LYP/6-31G* level using Spartan06. The X-ray diffraction study was performed on a RIGAKU Ultima III diffractometer. The thin films of polymer were irradiated by Cu-Kα (λ = 1.54 A°) and scanned from 1° to 40° (2Θ) at 0.04° interval at a rate of 2°/min. Thin films were prepared by drop casting polymer in chloroform (5.0 mg mL^{-1}) onto clean SiO$_2$ substrates. Tapping mode atomic force microscopy (TMAFM) analysis of the thin film was carried out using a Nanoscope IV-Multimode Veeco equipped with an E-type vertical engage scanner. Thin films were prepared by drop-casting polymer solution in chlorobenzene (1 mg mL^{-1}) on mica substrate and followed by slow evaporation in a saturated chlorobenzene chamber. The TMAFM images were acquired at room temperature in air using silicon cantilevers with a resonance frequency of 320 kHz and nominal spring constant of 42 Nm^{-1}.

4.3.3 Synthesis of Monomers

The synthesis of 3,3′-dihexyl-2,2′-bithiophene-5,5′ dicarbaldehyde was performed according to previously reported procedures, and the details are given below.[20] The detailed synthetic procedures of monomers and the NMR spectra are given below (Figure 4.2-4.12).

Synthesis of 2-(decyloxy) -4,6-dimethylpyrimidine (M1).
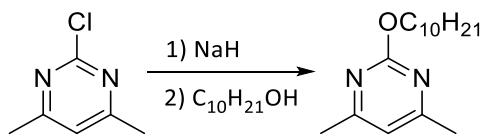
A suspension of 95% sodium hydride (1.09 g, 0.043 mol) in a solvent mixture of toluene and DMF (1:1, 200 mL) was heated at 90 °C, and 1-decanol (8.0 mL, 0.042 mol) was added drop-wise. The resulting mixture was heated at 115 °C for two hours. After two hours, 2-chloro-4,6-dimethylpyrimidine (4.00 g, 0.028 mol) in toluene (25 mL) was added slowly, and the reaction mixture was refluxed for 18 hours. The reaction mixture was cooled to room temperature and poured over ice. The product was extracted with diethyl ether (3×50 mL), washed with deionized water (3×50 mL), dried over anhydrous $MgSO_4$ and concentrated to yield a deep brown oil. The crude product was purified by column chromatography on silica gel with hexane: ethyl acetate (3:1) as the eluent, followed by vacuum distillation to obtain a clear oil. (6.30 g, 85.1%). ^{1}H NMR (500 MHz, $CDCl_3$): δH 6.62 (s, 1H), 4.30 (t, 2H), 2.38 (s, 6H), 1.77 (m, 2H), 1.45 (m, 2H), 1.25 (m, 12H), 0.86 (t, 3H); ^{13}C NMR (500 MHz, $CDCl_3$): δ 169.06, 165.21, 113.62, 67.29, 31.91, 31.60, 29.59, 29.42, 29.33, 29.01, 26.04, 23.85, 22.69, 14.12; EIMS (M$^+$) m/z calculated for C16H28N2O 264.41, found 264.30.
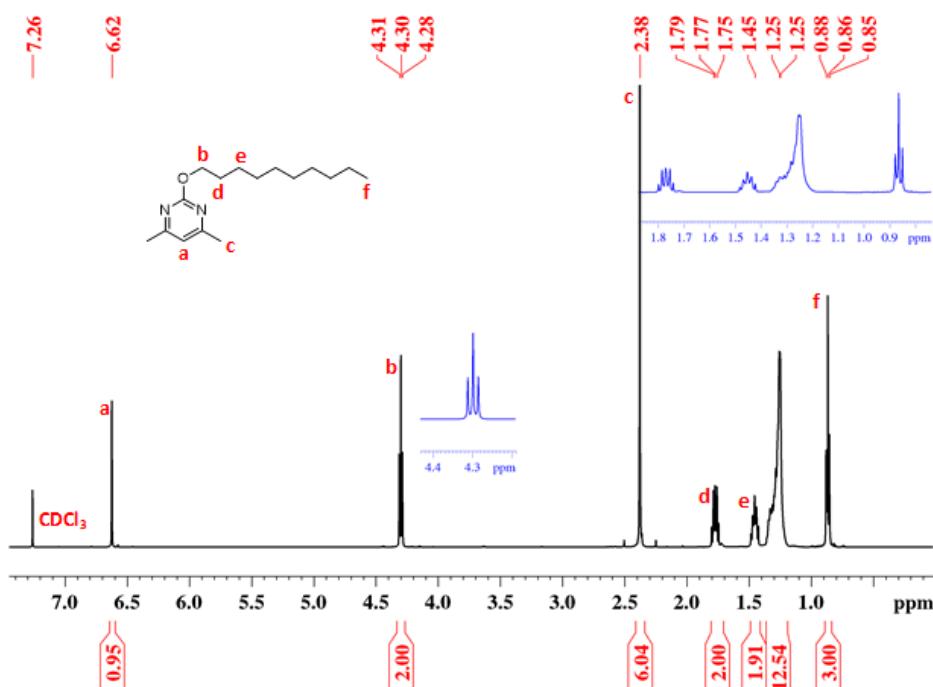
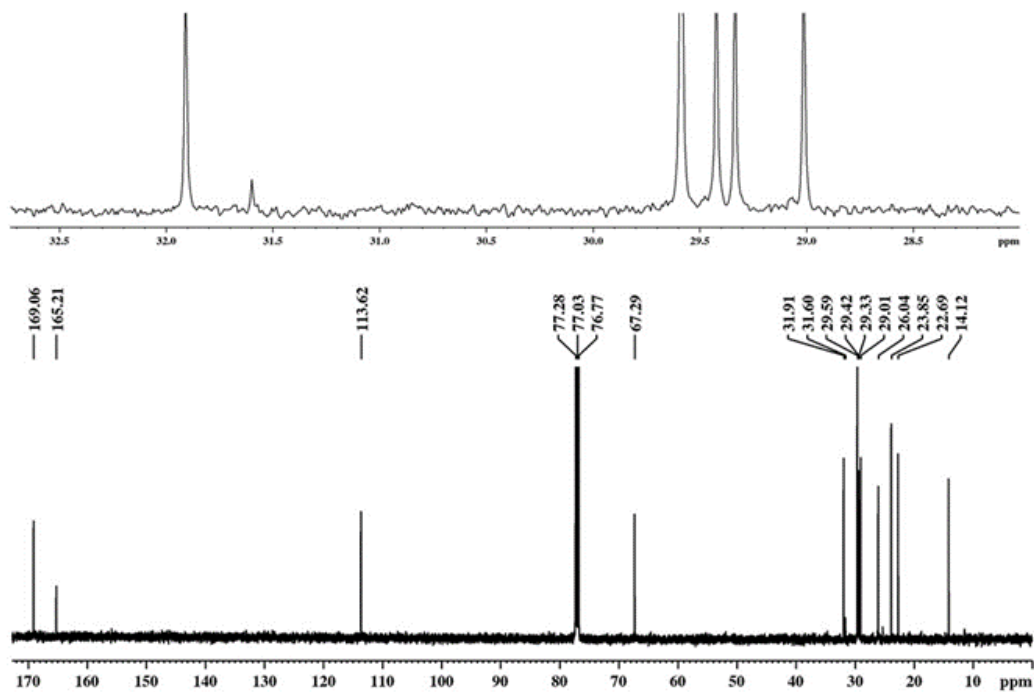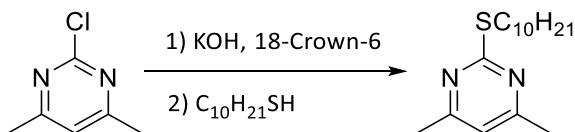**Figure 4.2.** ^{1}H NMR spectrum of 2-(decyloxy)-4,6-dimethylpyrimidine

Figure 4.3. ^{13}C NMR spectrum of 2-(decyloxy)-4,6-dimethylpyrimidine

Synthesis of 2-(decylthio)-4,6-dimethylpyrimidine (M2).

Decane-1-thiol (3.66 g, 0.021 mol) was added to a solution of potassium hydroxide pellets (1.29 g, 0.023 mol) and 18-crown-6 (6.08 g, 0.023 mol) in a mixture of THF and water (3:1, 200 mL) and the reaction mixture was refluxed for 2 hours. After 2 hours, 2-chloro-4,6-dimethylpyrimidine (2.00 g, 0.014 mol) was added, and the reaction mixture was refluxed for 24 hours. The reaction mixture was cooled to room temperature, quenched in water (200 mL) and extracted with diethyl ether (4×50 mL). The organic layer was washed with deionized water (3×200 mL), dried over anhydrous $MgSO_4$ and concentrated yield a clear oil. The product was purified by column chromatography on silica gel using hexane: ethyl acetate (9:1) as the eluent to obtain a clear oil (3.81 g, 97.0%). ^{1}H NMR (500 MHz, $CDCl_3$): δH 6.66 (s, 1H), 3.14 (t, 2H), 2.38 (s, 6H), 1.71 (m, 2H), 1.43 (m, 2H), 1.26 (m, 12H), 0.86 (t, 3H); ^{13}C NMR ($CDCl_3$, 500 MHz) δ: 171.50, 166.82, 115.38, 31.36, 30.73, 29.27, 28.55, 23.86, 22.53, 14.04; EIMS (M[+]) m/z calculated for C16H28N2S 280.47, found 280.10.
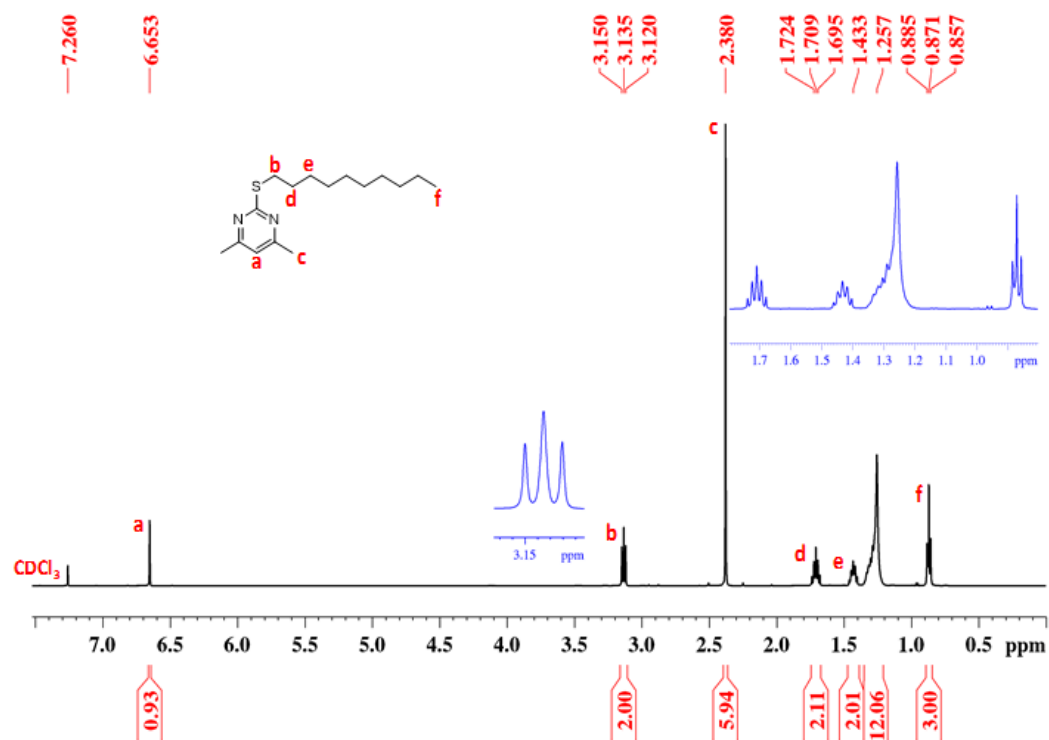
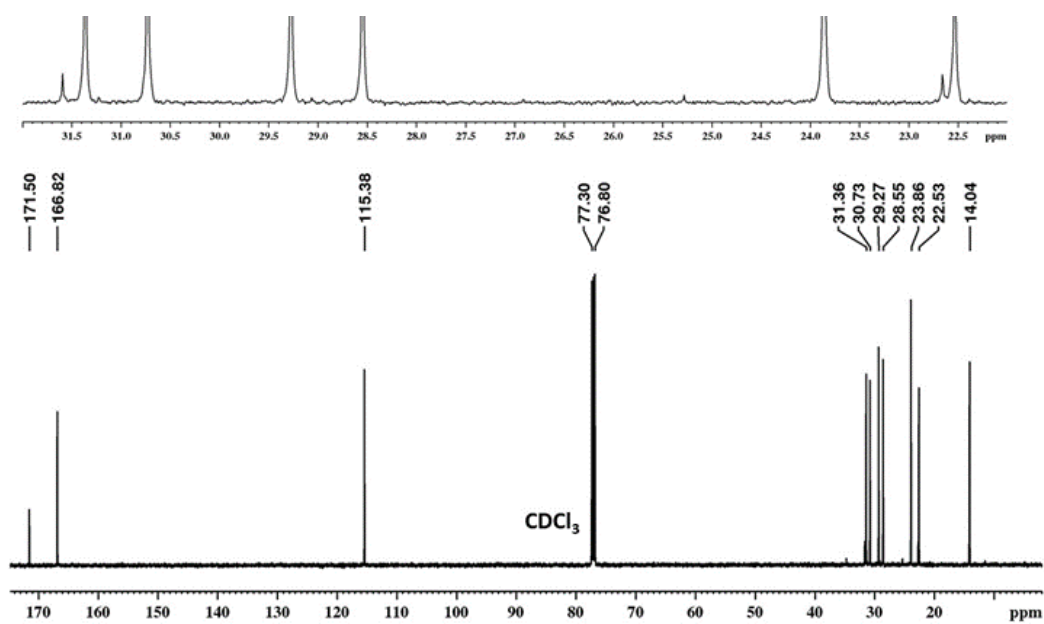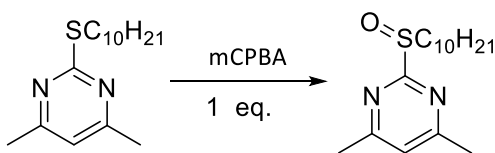**Figure 4.4.** ^{1}H NMR spectrum of 2-(decylthio)-4,6-dimethylpyrimidine

Figure 4.5. ^{13}C NMR spectrum of 2-(decylthio)-4,6-dimethylpyrimidine

Synthesis of 2-(decylsulfinyl)-4,6-dimethylpyrimidine (M3).

77% m-Chloroperoxybenzoic acid (1.57 g, 7.00 mmol) was dissolved in dichloromethane (40 mL) and added dropwise to a solution of 2-(decylthio)-4,6-dimethylpyrimidine (2.00 g, 7.14 mmol) in dichloromethane (10 mL). After 45 minutes, the reaction mixture was warmed to room temperature and stirred for 24 hours. Saturated potassium bicarbonate (10 mL) was added to the reaction mixture and stirred for 3 hours. The product was extracted with dichloromethane (3×50 mL), the organic phase was collected and washed with deionized water (3×50 mL). The organic layer was dried over anhydrous $MgSO_4$ and concentrated to yield a yellow oil. Crude was purified by column chromatography on silica gel with hexane: ethyl acetate (3:2) as the eluent to yield a pale-yellow oil. (1.41 g, 68.1%). ^{1}H NMR (500 MHz, CDCl$_3$): δH 7.05 (s, 1H), 3.01 (m, 2H), 2.55 (s, 6H), 1.90 (m, 1H), 1.64 (m, 1H), 1.42 (m, 2H), 1.21 (m,12H), 0.84 (t, 3H); ^{13}C NMR (500 MHz, CDCl$_3$): δ 172.76, 168.96, 121.04, 54.200, 32.130, 29.740, 29.600, 29.530, 29.390, 28.910, 24.240, 22.930, 22.550, 14.370; HRMS calculated for C16H28N2OS [(M+H)$^+$]:296.47, found: 297.20.
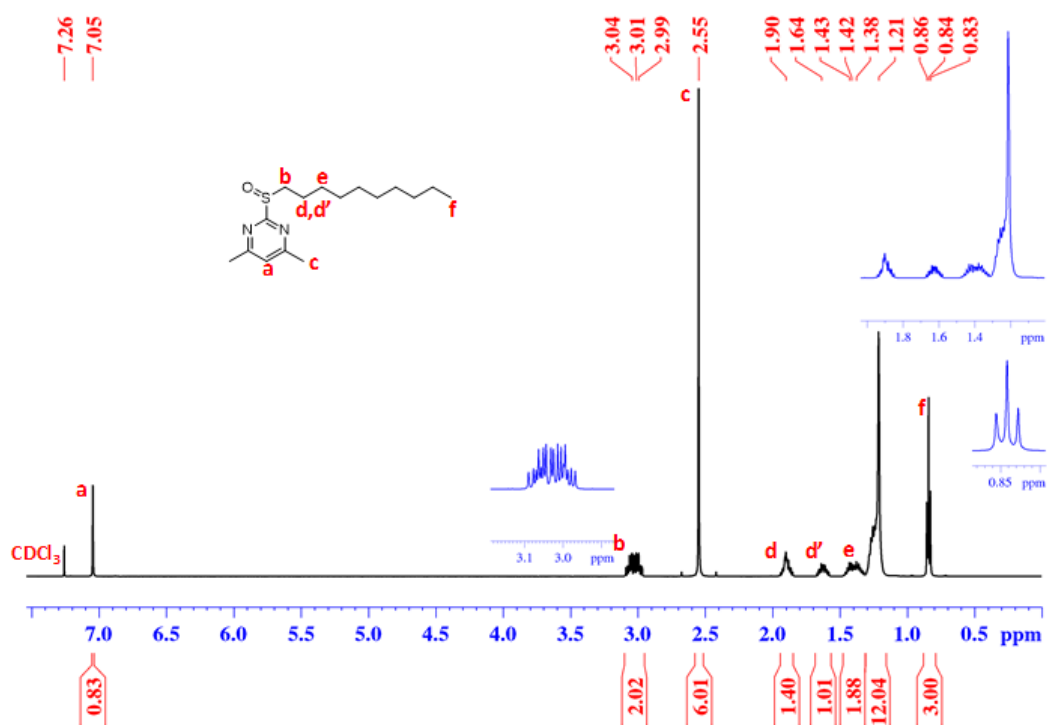
Figure 4.6. ^{1}H NMR spectrum of 2-(decylsulfinyl)-4,6-dimethylpyrimidine
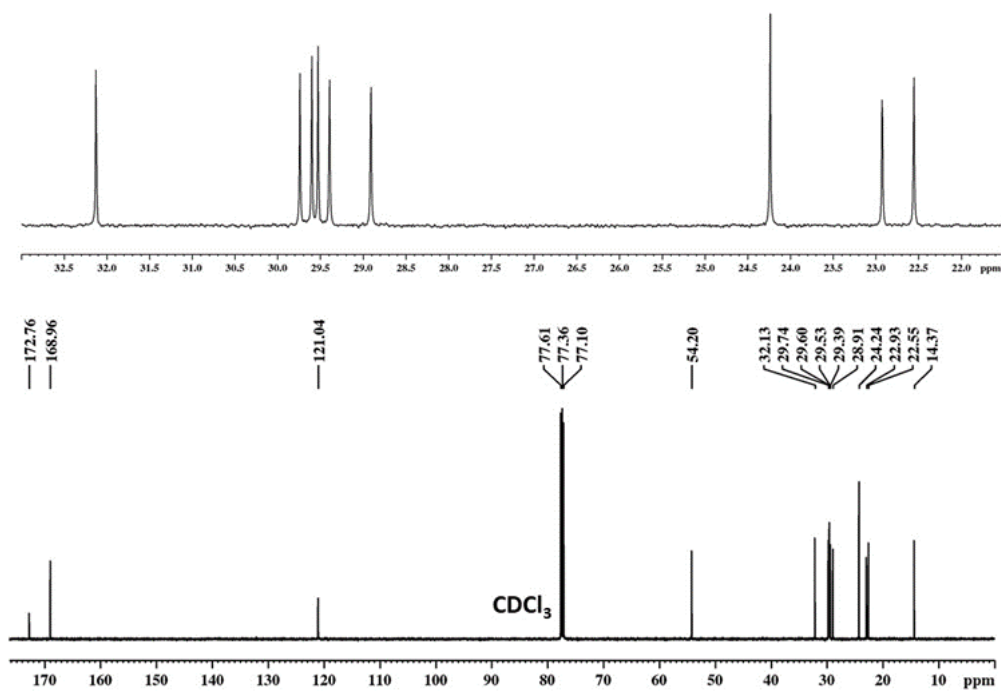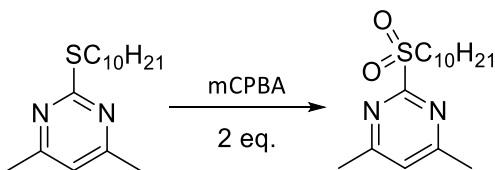

Figure 4.7. ^{13}C NMR spectrum of 2-(decylsulfonyl)-4,6-dimethylpyrimidine

Synthesis of 2-(decylsulfonyl)-4,6-dimethylpyrimidine (M4).

   2-(Decylthio)-4,6- dimethylpyrimidine (2.01 g, 7.17 mmol) was diluted with dichloromethane (100 mL) and cooled over an ice bath. 77% m- Chloroperoxybenzoic acid (3.53 g, 15.8 mmol) was dissolved in dichloromethane (100 mL) and added dropwise while stirring over an ice bath. After 45 minutes, the reaction mixture was removed from the ice bath and stirred for 14 hours at room temperature. Saturated potassium bicarbonate (20 mL) was added to the reaction mixture and stirred vigorously for 3 hours. The compound was extracted with dichloromethane (3×50 mL), the organic yield a colorless oil. Crude was purified by column chromatography on silica gel with hexane: ethyl acetate (3:2) as the eluent to yield a white solid (1.98 g, 88.6%). ^{1}H NMR (500 MHz, CDCl$_3$): δH 7.20 (s, 1H), 3.46 (m, 2H), 2.57 (s, 6H), 1.81 (m, 2H), 1.41 (m, 2H), 1.21 (m, 12H), 0.83 (t, 3H); ^{13}C NMR (500 MHz, CDCl$_3$): δ 169.44, 165.28, 123.08, 51.310, 32.070, 29.660, 29.470, 29.440, 29.180, 28.640, 24.220, 22.870, 22.220, 14.320; HRMS calculated for C16H28N2O2S [(M-H)$^+$]: 312.47, found: 311.18.
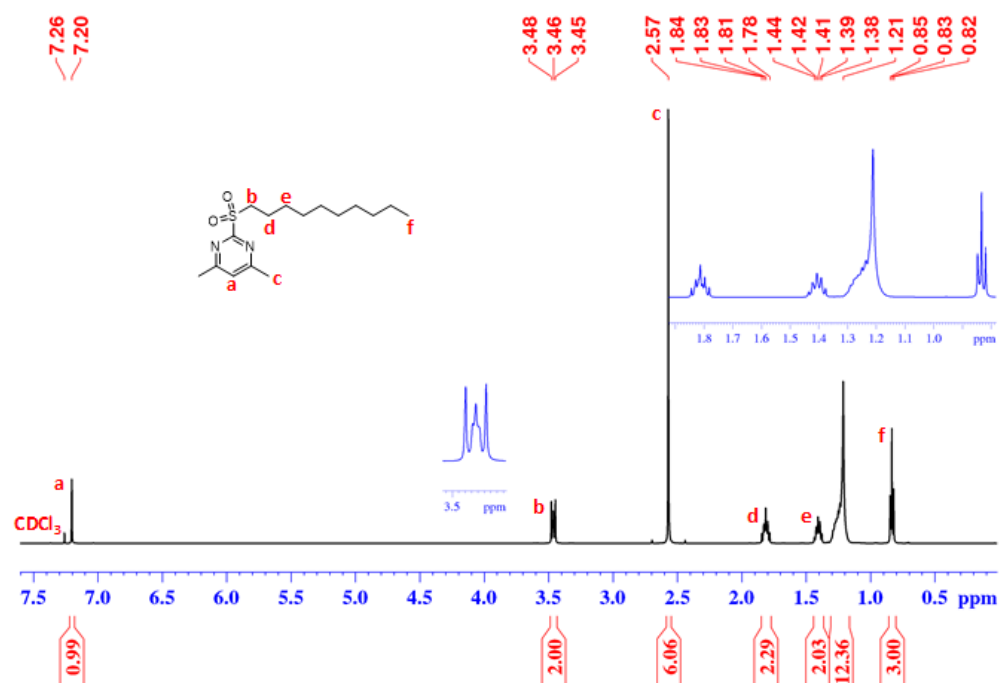
Figure 4.8. ^{1}H NMR spectrum of 2-(decylsulfonyl)-4,6-dimethylpyrimidine
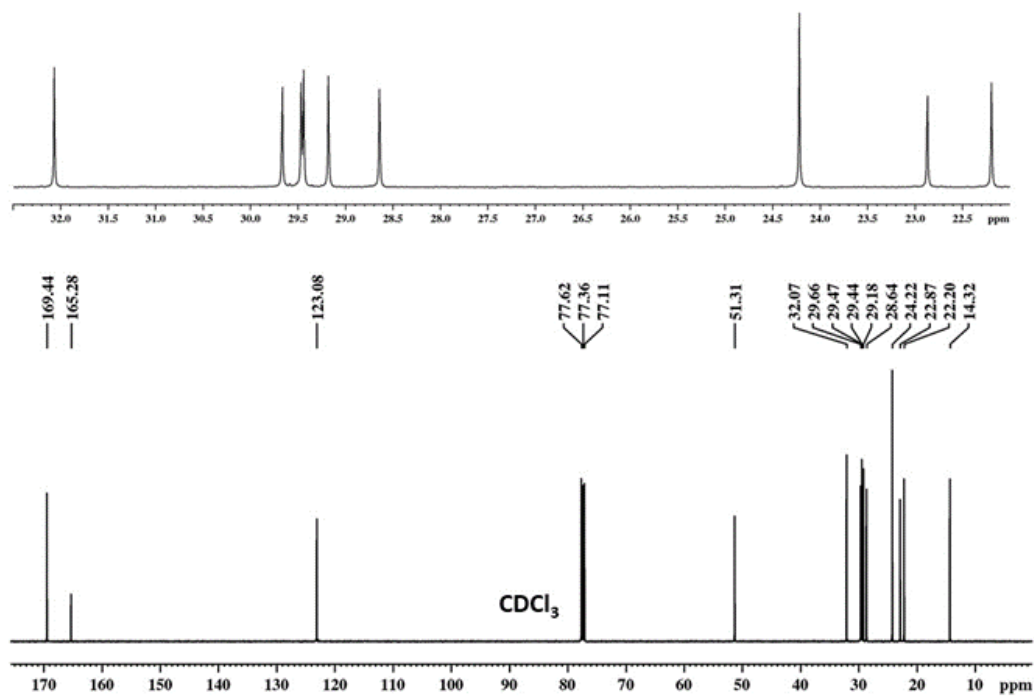

Figure 4.9. ^{13}C NMR spectrum of 2-(decylsulfonyl)-4,6-dimethylpyrimidine

93

Synthesis of 3,3'-dihexyl-2,2'-bithiophene-5,5'-dicarbaldehyde
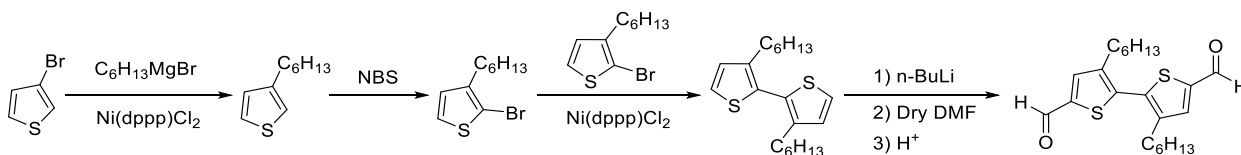
Synthesis of 3-hexylthiophene

Hexylmagnesium bromide (84.50 mL, 0.169 mol) was added slowly to a mixture of 3-bromothiophene (25.0 g, 0.153 mol), and Ni(dppp)Cl$_2$ (0.150 g, 0.277 mmol) in anhydrous diethyl ether (50 mL) and refluxed overnight under nitrogen atmosphere. The reaction mixture was cooled to room temperature and quenched in DI water (100 mL). The compound was extracted with diethyl ether (3×50 mL), the organic layers were combined, washed with DI water (3×50 mL), dried over anhydrous MgSO$_4$, and concentrated to yield a yellow oil. The oil was purified by vacuum distillation to obtain a clear oil (23.9 g, 92.8%). ^{1}H NMR (500 MHz, CDCl$_3$): δH 7.57 (d, 1H), 7.28 (s, 1H), 7.24 (d, 1H), 2.96 (t, 2H), 1.65 (m, 8H), 1.23 (t, 3H); EIMS (M$^+$) m/z calculated for C10H16S 168.30, found 168.10
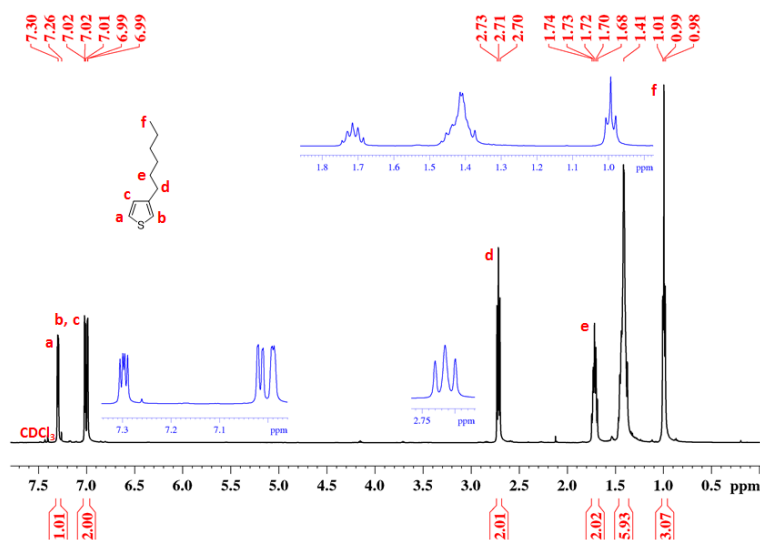
Figure 4.10. ^{1}H NMR spectrum of 3-hexylthiophene

Synthesis of 2-bromo-3-hexylthiophene

3-Hexylthiophene (5.20 g, 0.031 mol) was diluted with a mixture of chloroform and acetic acid (1:1, 100 mL), and N-bromosuccimide (5.23 g, 0.029 mol) was added slowly at room temperature. The compound was extracted with diethyl ether (3×50 mL), the combined organic layer was washed with DI water (3×100 mL), dried over anhydrous $MgSO_4$ and concentrated to yield a yellow oil which was purified by column chromatography on silica gel using hexane as the eluent to obtain a clear oil (6.98 g, 97.4%). ^{1}H NMR (500 MHz, CDCl₃): δH 7.19 (d, 1H), 6.80 (d, 1H), 2.56 (t, 2H), 1.58 (m, 2H), 1.35 (m, 6H), 0.89 (t, 3H); EIMS (M⁺) m/z calculated for C10H15BrS 247.19, found 248.00.
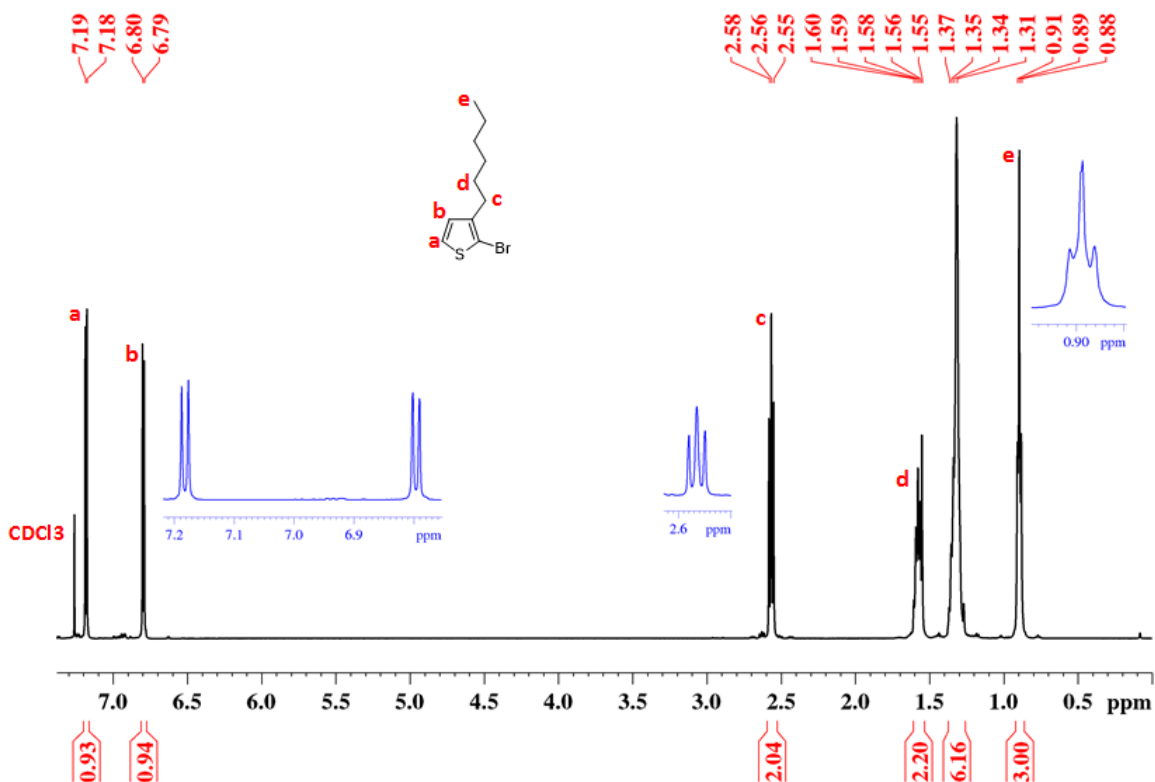
Figure 4.11. ^{1}H NMR spectrum of 2-bromo-3-hexylthiophene

Synthesis of 3, 3'-dihexyl-2, 2'-bithiophene-5, 5'-dicarbaldehyde

3, 3'-dihexyl-2, 2'-bithiophene (1.81 g, 5.40 mmol) was diluted with dry THF (80 mL), and n-BuLi (2.5 M in hexane) (4.8 mL, 12.0 mmol) was added dropwise under a nitrogen atmosphere, while stirring over an ice bath. After 45 minutes, dry DMF (10 mL) was added and stirred for an additional 10 minutes at room temperature. The reaction mixture was quenched in cold hydrochloric acid (1M, 100 mL). The compound was extracted with diethyl ether (3×50 mL), washed with water (3 × 100 mL), the organic layer was dried over anhydrous $MgSO_4$ and concentrated to yield a brown oil. The product was purified by column chromatography on silica gel using hexane: ethyl acetate (19:1) as the eluent to obtain a clear oil (2.00 g, 95.0 %). ^{1}H NMR (500 MHz, CDCl$_3$): δH 9.89 (s, 2H), 7.66 (s, 2H), 2.56 (t, 4H), 1.57 (m, 4H), 1.24 (m, 12H), 0.85 (t, 6H); EIMS (M$^+$) m/z calculated for C22H30O2S2 390.60, found 390.20
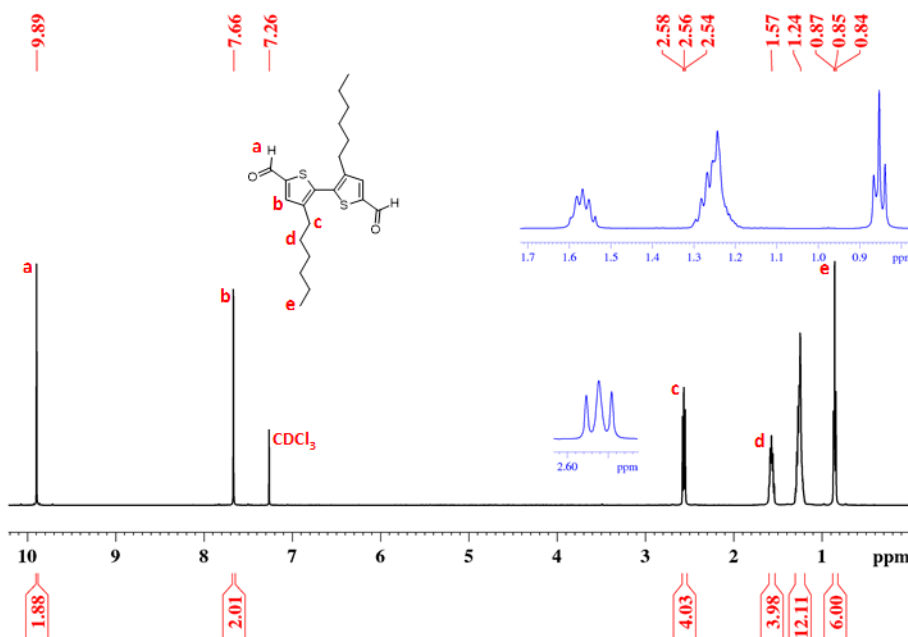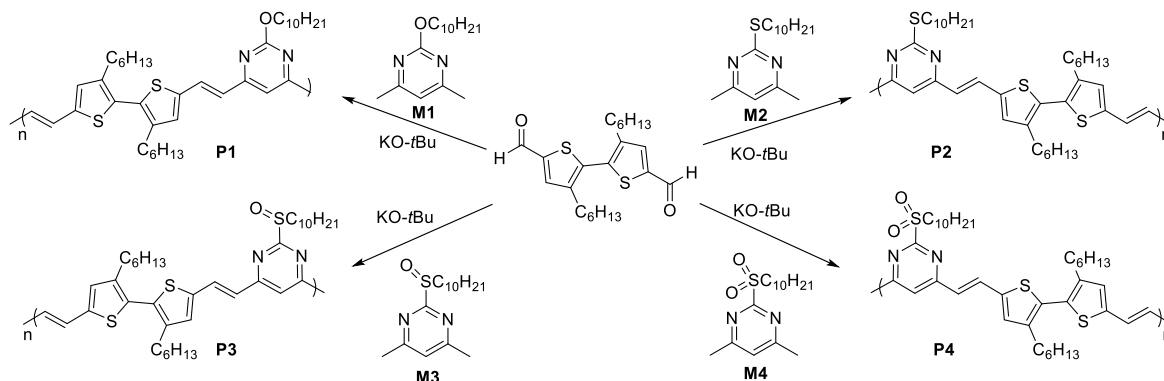

Figure 4.12. ^{1}H NMR spectrum of 3, 3'-dihexyl-2, 2'-bithiophene-5, 5'-dicarbaldehyde

4.3.4 Synthesis of Polymers

The D-A copolymers(P1-P4) were synthesized from 3,3′-dihexyl-2,2″-bithiophene-5,5′-dicarbaldehyde, and the corresponding functionalized pyrimidine monomers (Scheme 4.1.).

Scheme 4.1. The synthesis of pyrimidine-based donor-acceptor copolymers (**P1-P4**)

Synthesis of poly[2-(decyloxy)-4-(2-(3,3'-dihexyl-5'-vinyl-2,2'-bithiophen-5-yl)vinyl)-6vinylpyrimidine] (P1).

An oven dried 50 mL three neck round bottom flask was charged with 2-(decyloxy)-4,6-dimethylpyrimidine (0.249 g, 0.942 mmol) and degassed with nitrogen for 15 minutes. Potassium t-butoxide (0.212 g, 1.89 mmol) and 18-crown-6 (0.500 g, 1.89 mmol) were dissolved in dry THF (5 mL) under a nitrogen atmosphere, added to the round bottom along with dry toluene (10 mL) and heated at 85 °C for an hour. In a separate vial, 3,3'-dihexyl-2,2'-bithiophene-5,5'-dicarbaldehyde (0.368 g, 0.942 mmol) was diluted with dry THF (5 mL) under nitrogen atmosphere and added to the flask. The reaction mixture was heated at 85 °C under a nitrogen atmosphere for 24 hours. The reaction mixture was cooled to room temperature, the polymer was extracted with chloroform (4×100 mL), and the organic layers were combined. The organic phase was washed with deionized water (4×100 mL), dried over anhydrous MgSO$_4$ and concentrated in

vacuo. The polymer was precipitated in cold methanol, filtered and purified by Soxhlet extractions with methanol, hexane, and chloroform. The chloroform layer was evaporated *in vacuo* and precipitated in cold methanol. The polymer was filtered, vacuum dried to yield a red solid (0.285 g, 45.1%, Mn = 8.2 kDa, PDI = 2.1) and stored in glove box. ^{1}H NMR spectrum is shown in Figure 4.13. The peak at ~ 3.66 ppm may be due to the presence of soluble oxidized product of the **P1**, which has not been clearly identified or reported. Similar procedure was followed to synthesize 2-(decylthio)-4,6-dimethylpyrimidine (**P2**), 2-(decylsulfinyl)-4,6-dimethylpyrimidine (**P3**) and 2-(decylsulfonyl)-4,6-dimethylpyrimidine (**P4**), separately. The ^{1}H NMR spectra are shown in Figure 4.14., 4.15., and 4.16., respectively, and the SEC measurements are summarized in Table 4.1.

Figure 4.13. ^{1}H NMR spectrum of poly[2-(decyloxy)-4-(2-(3,3'-dihexyl-5'-vinyl-2,2'-bithiophen-5-yl)vinyl)-6- vinylpyrimidine] **(P1)**

Figure 4.14. ^{1}H NMR spectrum of poly[2-(decylthio)-4-(2-(3,3'-dihexyl-5'-vinyl-2,2'-bithiophen-5-yl)vinyl)-6-vinylpyrimidine] **(P2)**
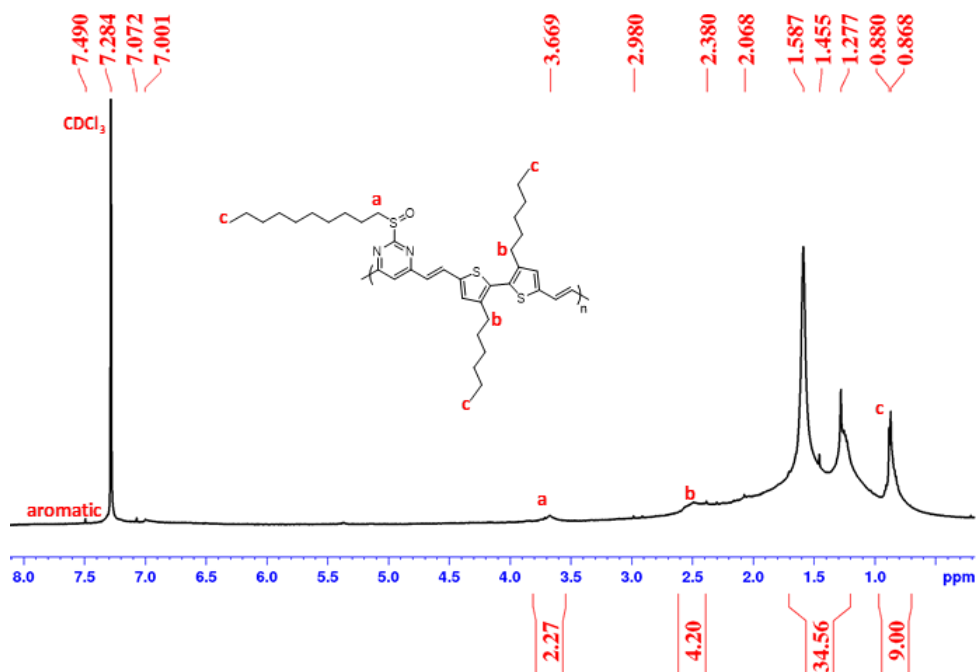
Figure 4.15. ^{1}H NMR spectrum of poly[2-(decylsulfinyl)-4-(2-(3,3'-dihexyl-5'-vinyl-2,2'-bithiophen-5-yl)vinyl)-6-vinylpyrimidine] **(P3)**
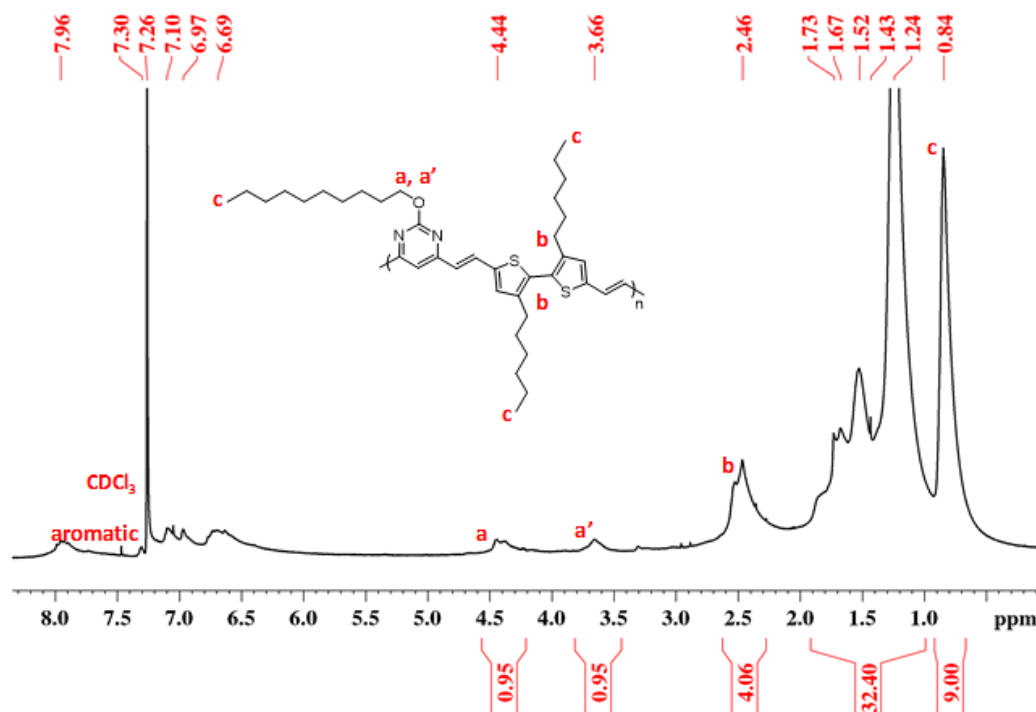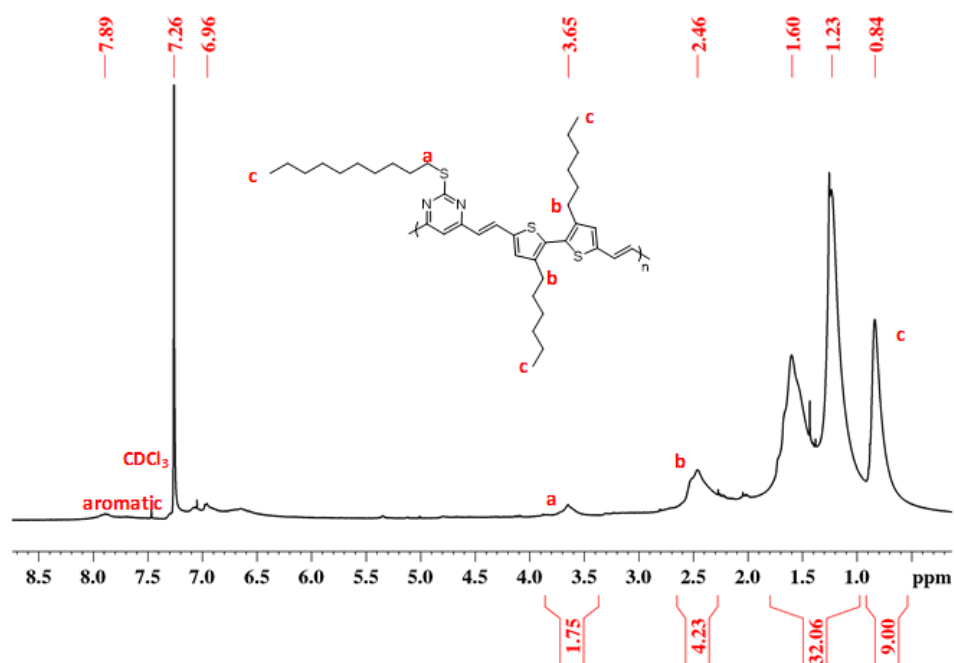
Figure 4.16. ^{1}H NMR spectrum of poly[2-(decylsulfonyl)-4-(2-(3,3'-dihexyl-5'-vinyl-2,2'-bithiophen-5-yl)vinyl)-6-vinylpyrimidine] **(P4)**
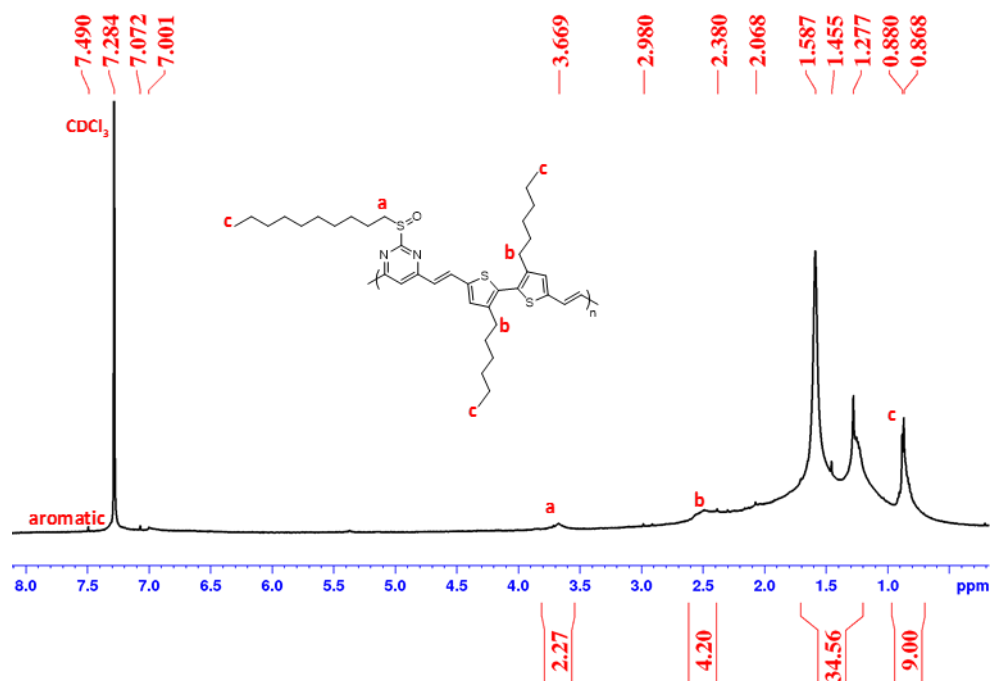
Table 4.1. Characteristics of Polymer **P1-P4**

Polymer	Mn (kDa)	PDI[a]	HOMO[b] (eV)	LUMO[c] (eV)	Eg[d] (eV)	Eg[e](eV)	λ_{max}[f] (nm)	λ_{max}[g] (nm)
P1	8.2	2.1	-5.28	-3.03	2.25	2.16	380	387
P2	7.4	2.4	-5.37	-3.14	2.23	2.19	385	389
P3	7.0	2.6	-5.45	-3.24	2.21	2.11	386	391
P4	6.1	2.6	-5.52	-3.36	2.16	2.02	394	400

[a] Measured by SEC using polystyrene standards with THF as eluent. [b] Estimated from the oxidation peak of the cyclic voltammograms. [c] Estimated from the reduction-oxidation peak of the cyclic voltammograms. [d] Calculated from LUMO [c] – HOMO [b]. [e] Calculated from the onset of UV-vis absorption in a thin film. [f] UV-vis in chloroform solution. [g] UV-vis in a thin film

4.4 Results and Discussion

4.4.1   Optical and electrochemical properties

The absorption spectra of the polymers in chloroform solution and solid state are shown in Figure 4.17. for all four polymers in solution and in thin film. The maximum of absorption indicates the transitions from π-π* states delocalized along the conjugated polymer backbone.[20,36–38] The much smaller bathochromic shift of the absorption band and the absence of the vibronic peak in the solid-state spectra indicate the poor intermolecular π-π stacking most likely due to the amorphous nature of polymer in the solid state.[39,40] HOMO and LUMO energy levels of polymers, **P1-P4**, were estimated from the oxidation and reduction curves (Figure 4.18.) measured by cyclic voltammetry using the equation: $E_{LUMO} = -(E_{red} + 4.8 - E_{1/2}, Fc/Fc^+)$ eV; $E_{HOMO} = -(E_{ox} + 4.8 - E_{1/2}, Fc/Fc^+)$ eV. The calculated HOMO and LUMO energy levels are given in Table 4.1. The HOMO/LUMO energy level of **P1** (-5.28/-3.03 eV) was higher than that of the HOMO/LUMO level of **P2-P4**, indicating the higher electron donating ability of decyloxy side chain attached to **P1** as compared to the less donating decylthio side chain (**P2**). Oxidation of the thioalkyl substituent of electron withdrawing decylsulfinyl (**P3**) or decylsulfonyl (**P4**) side chains, further lowered both HOMO and LUMO levels of the resultant polymer. Notably, the pyrimidine unit attached to the electron-withdrawing substituent lowered the HOMO/LUMO levels depending on the electron withdrawing strength.
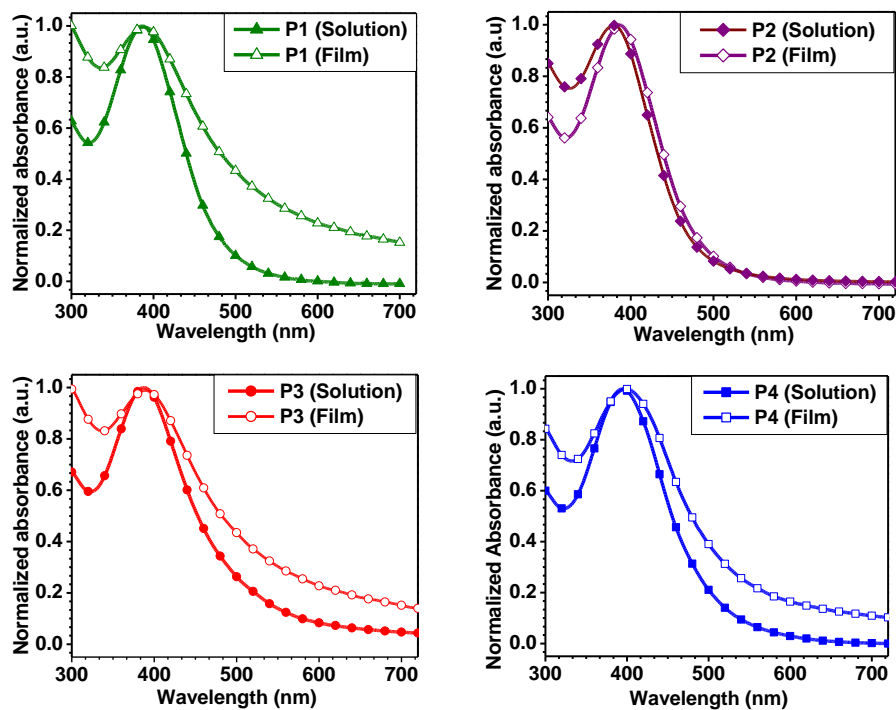
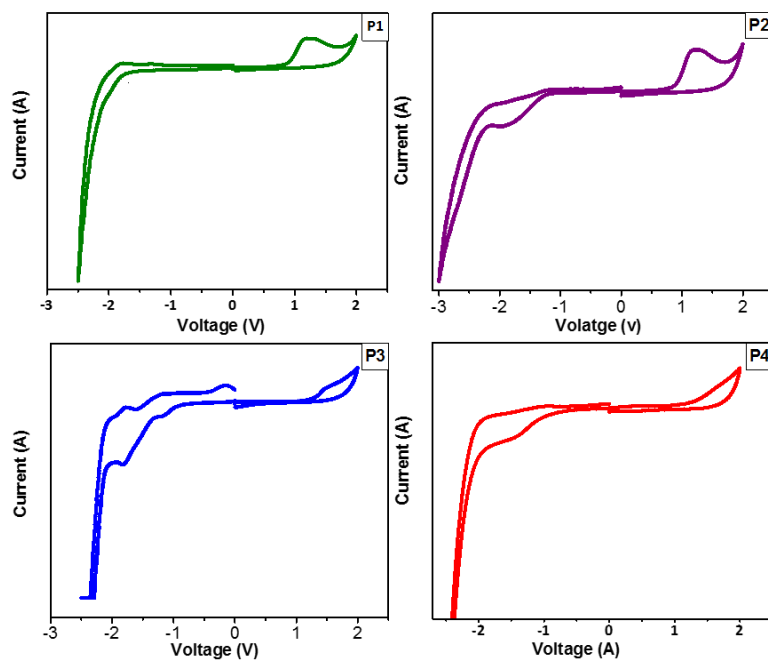**Figure 4.17.** UV-Vis spectra of polymers, **P1-P4**, in chloroform solutions and thin films

Figure 4.18. Cyclic voltammograms of polymers, **P1-P4**.

4.4.2 Structural Analysis

The estimation of the molecular geometry and electronic distribution of the frontier orbitals of the polymers was performed by density functional theory (DFT) calculations using Spartan 06 at the level of B3LYP/6- 31G*. The DFT calculations for dimers were performed, and all alkyl groups were replaced by methyl groups to simplify the calculation (Figure 4.19 and 4.20). The calculations demonstrated that the HOMOs were mostly concentrated on the donor moiety while the LUMO of the polymers were distributed over the entire conjugated backbone (Figure 2.20.). The calculated HOMO/LUMO energies of dimers of **P1**, **P2**, **P3**, and **P4** were −5.23 eV/−2.33 eV, -5.30 eV/−2.41 eV, −5.52 eV/−2.73 eV, and −5.57 eV/−2.83 eV, respectively. This data is consistent with the results obtained from the CV analysis and UV-vis absorption spectra (Table 4.1). As displayed in Figure. 4.19, polymer backbones, **P1**, **P2**, **P3**, and **P4** are not coplanar as the thiophene rings generated dihedral angles of 42.99°, 43.11°, 42.48°, and 40.05° with the adjacent thiophene rings, respectively.

P1) Φ_1 = 0.16° ; Φ_2 = 5.92° ; Φ_3 =42.99°   P2) Φ_1 = 0.19°; Φ_2 =5.78 °; Φ_3 =43.11°
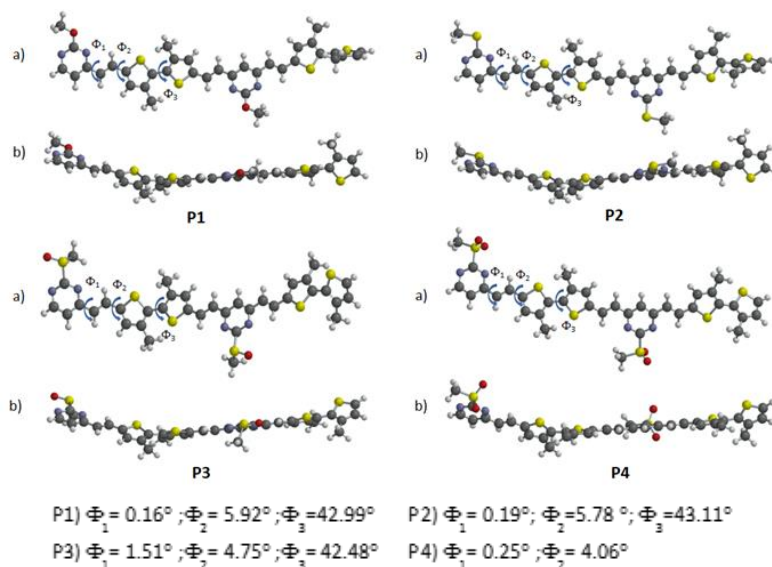P3) Φ_1 = 1.51° ; Φ_2 = 4.75° ; Φ_3 = 42.48°   P4) Φ_1 = 0.25° ; Φ_2 = 4.06°

Figure 4.19. (a) The top and (b) side views of molecular geometries of the respective two repeating units of polymers **(P1- P4)**.
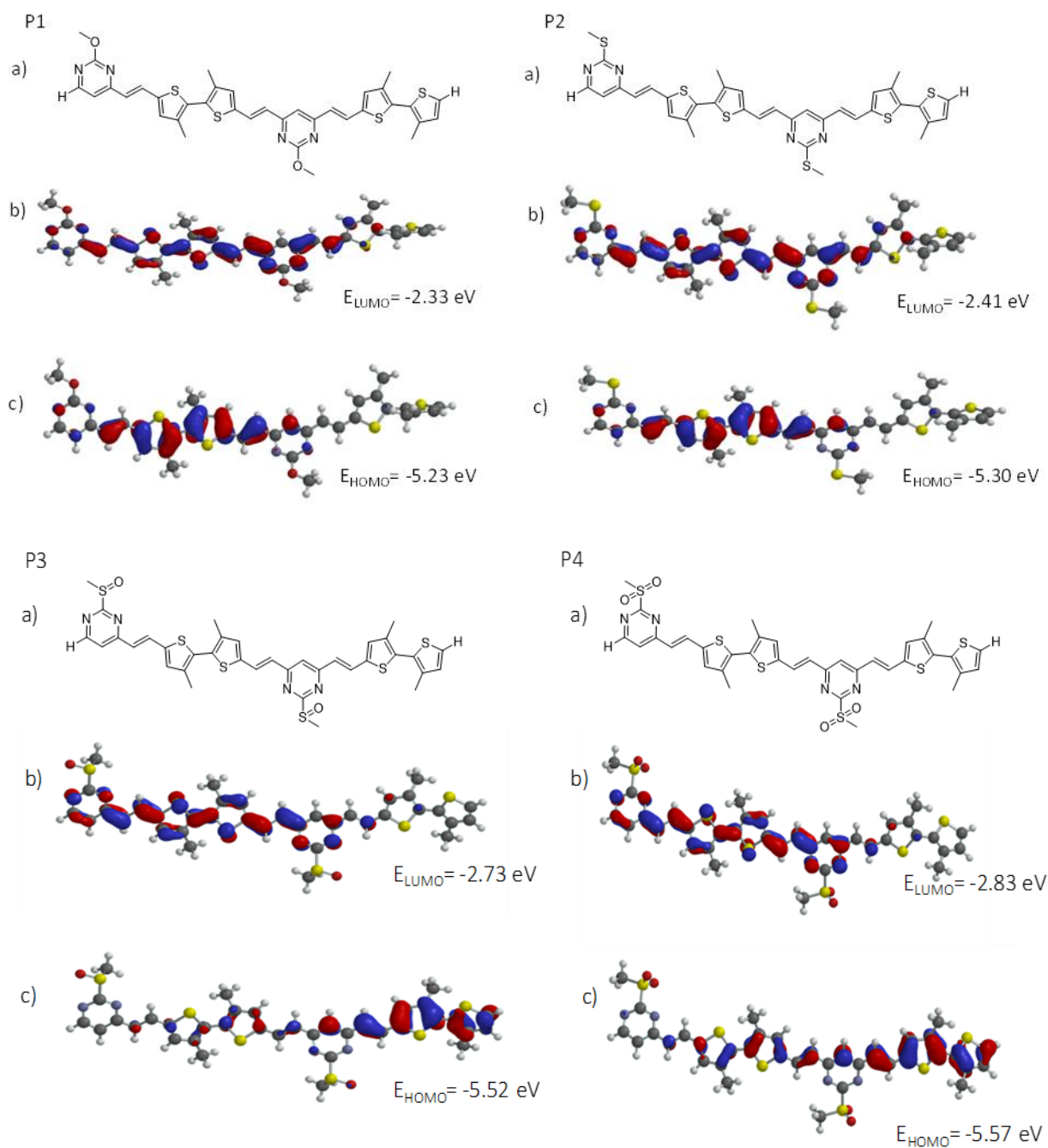
Figure 4.20. (a) Chemical structures, b) calculated LUMO, c) calculated HOMO of the respective two repeating units of polymers **P1**, **P2**, **P3**, and **P4**.

In the theoretical studies, a simplification has been established by replacing the long alkyl chains with methyl group. However, previously reported studies proved that the conjugated polymers with variable alkyl side chain length have a variable effect on the structural conformation and the electronic properties of the conjugated polymers.[41,42] Moreover, this computer modelling approach shows the results obtained for oligomers (two repeating units) and do not consider the interaction between adjacent alkyl chains.[41,43] Therefore, the results obtained from theoretical studies with simplifications would be sufficiently good approximation, but not precise.

4.4.3   X-ray and Morphology analysis

The crystallinity of the polymer thin films was investigated by X-ray diffraction analysis. The less intense, halo-like broad diffraction peaks centered around $2\theta \sim 20°$, shown in Figure 4.19, were observed for all four polymers which indicated the amorphous nature of the polymers, **P1-P4**.[20,40,44] The film morphology of the polymers, **(P1-P4)**, was investigated by TMAFM analysis. The polymer films displayed granular morphology (Figure 4.21, and 4.22) which resulted in a non-uniform surface. The TMAFM analysis also supports the amorphous nature of the polymers that was also proved by X-ray diffraction analysis results. Effort to fabricate bottom-gate bottom contact, and top-gate bottom contacted OFETs with all the synthesized polymers showed field effect mobility values lower than 10^{-6} cm^2/V^{-1}s most likely due to the amorphous nature of the polymers.

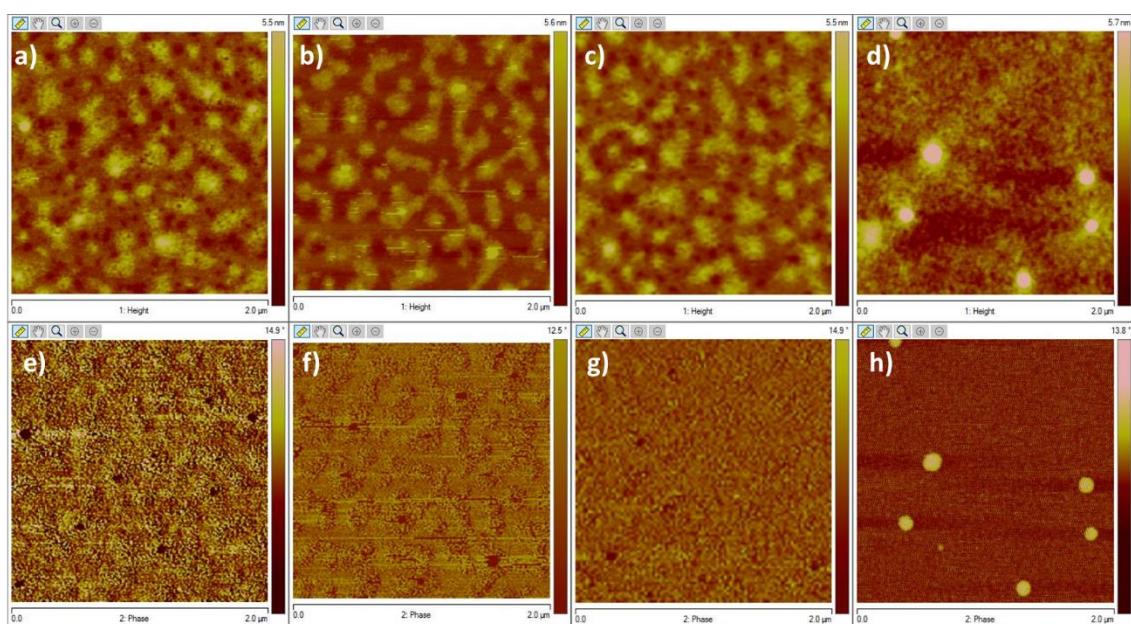**Figure 4.21.** Height and phase TMAFM images of thin film deposited on mica (2×2 µm); **P1** (a, e), **P2** (b, f), **P3** (c, g), and **P4** (d, h).
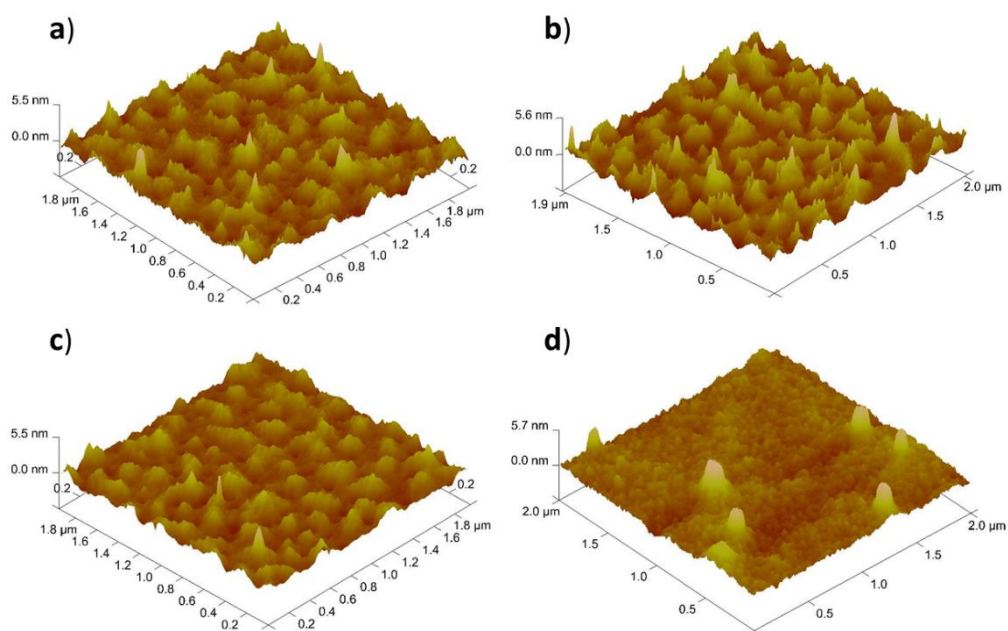

Figure 4.22. 3-D Height TMAFM images of thin film deposited on mica (a) **P1**, (b)**P2**, (c) **P3**, and (d) **P4**.

4.5 Conclusion

In summary, a series of pyrimidine containing donor–acceptor alternating copolymers, poly[2-(decyloxy)-4-(2-(3,3'-dihexyl-5'-vinyl-2,2'-bithiophen-5-yl)vinyl)-6-vinylpyrimidine] **(P1)**, poly[2-(decylthio)-4-(2-(3,3'-dihexyl-5'-vinyl-2,2'-bithiophen-5-yl)vinyl)-6-vinylpyrimidine] **(P2)**, poly[2-(decylsulfinyl)-4-(2-(3,3'-dihexyl-5'-vinyl-2,2'-bithiophen-5-yl)vinyl)-6-vinylpyrimidine] **(P3)**, and poly[2-(decylsulfonyl)-4-(2-(3,3'-dihexyl-5'-vinyl-2,2'-bithiophen-5-yl)vinyl)-6-vinylpyrimidine] **(P4)** were synthesized. The ability to perform the nucleophilic aromatic substitution on the pyrimidine ring coupled with the ease of substitution modification by oxidizing the sulfur atom of the substituent allowed pyrimidine to be functionalized with highly solubilizing flexible side chains that improved the solution processability of the polymers. Furthermore, opto-electronic properties of the polymers can be tuned by varying the electron withdrawing strength of the acceptor moiety. The reported pyrimidine-based polymers show favorable HOMO and LUMO energy levels that indicate some potential for application in optoelectronic devices. However, the structural disorder created an energy barrier to charge transport that adversely affected the charge carrier mobility by creating electronic traps. Improvement in the molecular weight with a good PDI value is currently under investigation which would be expected to give much a deeper lying LUMO energy levels that could yield to improved electron mobility and offer a path to develop novel, air-stable n-type semiconducting materials.

4.6 References

1.   Piliego, C., Holcombe, T. W., Douglas, J. D., Woo, C. H., Beaujuge, P. M., Fréchet, J. M. J. J. Am. Chem. Soc., 2010, 132, 7595–7597.

2.   Qin, R., Li, W., Li, C., Du, C., Veit, C., Schleiermacher, H.-F., Andersson, M., Bo, Z., Liu, Z., Inganäs, O., Wuerfel, U., Zhang, F. J. Am. Chem. Soc., 2009, 131, 14612–14613.

3.   Lijun, H., Shaoqing, Z., Xia, G., Feng, X., Yongfang, L., Jianhui, H. Angew. Chemie Int. Ed., 50, 9697–9702.

4.   A., S. R. Adv. Mater., 21, 2007–2022.

5.   Mei, J., Diao, Y., Appleton, A. L., Fang, L., Bao, Z. J. Am. Chem. Soc., 2013, 135, 6724–6746.

6.   Boroumand, F. A., Fry, P. W., Lidzey, D. G. Nano Lett., 2005, 5, 67–71.

7.   Tsumura, A., Koezuka, H., Ando, T. Appl. Phys. Lett., 1986, 49, 1210–1212.

8.   Jurchescu, O. D., Popinciuc, M., van Wees, B. J., Palstra, T. T. M. Adv. Mater., 2007, 19, 688–692.

9.   Minemawari, H., Yamada, T., Matsui, H., Tsutsumi, J., Haas, S., Chiba, R., Kumai, R., Hasegawa, T. 2011, 475, 364.

10.   Li, J., Zhao, Y., Tan, H. S., Guo, Y., Di, C.-A., Yu, G., Liu, Y., Lin, M., Lim, S. H., Zhou, Y., Su, H., Ong, B. S. 2012, 2, 754.

11.   Luo, C., Kyaw, A. K. K., Perez, L. A., Patel, S., Wang, M., Grimm, B., Bazan, G. C., Kramer, E. J., Heeger, A. J. Nano Lett., 2014, 14, 2764–2771.

12.   Diao, Y., Tee, B. C.-K., Giri, G., Xu, J., Kim, D. H., Becerril, H. A., Stoltenberg, R. M., Lee, T. H., Xue, G., Mannsfeld, S. C. B., Bao, Z. Nat Mater, 2013, 12, 665–671.

13.   Kang, I., Yun, H.-J., Chung, D. S., Kwon, S.-K., Kim, Y.-H. J. Am. Chem. Soc., 2013, 135, 14896–14899.

14.   Li, H., Tee, B. C.-K., Cha, J. J., Cui, Y., Chung, J. W., Lee, S. Y., Bao, Z. J. Am. Chem. Soc., 2012, 134, 2760–2765.

15.   Xu, X., Yao, Y., Shan, B., Gu, X., Liu, D., Liu, J., Xu, J., Zhao, N., Hu, W., Miao, Q. Adv. Mater., 2016, 28, 5276–5283.

16. Liu, Y., Zhao, J., Li, Z., Mu, C., Ma, W., Hu, H., Jiang, K., Lin, H., Ade, H., Yan, H. Nat. Commun., 2014, 5, 5293.

17. F., M. P., Iryna, Y., Jurriaan, H. Adv. Mater., 24, 5526–5541.

18. Mei, J., Bao, Z. Chem. Mater., 2014, 26, 604–615.

19. Casey, A., Ashraf, R. S., Fei, Z., Heeney, M. Macromolecules, 2014, 47, 2279–2288.

20. Gunathilake, S. S., Magurudeniya, H. D., Huang, P., Nguyen, H., Rainbolt, E. A., Stefan, M. C., Biewer, M. C. Polym. Chem., 2013, 4, 5216–5219.

21. Carsten, B., Szarko, J. M., Son, H. J., Wang, W., Lu, L., He, F., Rolczynski, B. S., Lou, S. J., Chen, L. X., Yu, L. J. Am. Chem. Soc., 2011, 133, 20468–20475.

22. McCullough, R. D., Williams, S. P. J. Am. Chem. Soc., 1993, 115, 11608–11609.

23. Wu, X., Chen, T.-A., Rieke, R. D. Macromolecules, 1995, 28, 2101–2102.

24. Lin, Y., Chen, X., Jiang, C., Zhao, M., Li, Y., Wang, H. Org. Electron., 2018.

25. Zhang, Q. T., Tour, J. M. J. Am. Chem. Soc., 1998, 120, 5355–5362.

26. Nielsen, C. B., Sohn, E.-H., Cho, D.-J., Schroeder, B. C., Smith, J., Lee, M., Anthopoulos, T. D., Song, K., McCulloch, I. ACS Appl. Mater. Interfaces, 2013, 5, 1806–1810.

27. Banno, M., Yamaguchi, T., Nagai, K., Kaiser, C., Hecht, S., Yashima, E. J. Am. Chem. Soc., 2012, 134, 8718–8728.

28. Li, H., Sundararaman, A., Venkatasubbaiah, K., Jäkle, F. J. Am. Chem. Soc., 2007, 129, 5792–5793.

29. Schneider, J. A., Dadvand, A., Wen, W., Perepichka, D. F. Macromolecules, 2013, 46, 9231–9239.

30. Xiong, Y., Qiao, X., Li, H. Polym. Chem., 2015, 6, 6579–6584.

31. Zhao, Y., Guo, Y., Liu, Y. Adv. Mater., 2013, 25, 5372–5391.

32. Guo, X., Facchetti, A., Marks, T. J. Chem. Rev., 2014, 114, 8943–9021.

33. Zhan, X., Tan, Z., Domercq, B., An, Z., Zhang, X., Barlow, S., Li, Y., Zhu, D., Kippelen, B., Marder, S. R. J. Am. Chem. Soc., 2007, 129, 7246–7247.

34. Yamamoto, T., Lee, B.-L. Macromolecules, 2002, 35, 2993–2999.

35. Gunathilake, S. S., Huang, P., Bhatt, M. P., Rainbolt, E. A., Stefan, M. C., Biewer, M. C. RSC Adv., 2014, 4, 41997–42001.

36. Shi, C., Yao, Y., Yang, Pei, Q. J. Am. Chem. Soc., 2006, 128, 8980–8986.

37. Liu, J., Zhang, R., Sauvé, G., Kowalewski, T., McCullough, R. D. J. Am. Chem. Soc., 2008, 130, 13167–13176.

38. Song, H. J., Kim, D. H., Lee, E. J., Haw, J. R., Moon, D. K. Sol. Energy Mater. Sol. Cells, 2014, 123, 112–121.

39. Noriega, R., Rivnay, J., Vandewal, K., Koch, F. P. V, Stingelin, N., Smith, P., Toney, M. F., Salleo, A. Nat Mater, 2013, 12, 1038–1044.

40. Kong, H., Lee, D. H., Seo, J.-I., Oh, J.-Y., Chung, D. S., Park, J.-W., Kwon, S.-K., Lee, Y. S., Park, C. E., Shim, H.-K. ACS Appl. Mater. Interfaces, 2010, 2, 1100–1106.

41. Oliveira, E. Mater. Res., 2014, 17, 1369.

42. Batagin-Neto, A., Oliveira, E. F., Graeff, C. F. O., Lavarda, F. C. Mol. Simul., 2013, 39, 309–321.

43. Zhuang, W., Lundin, A., Andersson, M. R. J. Mater. Chem. A, 2014.

44. Chen, C.-H., Hsieh, C.-H., Dubosc, M., Cheng, Y.-J., Hsu, C.-S. Macromolecules, 2010, 43, 697–708.

BIOGRAPHICAL SKETCH

Vasanthy Karmegam was born and raised in Matale, Sri Lanka. She completed her high school education at Pakkiyam National College, Matale and finished her undergraduate studies at University of Peradeniya, Sri Lanka, where she received her BS in Chemistry and Biology in 2010. In 2012, she completed her MS in Nanoscience and Nanotechnology at University of Peradeniya, Sri Lanka. In Fall 2013, she entered the Ph.D. program in Chemistry at The University of Texas at Dallas.

CURRICULUM VITAE

Vasanthy Karmegam

Address: Department of Chemistry and Biochemistry, BE 26
The University of Texas at Dallas
800 W Campbell Rd, Richardson, TX 75080
Email: vasanthykarmegam@gmail.com

Education:

The University of Texas at Dallas, Richardson, TX   November 2017
Ph.D. candidate in Chemistry
Dissertation: 'Functional Polymers for Drug Delivery and Opto-electronic Applications'
Advisor: Prof. Mihaela C. Stefan

The University of Peradeniya, Sri Lanka   June 2012
M.S. in Nanoscience and Nanotechnology
Dissertation: 'ZnO nanoparticle coated cellulose for anti-bacterial activity'
Advisor: Prof. RMG. Rajapakse

The University of Peradeniya, Sri Lanka   July 2010
B.S. in Chemistry and Biology

Graduate Research Experience:

Stimuli responsive, biodegradable functionalized poly(ε-caprolactone)s based micellar systems for drug delivery application
- Focused on multi-step synthesis of functionalized caprolactone monomers and ring-opening polymerization of -substituted caprolactone monomers
- Developed and characterized of micellar drug formulation for anti-cancer drug delivery
- Biological screening on micellar drug formulation for anti-cancer drug delivery

Nitrogen based semiconducting polymers for optoelectronic applications
- Focused on multi-step synthesis of functionalized pyrimidine monomers, purification and characterization
- Developed a series of solution processible semiconducting copolymers and analyzed the optoelectronic and morphological properties
- Studied the copolymers for optoelectronic application including OFETs and solar cells

Publications:

1. **Karmegam, Vasanthy**; Chinthake, Mahesh U.G.; Biewer, M.C.; Stefan, Mihaela C., Synthesis and Opto-electronic Properties of Functionalized Pyrimidine-based Conjugated Polymers, *Journal of Polymer Science Part A: Polymer Chemistry*, **2018**, 56, 2547-2553.
2. **Karmegam, Vasanthy**; Biewer, M.C.; Stefan, Mihaela C., Enhanced DOX Loading in Benzyl Functionalized- Polycaprolactone Micelles Based on Star-Polymer Architecture. (Journal of Material Chemistry B-Submitted).
3. **Karmegam, Vasanthy**; Biewer, M.C.; Stefan, Mihaela C., Star Polymer Micellar System for Co-delivery of Doxorubicin and Resveratrol (Manuscript in preparation).
4. **Karmegam, Vasanthy**; Soltantabar, Pooneh; Calubaquib, Erika Joy L.; Kularatne, Ruvanthi, N.; Stefan, Mihaela **C.** Biodegradable Aliphatic Polyesters for Drug Delivery, *Material Matters,* **2017,** *12*, 37-41.
5. Washington, K. E., Kularatne, R. N., **Karmegam, V.**, Biewer, M. C., Stefan, M. C. In *Stimuli Responsive Polymeric Nanocarriers for Drug Delivery Applications, Volume 1*, A. S. H. Makhlouf, and N. Y. Abu-Thabit, Eds.; Woodhead Publishing **2018**; pp. 501–529.
6. Washington, K. E.; Kularatne, R. N.; **Karmegam, V**.; Biewer, M. C.; Stefan, Mihaela C., Recent advances in aliphatic polyesters for drug delivery applications, WIREs Nanomedicine and Nanobiotechnology, **2017**,9,1446.

Presentations:

1. **Karmegam, Vasanthy**, Linear and Star-like Functionalized Polycaprolactone Micellar Systems for Doxorubicin Delivery, ACS Meeting April 2018, Southern Methodist University, Dallas, Texas, USA.
2. **Karmegam, Vasanthy**, Synthesis and Characterization of Novel Pyrimidine Donor-Acceptor Polymers, ACS Meeting Aug 2016, Philadelphia, USA.
3. **Karmegam, Vasanthy**, Antimicrobial Efficacy of Nano Zinc Oxide Coated Cross Linked Cellulose, Peradeniya University Annual Research Sessions (PURSE 2012) on July 2012, Peradeniya, Sri Lanka.

Awards:

1. Graduate Studies Scholarship in Chemistry, University of Texas at Dallas (September 2013-November 2018).
2. Second Place in Oral Presentation at ACS Meeting, Southern Methodist University, Dallas, Texas (April 2018).
3. Ph.D. Research Small Grant, University of Texas at Dallas (January 2016).
4. Best Result in Nanoscience and Nanotechnology, University of Peradeniya, Sri Lanka (June 2012).